Optimization of Cable-stayed Bridges at the Conceptual Design Stage

by

Olivia Oey

B.Eng. Civil Engineering
The University of Sydney, 2019

Submitted to the Department of Civil and Environmental Engineering
in partial fulfillment of the requirements for the degree of

Master of Engineering in Civil and Environmental Engineering

at the

MASSACHUSETTS INSTITUTE OF TECHNOLOGY

May 2022

Author .....
Department of Civil and Environmental Engineering
May 06, 2022

Certified by .....
John A. Ochsendorf
Class of 1942 Professor of Civil and Environmental Engineering and Architecture
Thesis Supervisor

Accepted by .....
Colette L. Heald
Professor of Civil and Environmental Engineering
Chair, Graduate Program Committee

Optimization of Cable-stayed Bridges at the Conceptual Design Stage

by

Olivia Oey

Submitted to the Department of Civil and Environmental Engineering
on May 06, 2022, in partial fulfillment of the
requirements for the degree of
Master of Engineering in Civil and Environmental Engineering

Abstract

Conceptual design of cable-stayed bridges, which defines the structure's geometry and typology in the early stages of design, has significant influence on the structure's efficiency, cost, aesthetics, and constructability. However, conventional design approaches for bridge design places greater emphasis on detailed structural analysis than conceptualization, resulting in designers being stuck in an iterative design loop with a structurally inefficient system.

This thesis looks at developing a user-friendly conceptual design tool in the form of efficiency curves, which relates the geometrical aspect ratio L/H of different cable-stayed typologies to its structural performance in terms of volume. By developing a parametric model in the Grasshopper environment, numerous design variables such as number of stay cables, span lengths, materiality, loading conditions, boundary conditions, and flexural rigidity in the towers and decks are able to be investigated and incorporated to obtain a more realistic behavior of the structurally indeterminate cable-stayed bridge.

A series of design curves are proposed for the harp, fan, web, and semi-fan cable configurations. The performance of the forms improves from the web, fan, semi-fan to harp configuration under symmetric loads, and under asymmetric loads, the fan configuration performs better than the harp configuration. Furthermore, since the design curves converge with increasing number of cables, the use of a truss analysis is sufficient for conceptual design, provided that the number of cables is adequate; this design approach, however, does not apply for the web configuration. Furthermore, a region of 'flatness', equivalent to a range of L/H ratios that lies within a 10% variation of the optimum design solution, is proposed for different typologies, material, and boundary conditions. Overall, the web configuration has the most restrictive design curve out of all the typologies, with a very tight range of optimum L/H ratio.

Thesis Supervisor: John A. Ochsendorf
Title: Class of 1942 Professor of Civil and Environmental Engineering and Architecture

Acknowledgments

I would first like to thank my advisor Professor John Ochsendorf who has always been very supportive and insightful throughout my time here at MIT. You have challenged me in the best way possible and sparked my love for structural engineering even more than I could have ever imagined. I have a newfound love for structures, as I no longer merely see structures as science but also as an art form. It has been a great pleasure working alongside you, and I thank you for instilling great wisdom in both my professional endeavors and core values.

Thank you to Professor Caitlin Mueller for your inspiration. It is truly an honor to learn from you and work on this thesis in its early stages with you. Your feedback and guidance have been instrumental in making this thesis possible.

I would also like to thank Demi Fang for her interest and invaluable insights into this thesis. Thank you for referring me to relevant literature and providing guidance whenever I needed help with my Grasshopper script.

Thank you to the CEE Academic Programs Office for their constant support and work in ensuring the best for us.

I would also like to thank my classmates from the Master of Engineering program in Course 1. Your positive support, great company, and incredible knowledge have made the degree a lot easier than it actually is. I am very grateful for our invaluable friendship.

Lastly, I would like to thank my family for their constant love and encouragement despite being miles away. Especially to my parents, thank you for always believing in me and my passion for structural engineering. I would not be where I am today if it were not for all of you.

Contents

List of Figures

List of Tables

Chapter 1

Introduction

The concept of a cable-stayed bridge has been in existence ever since the 17th century, yet its construction was only achieved in the late 18th century. In 1784, the first known cable-stayed system was built by German carpenter C.J Loscher. The bridge consisted of a wooden deck supported by stay anchored to wooden towers. There were a number of cable-stayed bridges that emerged ever since then, such as the Kings Meadow footbridge in 1817, the Tweed River bridge in 1818, and the Nienburg bridge in 1824 (Bessas, 2005). However, the collapse of the Tweed River bridge and Nienburg bridge due to the lack of technical knowledge on fatigue and structural indeterminacy halted the supposedly growing prevalence of cable-stayed bridges for the next 125 years (Svensson, 2011).

Only through the development of high-strength steel cables in the 19th century, there was once again renewed interest in the concept of cable-stayed bridges. The first concept of a modern cable-stayed bridge was then realized in 1955 through the construction of the Strömsund Bridge in Sweden, with a main span length of 182 m. Following this success, rapid interest in its design and construction has led to extensive growth in its numbers and span length, as indicated by Figure 1-1. The appeal for cable-stayed bridges can be attributed to a number of factors. Apart from aesthetics, some of the advantages provided by cable-stayed bridges include their ease of construction through free-cantilevering and incremental launching method, the structural redundancy provided by the stay cables, and the efficient utilization of materials to span longer lengths (Svensson, 2011).

The growing demand for cable-stayed bridges poses a massive challenge for engineers in determining the most optimum design, given the highly statical indeterminate nature of the structure (Agrawal, 1997). One aspect of improving the efficiency of a cable-stayed structure involves defining a structurally optimal geometry for a given typology. Although the structure can easily be subdivided into three main compo-

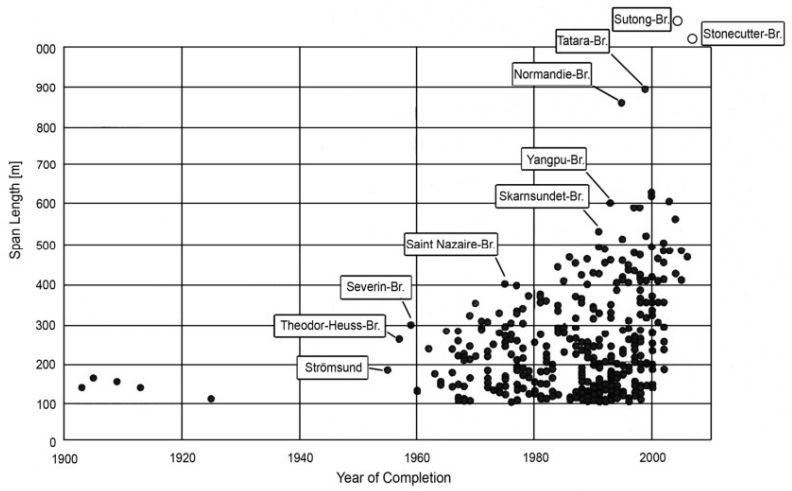

Figure 1-1: Growth of cable-stayed bridges over the past century (Svensson, 2011)

nents (Figure 1-2) - girders, towers, and stay cables - the high structural redundancy and numerous design variables such as cable arrangement and number of stay cables, main span length, and pylon height make the design and optimization procedures of cable-stayed bridges difficult. The design variables of some recent bridges are summarized in Table 1.1 below.

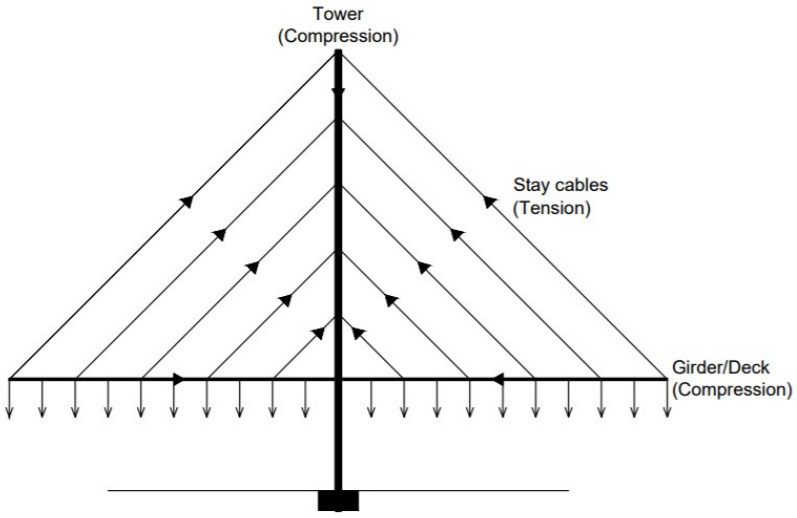

Figure 1-2: Simple illustration of a cable-stayed bridge

There is a wide range of geometry L/H within the list provided in Table 1.1, ranging between 3.20 to 5.50. The geometrical aspect ratio is an integral design variable defined early in the design phase. The conceptual design phase of cable-stayed bridges, which comprises the early stage of the structural design process, involves determining the right typology and geometry of the cable-stayed structure to satisfy

Table 1.1: List of some cable-stayed bridges around the world

Name	Main span length L (m)	Tower height H (m)	L/H	Year built	Type	Material
Pasco-Kennewick Bridge	273	73	3.75	1978	Fan	Concrete
Barrios de Luna Bridge	322	90	3.57	1983	Harp	Concrete
Knie Bridge Dusseldorf	450	95	4.76	1969	Harp	Steel
Second Severn Crossing	456	101	4.51	1996	Semi-fan	Composite
Skarnsundet Bridge	530	152	3.49	1991	Semi-fan	Concrete
Stonecutters Bridge	729	225	3.25	2009	Semi-fan	Composite
Tatara Bridge	765	180	4.25	1999	Semi-fan	Composite
Pont de Normandie	856	156	5.50	1995	Semi-fan	Composite
Sutong Cable-stayed Bridge	1088	306	3.56	2007	Semi-fan	Composite

the design constraints. This particular stage of design has significant influence on the structure's efficiency, cost, aesthetics, and constructability (Reich and Fenves, 1995).

Conventional design approaches for bridges, however, place greater focus on detailed structural analysis than design conceptualization (Romo et al., 2015), and for many years, this critical predesign stage has depended heavily on the experience of expert engineers. It is important to acknowledge that the lack of focus and available tools in design exploration during the early stages of conceptual design needs to be addressed to ultimately achieve the main objective of designing a structurally sound and efficient system.

Defining a suboptimal conceptual design is necessary to streamline the design process as it serves as the premise for detailed design works to be based upon. Furthermore, there is substantial design freedom in the early stages of design to manipulate the system's form and geometry, which would result in a preliminary design that performs satisfactorily against the design constraints. Significant changes further down the design process are unfavorable and mostly limited by cost and resource constraints (Romo et al., 2015).

Therefore, the importance of obtaining an efficient form in the early stages of design emphasizes the need for conceptual design tools that are simple to implement and could provide designers with good approximations of the structural performance of different cable-stayed typologies without restricting free exploration of the design space. This led to the development of the theory of morphological indicators (MI) by Philippe Samyn in 1999, allowing for typology optimization at the conceptual level. Morphological indicators (MI) are essentially dimensionless quantities that represent the physical performance of a structure (De Wilde et al., 2015).

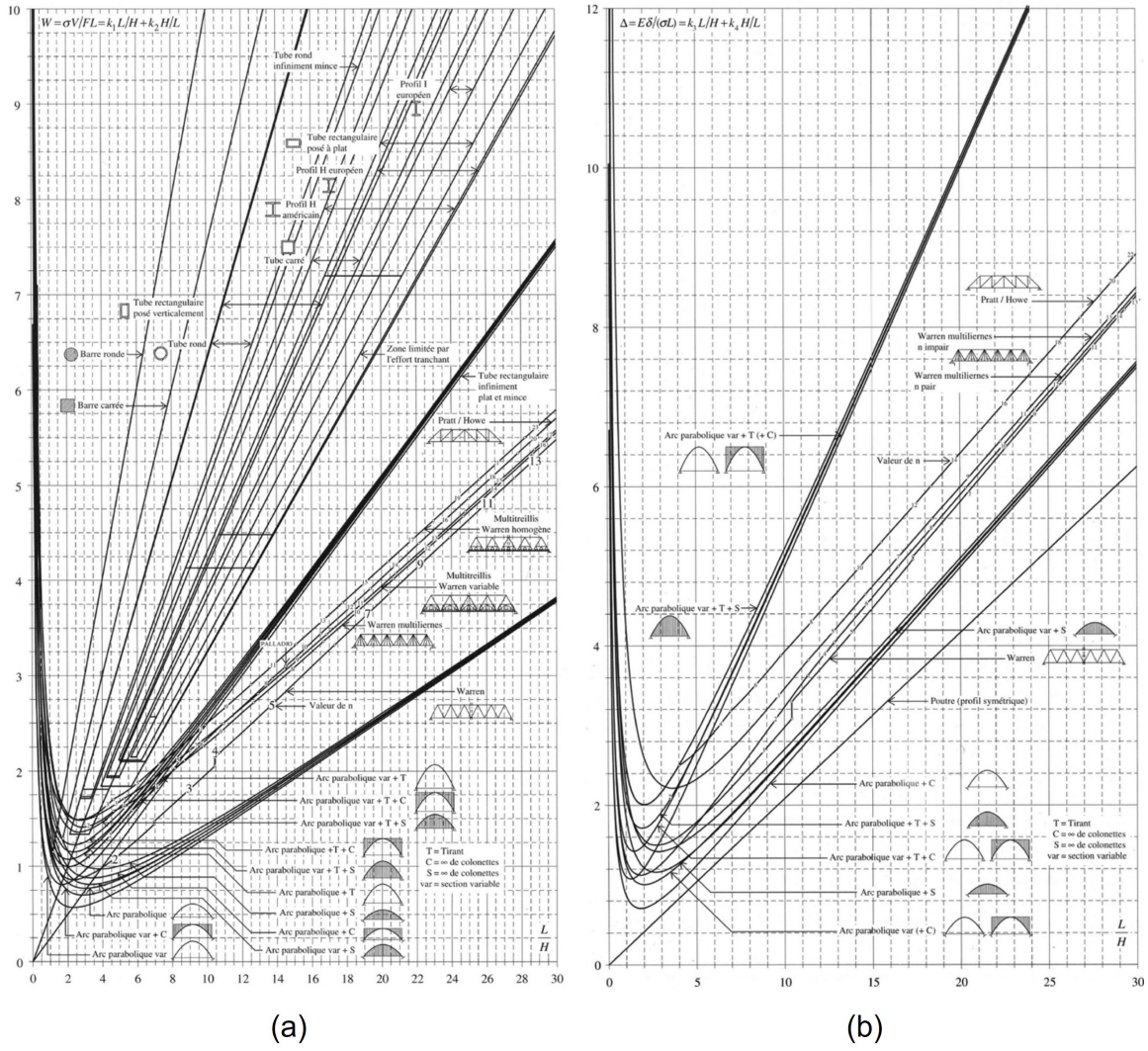

(a) (b)

Figure 1-3: (a) Volume indicator W and (b) Displacement indicator Δ of classical systems considering only resistance (Samyn, 1999)

Considering only resistance, two fundamental indicators, namely volume W and displacement indicators Δ, were developed (Samyn, 1999), with each dimensionless indicator representing the structure's strength and stiffness. When these indicators were plotted against the structure's geometric slenderness L/H, a series of efficiency curves shown in Figure 1-3 was obtained. The curves concisely summarize the optimum geometrical slenderness L/H corresponding to the least volume and displacement for various structural typologies and topologies.

1.1 Problem Statement

The theory of morphological indicators (MI) as a conceptual design tool allows for the structural performances of different cable-stayed typologies to be objectively compared using minimal design variables, rendering it a user-friendly conceptual design tool. However, the wide range of variables involved in the design of cable-stayed bridges requires a conceptualization design tool that is versatile enough to encompass these increasingly new variables.

Based on the previous concepts built by Samyn (2004) on cable-stayed structures, this thesis aims to provide design guidance in the form of efficiency curves that objectively and accurately quantify the volume and displacement performances of different cable-stayed typologies: harp, fan, and web. This is done by:

1. Accounting for the self-weight of the main elements.
2. Incorporating bending stiffness EI of the tower and deck elements to simulate bending deformations.
3. Utilizing different materials such as steel and concrete for the deck and tower elements.
4. Considering asymmetrical loading conditions.

Additionally, an optimum range of L/H ratios will be proposed for various typologies, loading, and support conditions. The optimum range is defined as the region of "flatness" in the efficiency curves, corresponding to a 10% variation of the minimum optimal performance.

Chapter 2

Literature Review

2.1 Morphological Indicators

Zalewski and Kus (1996) formed the basis for the development of morphological indicators (MI). Without considering the effects of instability, the study compared the weights and displacements of two-dimensional (2D) trusses with different typologies based on the flow of forces and flux of stresses in beams and plates. This was the first time that a relationship between geometrical slenderness L/H and the volume and displacement of a truss system was drawn.

The theory of MI was explored by Samyn (1999) in his doctoral thesis, where the volume V and displacement δ of statically determinate planar structures were expressed as dimensionless quantities, namely W and Δ. While neglecting the effects of buckling instabilities, W and Δ were determined to be functions of the structure's geometrical slenderness L/H, with L being the larger dimension in which the structure was inscribed in.

The derivation of the volume indicator W can be demonstrated by considering a statically determinate structure with principal dimensions L and H and subjected to a total resultant force F. For any given element i of the structure, its volume V_i under a fully-stressed state can be computed as:

$$V_i = \frac{N_i l_i}{\sigma} \tag{2.1}$$

where N_i and l_i are the axial force and length of member i, and σ is the allowable strength of the members.

The axial force N_i of any given member i can be denoted as a fraction of the total resultant force F, $k_i F$, in which the coefficient $k_i = f(L/H)$. Upon expressing the member length l_i as a quotient of L and the axial force N_i as $k_i F$, Equation 2.1 can

be expressed as:

$$V_i = \frac{k_i F}{\sigma} \frac{l_i}{L} L = \frac{FL}{\sigma} \left(k_i \frac{l_i}{L} \right) \tag{2.2}$$

Since k_i and l_i/L depend only on L/H, the expression for the total volume V can thus, be simplified using a dimensionless volume indicator W as:

$$V = \frac{FL}{\sigma} \sum k_i \left(\frac{l_i}{L} \right) = \frac{FL}{\sigma} W \tag{2.3}$$

The dimensionless volume indicator W quantifies the volume of an isomorphic structure with a unit span length L (1 m) and elements sized at a unit allowable stress σ (1 Pa) when subjected to a unit resultant force F (1 N).

The dimensionless displacement indicator Δ was also derived in a similar approach. It represents the maximum displacement δ of an isomorphic structure with unit span L (1 m), in which the elements are sized at a unit allowable stress σ (1 Pa) and made up of material with unit Young's modulus E (1 Pa) when subjected to a unit resultant force F (1 N).

By expressing these indicators as a function of only the structure's geometrical slenderness L/H, Samyn (1999) successfully derived analytical equations for both volume W and displacement Δ indicators in Equation 2.4 and 2.5 based on only resistance criteria. This allows for the volume of material and stiffness of different structural systems to be compared objectively, provided that they are subjected to the same loading and support conditions.

$$W = \frac{\sigma V}{FL} \tag{2.4}$$

$$\Delta = \frac{E\delta}{\sigma L} \tag{2.5}$$

Using Equations 2.4 and 2.5, Samyn (2004) plotted efficiency curves for the volume W and displacement Δ indicators of various structural typologies, including trusses, beams, arches, cables, cable-stayed structures, masts and frames, as shown in Figure 1-3. It shall be noted that these curves were derived under strict design hypotheses, simple load cases, and support conditions.

For the purpose of this thesis, morphological indicators (MI) derived for the cable-stayed structures will be discussed further in depth.

2.1.1 Cable-stayed structures

In deriving the volume W and displacement Δ indicators for cable-stayed structures, Samyn (2004) analyzed the system as a truss, where the elements had no bending rigidities and acted only in pure axial compression/tension. Because the elements had pin-jointed connections, the uniformly distributed load p was transformed to equivalent point loads acting at the joints. A detailed description of a typical cable-stayed model with deck span L and tower height H is provided in Figure 2-1.

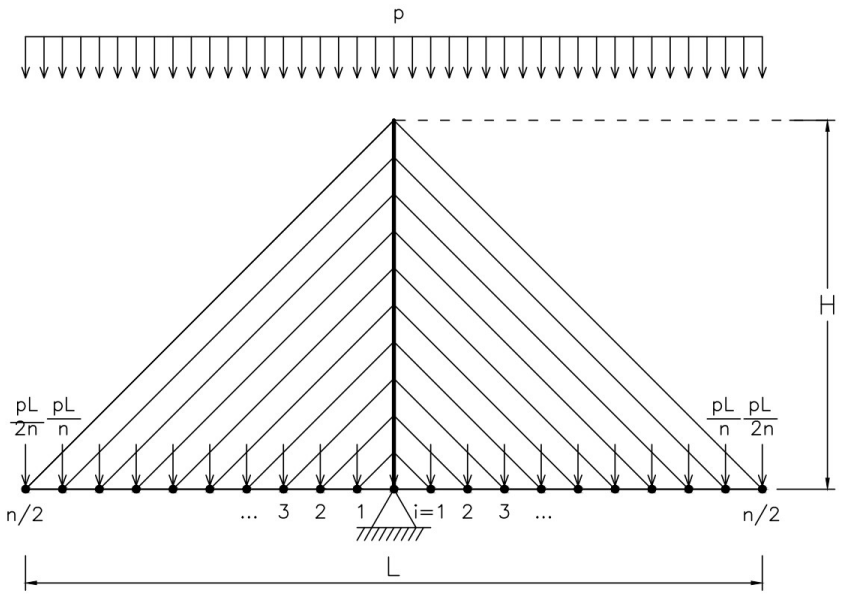

Figure 2-1: Samyn's (2004) cable-stayed model

Three cable-stayed configurations were explored in the study: fan, harp, and semi-harp. The cables in a fan configuration coincided at the highest point of the tower, while the cables in a harp and the semi-harp configuration were evenly spaced over the entire tower height and two-thirds of the tower height, respectively.

For each cable-stayed typology, the towers remained pinned while three modifications to the support conditions at the deck ends were made, which imposed distinct axial forces in the deck, such that:

- The deck was under full compression as the deck ends were unrestrained;
- The deck was under full tension;
- The deck was under compression and tension symmetrically about the tower as horizontal translational was restricted.

The maximum static displacement Δ indicator referred to in this study considered both horizontal $\Delta_{deck,h}$ and vertical displacement $\Delta_{deck,v}$ at the deck ends as well as the vertical displacements (axial shortening) of the towers Δ_{tower}. Where the decks

had tensile forces acting on them, no horizontal displacements were recorded due to the lateral restraint provided by the rollers. These displacements are labeled in Figure 2-2.

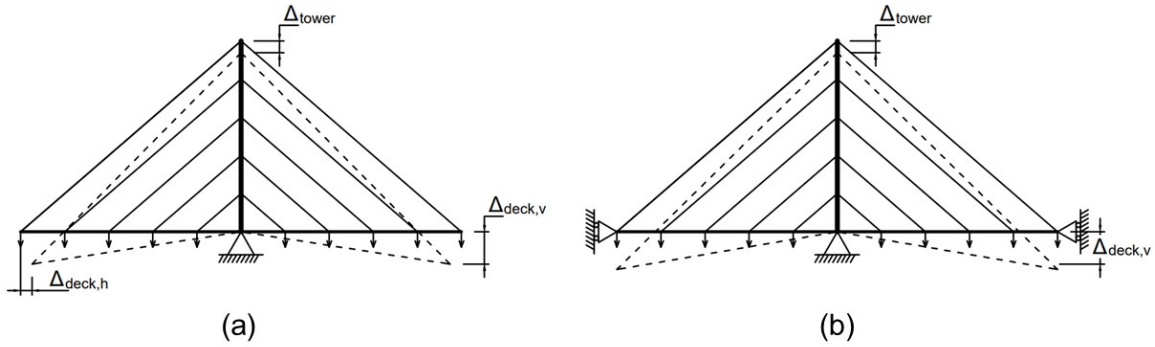

Figure 2-2: Maximum displacement Δ of the system for (a) unrestrained deck ends, and (b) laterally restrained deck ends

Under the assumption of a fully stressed state and resistance-based design, analytical solutions to volume W and displacement Δ indicators for the three bridge typologies listed above with different support conditions were eventually derived. Efficiency curves depicting the strength and stiffness performances of different systems were also developed over an extensive range of L/H ratios between 0.1 to 18.0, as shown in Figure 2-3. Therefore, the development of morphological indicators provided a relatively quick measure of the system's efficiency based only on the geometrical parameter L/H (De Wilde et al., 2015).

2.1.2 Working Hypotheses

The performance curves in Figure 2-3 developed by Samyn (1999, 2004) effectively and concisely summarized the most desirable geometry for any cable-stayed typology, which would aid in predimensioning an aspect ratio L/H that satisfies both form and function at the early stages of design. However, the simplicity of the approach, as previously mentioned in Section 1.1, was made possible by imposing the following design hypotheses:

- The structure had only one dominant load case, which was the uniformly distributed load, p.
- The members were not subjected to bending, given that the number of cables n was assumed to approach infinity.
- The structure was made of a homogenous, linear elastic material.
- The structure was in a fully stressed state, whereby the elements were optimally sized to resist the applied loads.

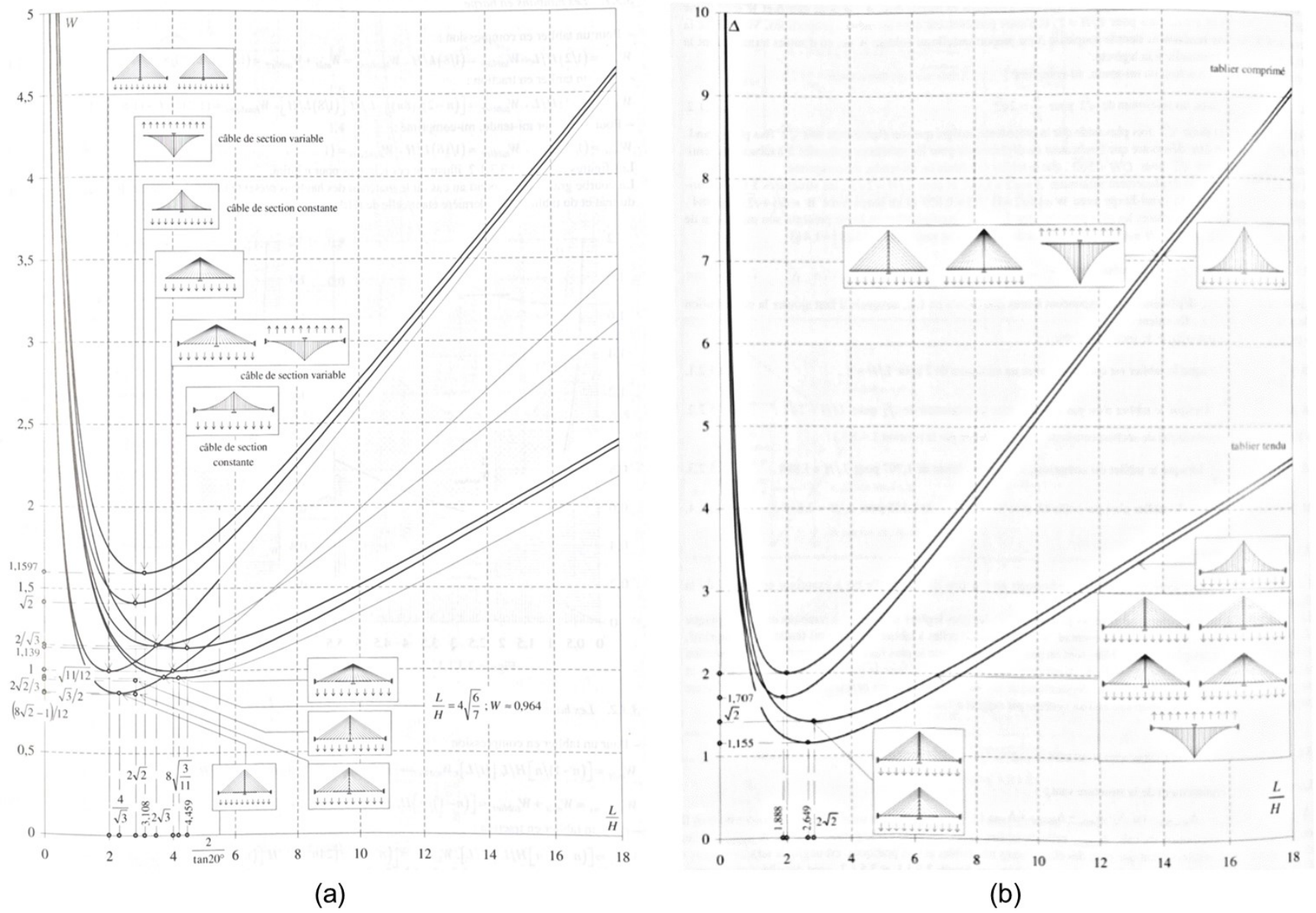

Figure 2-3: (a) Volume W and (b) Displacement indicator Δ of cable-stayed structures considering only resistance by Samyn (2004)

- Instabilities such as buckling were neglected.
- Self-weight and second-order effects were neglected.
- Fatigue and dynamic effects were ignored.

Considering the high degree of redundancy and wide range of design variables involved in the design of cable-stayed bridges (Romo et al., 2015), these working hypotheses restricted the applicability of MI to be utilized as an effective conceptual design tool for cable-stayed bridges.

2.2 Structural Optimization of Cable-stayed Bridges

The world of structural optimization within cable-stayed bridges is not only limited to the concept of morphological indicators. There have been numerous attempts and studies that looked at optimization at the conceptual level and detailed phase as well.

P. Wang et al. (1993) proposed a system of nonlinear equations that were solved using the Newton-Raphson method to determine an efficient initial shape of cable-stayed bridges under dead loads and pretension loads in the stay cables. Structural optimization on detailed analysis of cable-stayed bridges was conducted by Hassan et al. (2013) in which a numerical design tool with an objective function of minimizing the total cost was developed using finite element modeling, genetic algorithm (RCGA), and B-spline curves. In this study, a total of nine design variables were considered for a three-span composite, semi-fan cable-stayed bridge.

Like many other research on optimizations, the aforementioned optimization methods are derived from a very specific set of design variables with a predefined geometry or shape to obtain a single optimal solution through the use of mathematically formulated objective and constraint equations. Furthermore, since these studies emphasized primarily on quantifiable objectives and less on architectural expression, it lends itself as being impractical to implement as it limits design freedom during the early design exploration stage.

Therefore, there needs to be a structural optimization tool that caters to the early conceptual design of cable-stayed bridges while effectively translating the designer's intent and objectives. This way, issues with existing optimization strategies which are known to be stringent and too numerically complex to be implemented for conceptual design, can be mitigated.

2.3 Design Variables of Cable-stayed Bridges

The performance of a cable-stayed system, which includes its volume of material, static displacement, as well as dynamic response, is dependent on multiple design variables interacting with one another. Identifying the critical variables early in the design stage is necessary to achieve a suboptimal conceptual design which would make size and shape optimization performed in the detailed analysis phase worthwhile.

As proven by the distinct curves plotted in Figure 2-3 for the fan, harp, and semi-harp configurations, an obvious design parameter would be the form or typology of the cable-stayed system. Other than typology, previous studies have also discovered that various design variables such as number of stay cables, tower height, span length, support conditions, and load cases affect the both static and dynamic aspects of a cable-stayed structure.

The effect of bridge typology on the volume performance of cable-stayed bridges was also corroborated by a parametric study conducted by Agrawal (1997). The study examined the effect of the number of cables and side-to-main span ratio on a two-plane harp and fan cable-stayed bridge. The study revealed that for a smaller number of cables, the total volume for a fan configuration was larger than a harp configuration. The total volume for both configurations evened out as the number of cables was increased.

With respect to the dynamic response of cable-stayed bridges, Kawashima et al. (1993) and Akhoondzade-Noghabi and Bargi (2016) discovered that the damping ratio increases in the order of semi-fan, fan, and harp under free-oscillation tests. These findings further reinforced the importance of identifying a form that would work the most efficiently under the predefined design criteria.

Within Clune's (2013) Ph.D. thesis of automating algorithm selection for structural optimization, the design problem of a cable-stayed bridge with fan configuration was considered. While keeping the tower height as a variable parameter, the study recorded the mass of the optimized solution for three-span lengths - 300 m, 500 m, and 800 m. The study demonstrated an approximately linear relationship between the mass per unit area and the span length of the structure. Further, the change in tower height mainly affected the distribution of weight (stiffness) between the deck and cable elements. A shorter tower height required a much stiffer deck to compensate for the lack of vertical stiffness in the cables, which would have otherwise been provided by a taller tower.

In a recent study provided by Fairclough et al. (2022), the importance of support conditions in cable-stayed bridges was demonstrated. An optimized cable configuration was obtained for a self-anchored bridge where vertical supports were provided at

the ends of the deck and a partially ground-anchored bridge where horizontal displacements were partially restrained. The final form obtained for both cases are shown in Figure 2-4 and the optimum span-dip ratio was determined to be 2.00 and 3.28, respectively. In addition, the total weight of the entire structure was also quantified, in which the self-anchored system required almost twice the amount of material relative to a ground-anchored bridge.

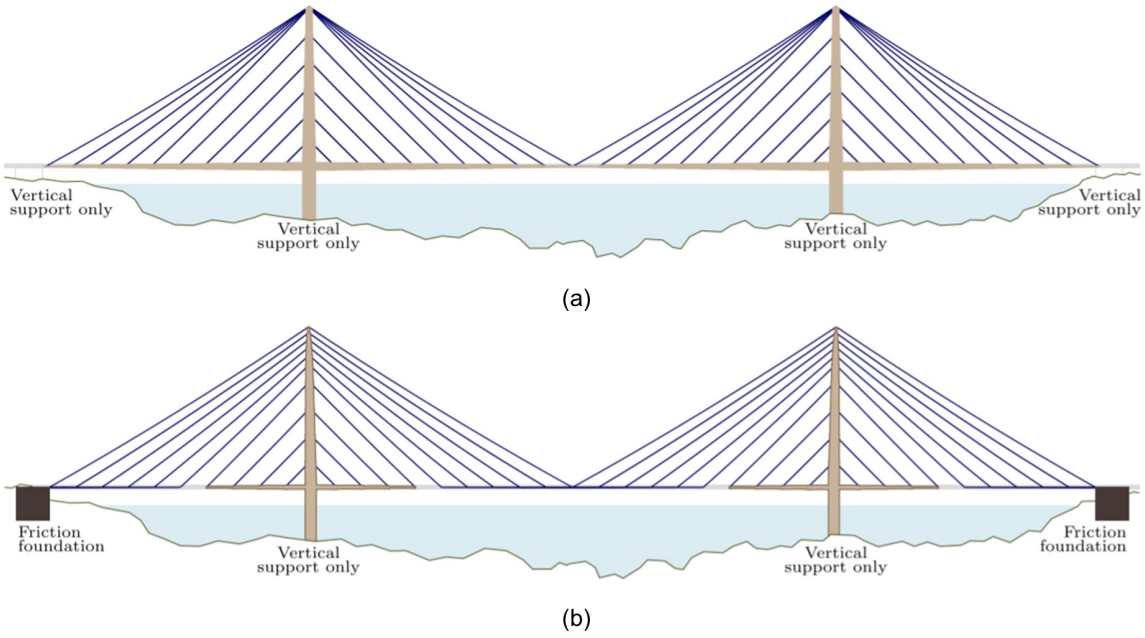

Figure 2-4: Optimized design for a (a) self-anchored cable-stayed bridge with purely vertical supports, and (b) ground-anchored cable-stayed bridge with frictional supports (Fairclough et al., 2022)

2.4 Conclusion

The existing literature supports the lack of conceptual design tools that would enable structural optimization to be performed in the early stages of cable-stayed bridge design with minimal disregard for critical design variables and hypotheses. The concept of morphological indicators developed by Samyn (2004) shows the potential for free design exploration through simple yet user-friendly efficiency curves defined by the geometry of the structure L/H. The main limitation exhibited by MI is its lack of integration of multiple design variables and its strict design assumptions, which are attempted to be resolved in this thesis.

More versatile and robust conceptual design tools are necessary to simplify the initial design process as it aids designers in dimensioning an optimum geometry of a

cable-stayed system based on a set of preliminary design constraints and requirements. Through this thesis, the concept of MI is augmented to incorporate critical design variables and important design assumptions. By the end of this study, a series of volume efficiency curves described by the system's geometric slenderness L/H will be derived for elements with flexural rigidity, different materiality, typologies, load cases, and support conditions.

Chapter 3

Methodology

3.1 Concept

Incorporating the effects of materiality into the model invalidates the use of morphological indicators to assess the efficiency of different cable-stayed typologies. This can be demonstrated when the volume indicator W in Equation 2.4 is expressed in terms of the structure's total "load path" (Maxwell, 1864), defined as the sum of the product of the member's axial force and its corresponding length, $\Sigma|N_i|l_i$. By Maxwell's Load Path Theorem, the total volume V of a fully stressed structure with negligible flexural deformations can be described as (Baker et al., 2015):

$$V = \frac{\Sigma|N_i|l_i}{\sigma} \tag{3.1}$$

where N_i = axial tension (or compression) force of member i, l_i = length of members i, and σ = allowable stress.

When the dimensionless volume indicator W is represented as a function of the total load path (Equation 3.1), W reduces to Equation 3.2 and is shown to be independent of the material property, rendering it ineffective to capture the effect of different materiality in the study.

$$W = \frac{\sigma V}{FL} = \frac{\sigma \times \frac{\Sigma|N_i|l_i}{\sigma}}{FL} = \frac{\Sigma|N_i|l_i}{FL} \tag{3.2}$$

where F = resultant of the external forces, and L = span length of the structure.

Other than materiality, the inclusion of bending rigidities in the structural elements, whereby $EI \neq 0$, made the use of Maxwell's Load Path Theorem an inaccurate approach to quantifying the structural efficiency of a system. The "load path" approach would compute a much more conservative volume of material given that

members are sized only to resist the applied axial force.

It can also be postulated that bending in the elements would introduce an additional dependent variable, flexural rigidity EI, affecting the final volume of material V. Since it is established earlier in Section 2.1 that the volume indicator W was derived under the assumption that the axial force acting on any member N_i is proportional to the resultant force F of the entire system (Section 2.1) with no explicit mention on the effects of flexure, the use of volume indicator W would not be appropriate for this study.

Therefore, the performance metrics in this study will be evaluated using absolute values in order to comprehensively capture the full effect of materiality and flexure within the performance curves.

3.2 Parametric Model

A single-plane cable-stayed parametric model based on Samyn's (2004) existing work is developed using Grasshopper in Rhinoceros (McNeel). The additional complexities incorporated into the model are best achieved through the use of a parametric model, given the large number of variables being studied. Changes in the shape of the model geometry, such as its dimensions L and H, the number of cables n, load cases, and material properties are easily modified (Romo et al., 2015) through the use of sliders in Grasshopper.

As outlined in Section 1.1, four important details are integrated into the parametric model to accurately simulate the behavior of cable-stayed structures. Two of the simpler adjustments made to the parametric model involve the consideration of the system's self-weight and the material type.

Apart from the stay cables, the deck and tower elements are modeled with bending rigidities EI to simulate the elements bending between the cable supports. Figure 3-1(b) provides a visual interpretation of the deck and tower elements modeled as beam elements with flexural rigidities compared to a system entirely composed of truss elements (Figure 3-1(a)).

The system is ensured to be 'fully stressed' by sizing the elements to provide minimum resistance against the applied bending moments M_i and axial loads N_i. Given that bending moment is quadratically proportional to the length of tower or deck elements between consecutive cable supports, the number of cables n is identified as a critical variable that has to be considered in the study.

Lastly, the optimum geometry for the four typologies under asymmetric loading condition is also explored in this study.

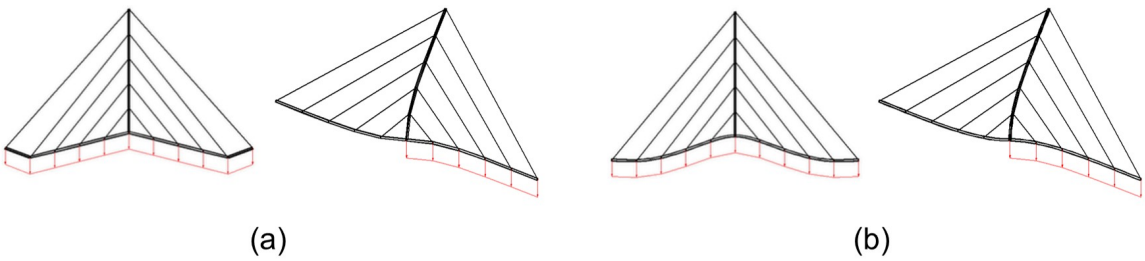

Figure 3-1: Deck and tower elements modelled as (a) truss elements, without bending rigidities, and (b) beam elements, with bending rigidities

Design principle

The design of the cable-stayed structure in this study adopts the Allowable Stress Stress Design (ASD) principle, where sizing of the structural elements is performed based on the allowable stress of the material at service (unfactored) load combinations.

The tower and deck elements are modeled as steel and concrete, while the cable elements are modeled as Grade 250 low-relaxation, seven-wire steel strands. Given that the stay cables are the elements that transfer the applied loads on the deck to the towers through axial action, the safety of the entire system is highly dependent on the performance of the stay cables. To ensure sufficient robustness and redundancy within the system, a safety factor of 2.2 (or 0.45 σ_{UTS}) is recommended for the design of stay cables as per the Post-Tensioning Institute Manual (PTI, 2015).

The relevant material properties are listed in Table 3.1, including the densities ρ used in computing the dead loads of the overall structure. These values are obtained from ASTM (2019a), ACI 314-R (2014) and ASTM (2019b), respectively.

Table 3.1: Assumed material properties

Material	Allowable Stress σ (MPa)	Young's Modulus E (GPa)	Density ρ (kg/m^3)
Steel	250	200,000	7,850
Concrete	35	29,560	2,400
Prestressing steel	775	200,000	7,840

3.2.1 Design variables

L/H ratio

A narrower range of L/H ratio between 1 to 10 is focused on to ensure that the proposed curves are practical enough to be implemented in the actual design of cable-

stayed bridges. The high L/H ratio is adopted to encompass a new structural form of cable-stayed bridges known as extradosed bridges, characterized by shorter towers with L/H ratios of approximately ten (Stroh, 2015).

To account for the effect of span length on the overall loading conditions, such as the case where dead loads govern the loading criterion of long-span bridges, (Ochsendorf and Billington, 1998), three classes of cable-stayed bridges are investigated: short-span, medium-span, and long-span, each with span lengths L of 200 m, 500 m, and 800 m, respectively. For each of the three span length categories, the geometric design variables H are varied to cover the L/H range between 1 to 10.

Number of stay cables n

The bending moment induced in the decks and towers is controlled by the spacing of the cable supports. A higher number of cable supports would reduce bending moments and allow for a more slender stiffening girder. The spacing of the cables in the deck and tower is influenced by the chosen typology (Section 3.2.3) as well as the number of cable supports.

In this study, the number of cables n referred to the number of cable supports on only one side of the tower, supporting half the total span length L. The number of cables n is incremented consecutively to determine the optimum number of cables for the three span length categories and typologies.

Section properties

To make the sizing procedure of the individual bridge elements more manageable, the overall cross-sectional geometry of the towers and decks are estimated as geometrical ratios of the span length L and tower height H. The cross-section dimensions of the deck (W_{deck} and D_{deck}) and tower (W_{tower} and D_{tower}) elements referred to in this study are clearly labeled in Figure 3-2 and 3-3.

Each bridge is designed to accommodate six lanes of traffic. In compliance with the design specifications set in the LRFD Manual for Highway Bridge Superstructures by AASHTO (2015), the decks are modeled as 22 m wide box girders. The depth of the decks D_{deck} is expressed as a function of the bridge span L, whereby a linear relationship described in Equation 3.3 is obtained by curve-fitting the variables D_{deck}/L against L of actual cable-stayed bridges as shown in Figure 3-4.

$$D_{deck}/L = -6.0 \times 10^{-6} L + 0.009 \tag{3.3}$$

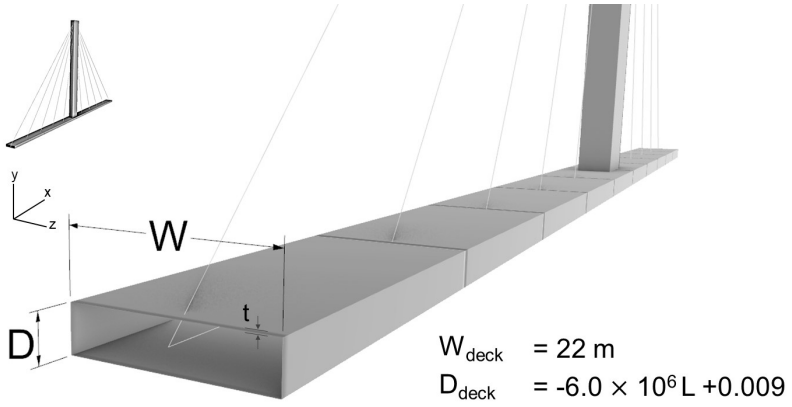

Figure 3-2: Depth D_{deck} and width W_{deck} of the bridge deck

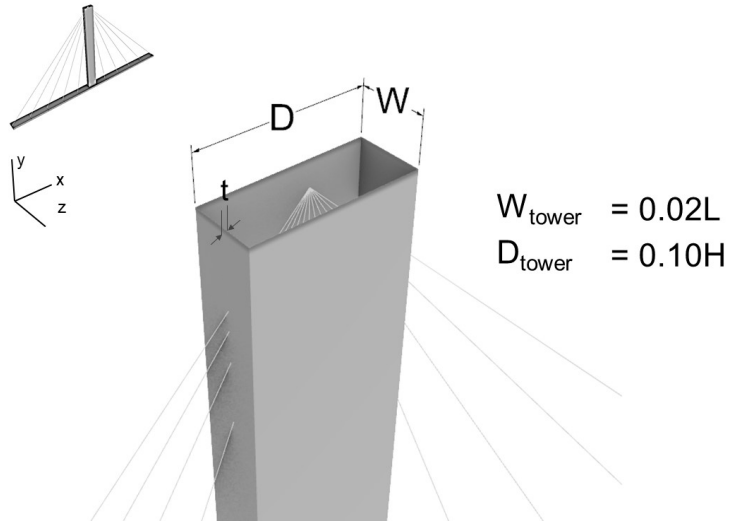

Figure 3-3: Depth D_{tower} and width W_{tower} of the bridge tower

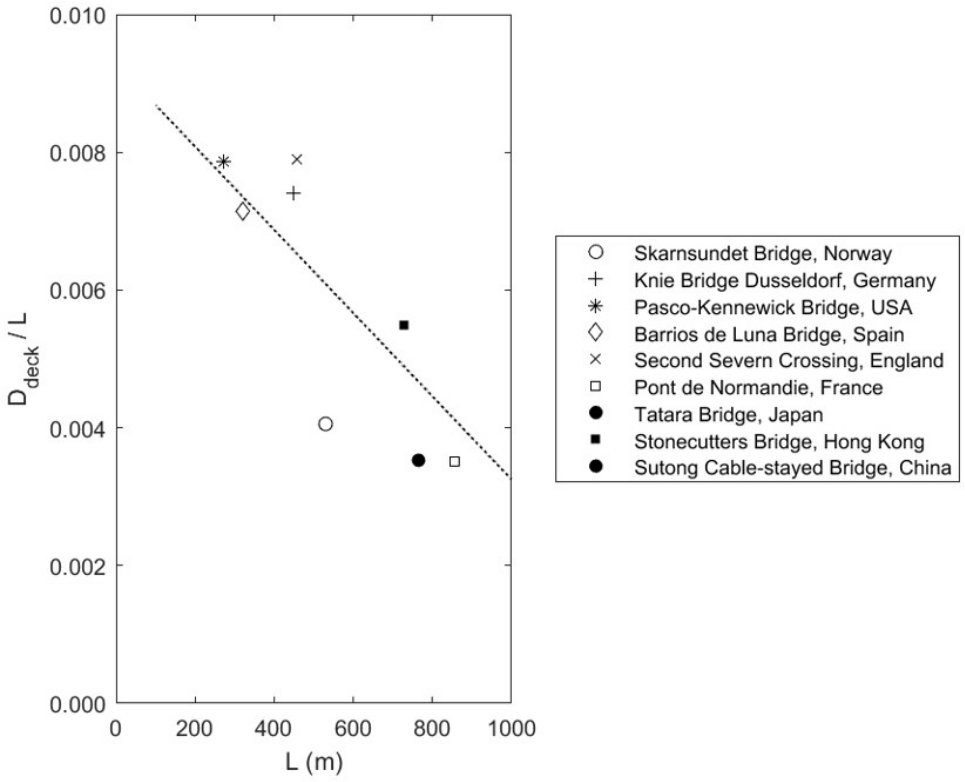

Figure 3-4: Linear interpolation between D_{deck}/L and bridge span L of existing cable-stayed bridges

Additionally, the width W_{tower} and depth D_{tower} of the tower sections are empirically determined as $0.02L$ and $0.10H$, respectively.

For each of the short, medium, and long-span cable-stayed bridges, Table 3.2 outlines the deck and tower cross-section dimensions for the corresponding upper and lower bounds L/H ratio of 10 and 1.

Table 3.2: Upper and lower bounds of the deck and tower cross-sectional properties for the various design variables studied

Span length L (m)	200 m		500 m		800 m	
L/H	1	10	1	10	1	10
Deck width W_{deck} (m)	22	22	22	22	22	22
Deck depth D_{deck} (m)	2	2	3	3	4	4
Tower height H (m)	200	20	500	50	800	80
Tower width W_{tower} (m)	4	4	10	10	16	16
Tower depth D_{tower} (m)	20	2	50	5	80	8

3.2.2 Design loads

The design vehicular live load assigned to the parametric models conforms with AASHTO Load and Resistance Factored Design (LRFD) for Highway Bridge Superstructures code (2015). A minimum 3.66 m (12 ft) design lane width for a lane of traffic is required, in which the longitudinal design lane load equivalent to 10 kN/m shall be located within a 3.0 m (10 ft) width of the 3.66 m (12 ft) design lane width.

Since the study focused on initial conceptual design, the longitudinal live loading criterion of the bridges only considers the uniformly distributed design lane load. To mitigate unconservatism in disregarding design truck and tandem loading, the design lane load is increased to 15 kN/m longitudinally for a design lane.

As previously mentioned, the parametric bridges are modeled as 22 m wide box girders, equivalent to six lanes of traffic. As a result, a cumulative 90 kN/m uniform line load is applied longitudinally along its span L.

Asymmetrical load pattern is also explored, given the highly stochastic nature of traffic loads. The emphasis on investigating the implications of asymmetrical loads lies in the fact that it generally is the governing design criteria of cable-stayed bridges. This loading criterion is achieved by modeling the design lane load of 90 kN/m to only half the bridge span L. The imposed bending in the tower towards the loaded span would result in a higher quantity of material.

All the bridge models are optimally sized to withstand the same design vehicular loads, in addition to dead loads. The dead load consists of the structure's self-weight and an additional 250 mm thick concrete deck (AASHTO, 2015), equivalent to a uniform line load of 130 kN/m.

The two design load cases mentioned in this section are illustrated in Figure 3-5.

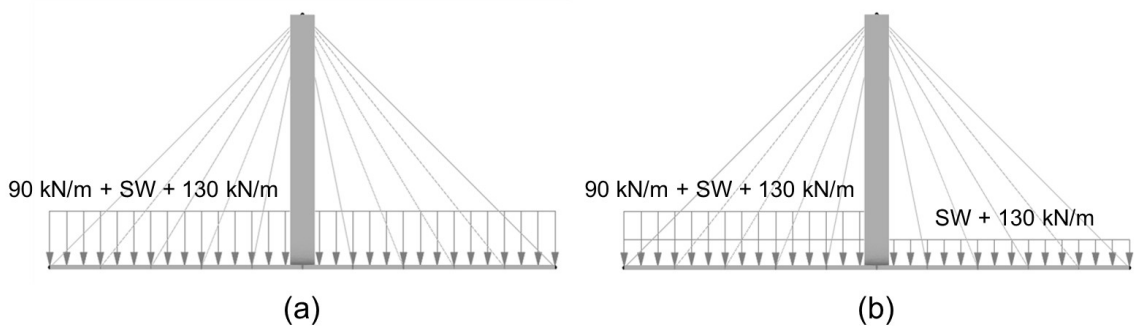

Figure 3-5: (a) Symmetrical (b) Asymmetrical loading conditions

3.2.3 Typologies

Four main cable configurations, as depicted in Figure 3-6 are investigated in this study. The typologies are:

1. Harp, where the cables are evenly spaced across the deck and tower. Thus, the cables are all inclined at equal angles;
2. Fan, where the evenly spaced cables on the deck coincide at the top of the tower.
3. Web, inspired by the Margaret Hunt Hill Bridge in Dallas. Designed by the engineer and architect Santiago Calatrava, the cables are arranged reversely with the highest cable support at the tower connected to the closest support in the deck and vice versa. Closer to the towers, the cables are steeply inclined, and transitions to a gentler inclination angle further down the deck and away from the tower. Another close precedent to the web typology is the Ruck-a-Chucky Bridge, a cable-stayed bridge design proposed by T.Y. Lin International, Hanson Engineers, and Skidmore, Owings & Merrill (SOM) in 1978 to span the American River in California. Although the inclinations of the cables are not as extreme as that of the Margaret Hunt Hill Bridge, it simulates the idea of the cables interlacing one another in addition to the gentle slope of the cables. The two bridges are shown in Figure 3-7.
4. Semi-fan, with the cables evenly distributed across one-third of the tower height.

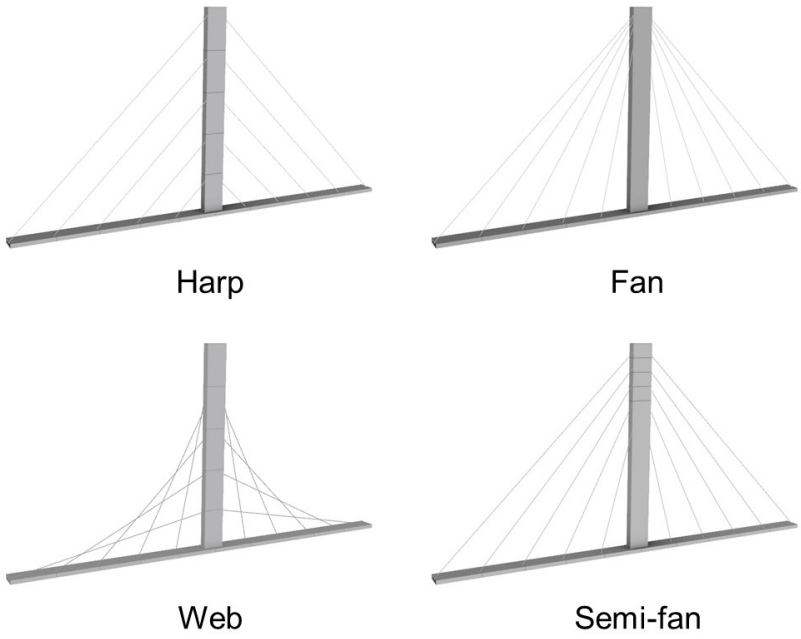

Figure 3-6: Four cable configuration studied in this paper: Harp, Fan, Web, and Semi-fan

Figure 3-7: Margaret Hunt Hill Bridge in Dallas, Texas (Photo obtained from Alan Karchmer and SOM)

3.2.4 Support Conditions

Equilibrium of the bridge models is established by setting up appropriate boundary conditions at the deck ends (midspan of the bridge), and the tower supports. In this study, a self-anchored and a partially ground-anchored system are investigated. A self-anchored cable-stayed system is simulated by releasing the deck ends from any rotational and translational restraint, which causes the deck to be entirely under compression. The partially ground-anchored system is modeled by restricting translation in the horizontal direction. The reaction force provided by the roller supports would force the decks next to the support to be under tension while remaining under compression near the tower. The support conditions are illustrated in Figure 3-8 along with its equilibrium states.

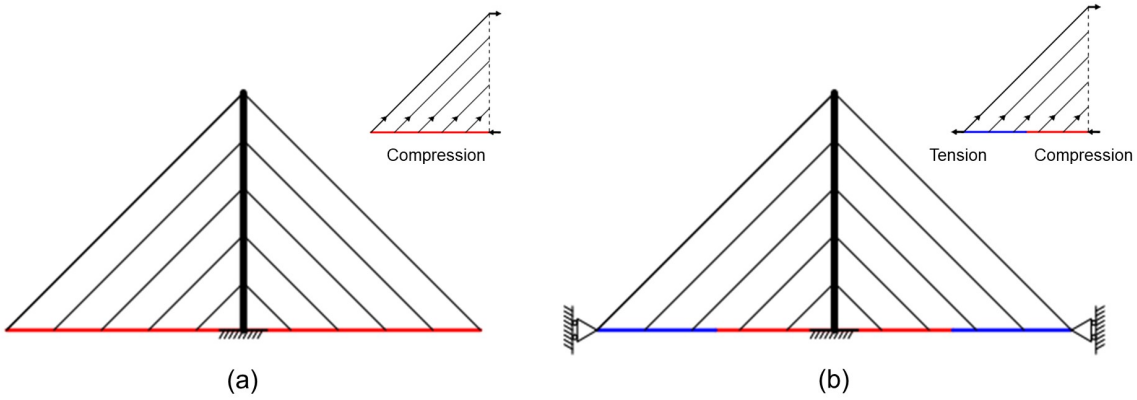

Figure 3-8: Support conditions for (a) self-anchored bridge model and (b) partially anchored bridge model

To limit the study to a two-dimensional plane, out-of-plane translational displacements are restrained. It shall be noted that the connection between the tower and deck is kept rigid to prevent instability issues from arising during the analysis using Karamba3D. The rotational restraint provided at the tower-deck connection limits excessive global deflections of the towers under asymmetrical loads, which is the generally the case for multiple cable-stayed span bridges due to the absence of the back-staying effect otherwise provided in a single-span cable-stayed bridge (Virloguex, 2001).

3.2.5 Cable elements

One of the limitations of the plug-in Karamba3D in performing finite element analysis of the parametric models is the absence of cable elements to model the stays of the bridges. This issue is circumvented by defining the cables as truss elements by setting

its flexural rigidity to zero and deactivating buckling. In an instance where the cables undergo compression, the cables are forced into tension by applying a positive prestrain (or elongation) as indicated in Figure 3-9.

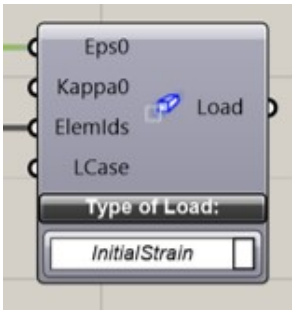

Figure 3-9: Prestrain load in Karamba applied to the cables that undergo compression

It is important to also realize that while modeling the stay cables as equivalent truss element suffices in the preliminary design stage, it eliminates two inherent properties of cable elements, that is the sag effect and its nonlinear behaviour which causes its stiffness to vary with the applied loads. These factors are important and must be considered in the detailed analysis.

This design workaround is later verified using a standard finite element analysis software Strand7 (2010) where the stays are modeled as actual cable elements. The model setup will be discussed in detail in Section 3.5.

3.3 Design approach

Each design solution generated for a unique set of design variables represents the optimum design to a corresponding L/H aspect ratio subjected to specific design constraints defined in Section 2.3 in the infinitely large design space.

The overall framework implemented in optimally sizing individual elements is outlined in Figure 3-10 and is distinguished into two major phases, which will be discussed further in Section 3.3.1 and 3.3.2. Finite element analysis of the parametric models is performed using the structural analysis plug-in Karamba3D in Grasshopper. Based on linear analysis, the final design of the bridge shall have sufficient strength to resist the imposed dead and live (traffic) loads according to the material's allowable strength σ listed in Table 3.1.

The sizing of the individual elements to obtain a fully-stressed state design is achieved by treating the cross-section dimensions as a continuous variable instead of a discrete one. Since the computational time required to perform discrete optimization of the cross-sections using Karamba's 'Optimize Cross Section' algorithm is highly

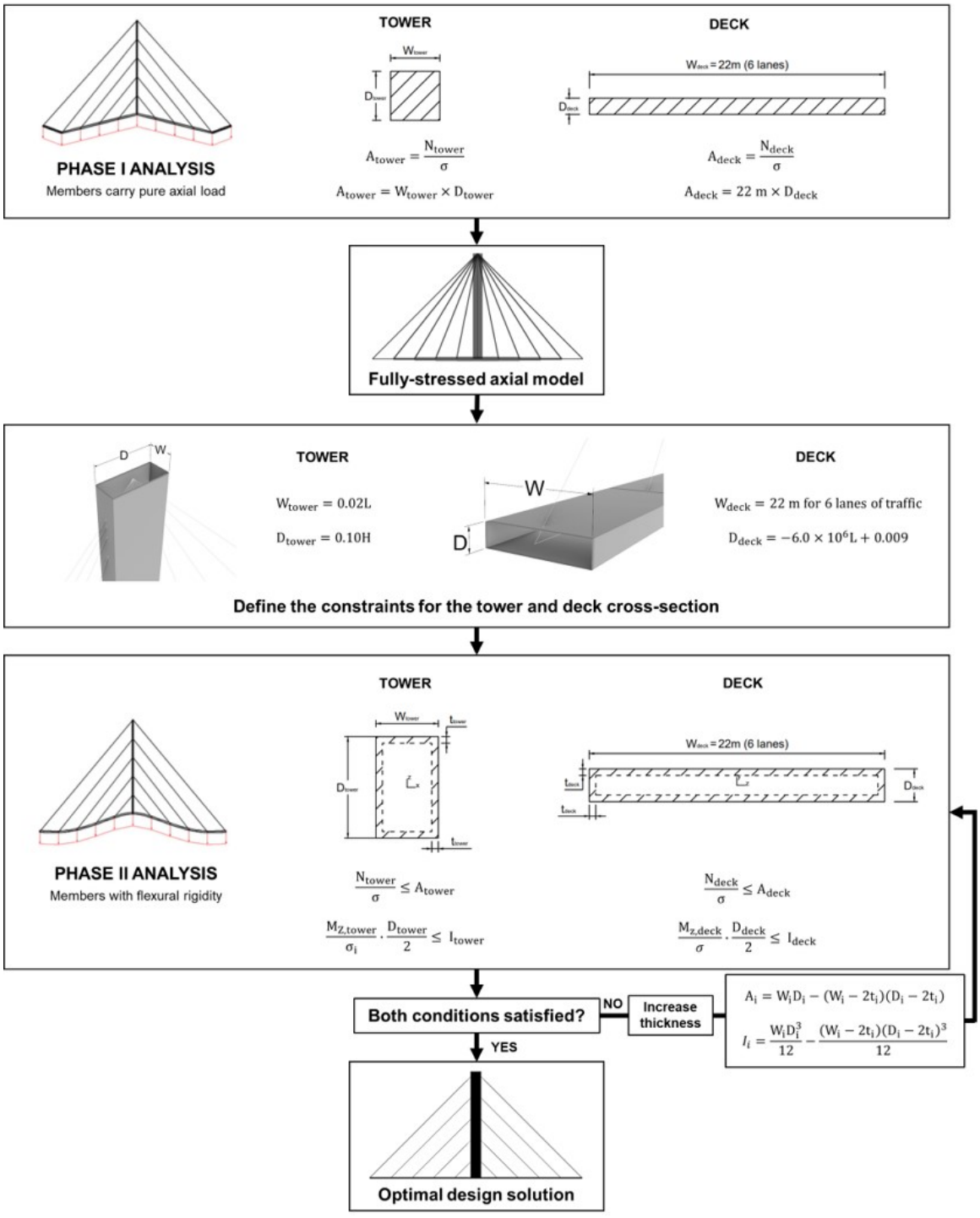

Figure 3-10: Overview of the design framework implemented in analyzing and structurally optimizing the parametric models into a fully-stressed state

inefficient, the cross-section's dimension or more specifically its thickness t is varied incrementally with the help of a GhPython script embedded within the Grasshopper environment.

A sample calculation outlining the design procedure for a medium-span parametric cable-stayed bridge with harp typology is provided in Appendix A.

3.3.1 Phase I: Axial-only analysis

Similar to Samyn's (2004) study, the first phase of the analysis discussed in this section involves analyzing the structure as truss members, where every structural member has zero flexural stiffness. Analyzing the system as a truss implies that all the elements are either in pure compression or tension and hence, are effectively sized as solid sections. The minimum area A_i required for each individual member to resist the applied axial loads is computed as:

$$A_i = \frac{N_i}{\sigma} \tag{3.4}$$

where N_i = axial force, either in tension or compression acting on member i, and σ = allowable stress of the material.

Because this phase of the analysis adopts the same design assumptions as P. Samyn's (2004) work discussed in Section 2.1.1, the total volume of material V and the maximum displacement Δ_{max} of the optimum design solution is corroborated against Samyn's (2004) results. The resulting fully-stressed model is utilized as the input model for the second analysis to be performed on.

Under asymmetric loads, the members no longer qualifies as a two-force member, rendering a truss analysis ineffective in resolving the system to equilibrium. Figure 3-11 shows by method of joints that the resultant force acting at the member ends are no longer collinear along the longitudinal axis of the member, which introduces bending moments in the tower to counteract this couple. Therefore, for both symmetric and asymmetric loads, the input model for beam analysis (Phase II) will use the structurally optimized system under symmetric loads.

3.3.2 Phase II: Axial and bending analysis

Modeling flexural rigidity EI into the tower and deck elements in the second phase of the analysis increases the complexity of the optimization problem. Since the parametric model is now a statically indeterminate structure, the imposed bending moments, axial and shear forces vary with cross-section and moment of inertia. This implies that the sizing of the members to provide minimum resistance against the imposed

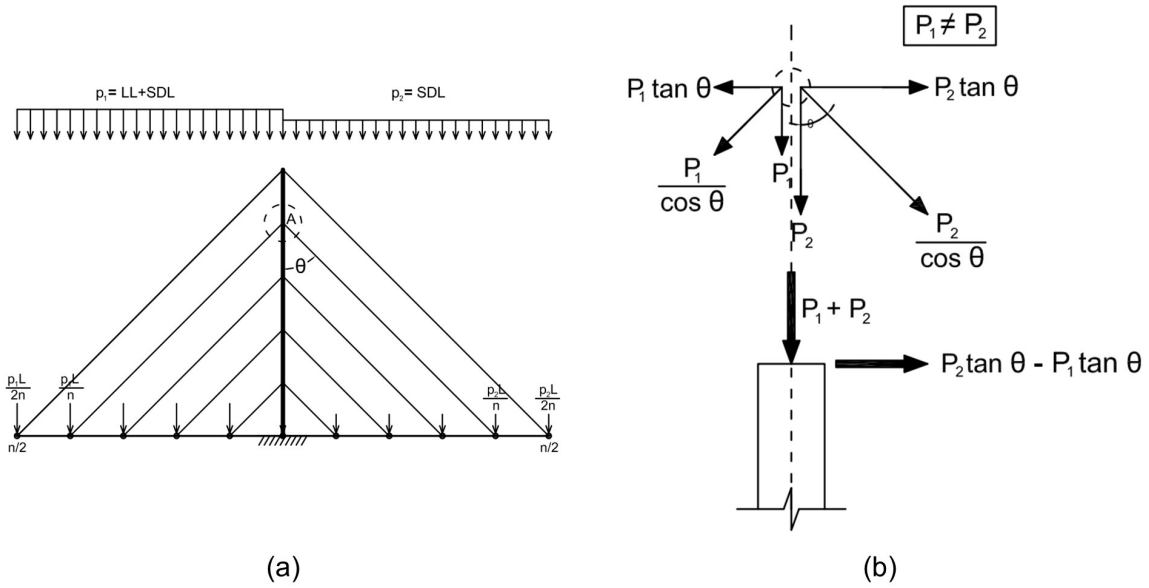

Figure 3-11: (a) Cable-stayed systen under asymmetric load condition (b) Resolving forces at node A by method of joints

bending and axial stresses depends on the initial model on which the analysis is performed. The problem of structural indeterminancy is resolved by utilizing the parametric model that has been optimally sized based on pure axial compression/tensile loads in Section 3.3.1 as the input model for which the second analysis is performed on. In this stage, the fully-stressed solid structural elements obtained from Phase I are analyzed as beam elements with bending rigidities.

To ensure that the structural elements have adequate bending stiffness to resist the applied bending stresses, a hollow cross-sectional shape is adopted for the tower and deck elements. Using the empirical relationships developed earlier in Section 3.2.1, the sizing process for any given member is simplified by constraining the bounds for which the material can be distributed across its cross-section. Therefore, the only design variable determining the final size of the elements is the thickness t_i of the hollow sections.

A hollow cross-section is selected due to its improved bending resistance relative to a solid section of a similar gross area. The considerable bending stiffness of hollow sections can be attributed to the fact that most of the area is concentrated away from the neutral axis. In this study, by increasing the thickness of the profile and concentrating material closer to the perimeter of the cross-section, sufficient moment of inertia would be developed by the cross-section to resist the applied bending moments. The minimum moment of inertia for a member to resist bending moment M_i can therefore, be computed as:

$$I_{i,min} = \frac{M_i}{\sigma} \cdot \frac{D_i}{2} \tag{3.5}$$

where M_i = bending moment acting on member i, σ = allowable stress of the material, $\frac{D_i}{2}$ = perpendicular distance from the neutral axis to the extreme fiber of the section.

In sizing the tower and deck elements, two critical requisites have to be satisfied. Equation 3.6 describes the axial capacity of the section, which determines the minimum area required for the element to effectively resist axial compression/tension. On the other hand, Equation 3.7 describes the bending capacity of the section, representing the distribution of the area within the specified cross-sectional domain.

$$\sigma \cdot A_i \geq N_i \tag{3.6}$$

$$\frac{\sigma I_i}{D_i/2} \geq M_i \tag{3.7}$$

The thickness of the profile t_i is incremented until the strength conditions in Equations 3.6 and 3.7 are satisfied using a GhPython script that is fed as an input to the Karamba's 'Cross-section' Tool. The sizing procedure is depicted more clearly in Figure 3-12.

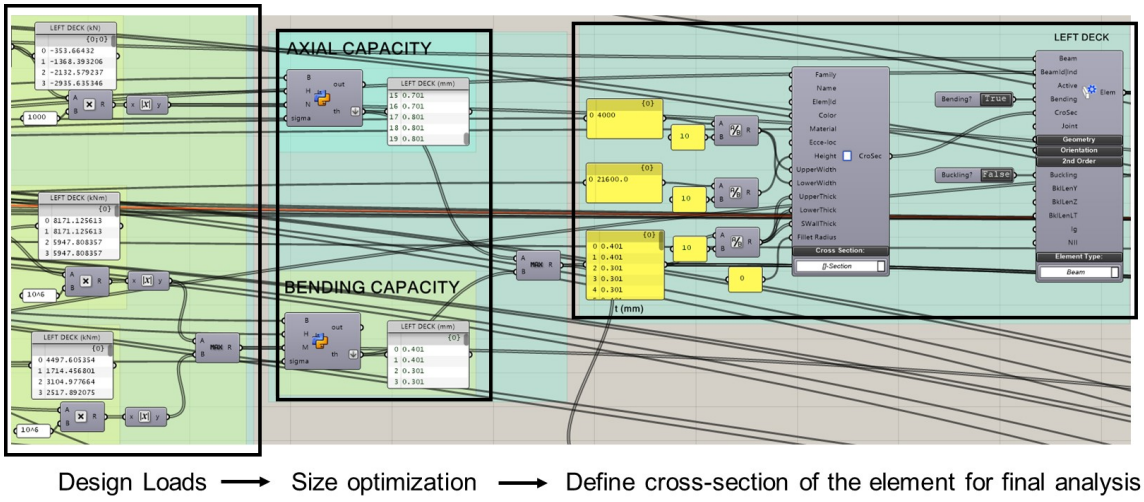

Figure 3-12: Sizing optimization using GhPython and Karamba3D

3.4 Data Generation

The diverse range of the design variables suggests that a large number of data set of varying tower heights H corresponding to a L/H range between 1 to 10 has to be

generated for the three span length (L = 200 m, 500 m, 800 m) categories, typologies, and materials. Using the Design Space Exploration (DSE) plug-in tool developed by Digital Structures at MIT (Brown, 2017), design solutions calculated from the design and analysis phase are able to be captured and processed efficiently in Grasshopper.

3.4.1 Sampling and capturing the data

The Sampler and Capture Tool from the DSE Toolbox shown in Figure 3-13 are utilized to sample through the design space and record the necessary objectives of the optimal design solution. For a unique set of design variables, a total of 25 data points are sampled over the design space using the uniform grid sampling method. The objectives that are captured include the volume of individual elements (tower, deck, and cables), maximum displacements of the deck and tower, and the structure's self-weight.

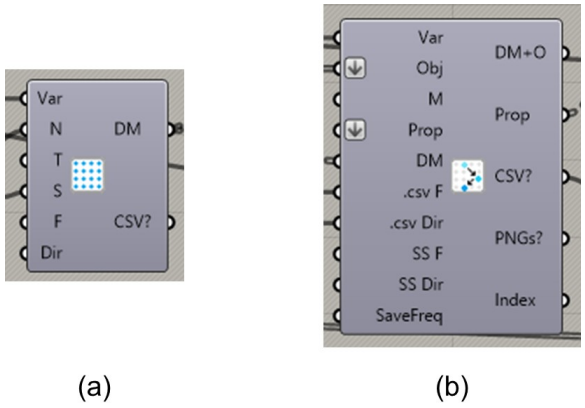

Figure 3-13: (a) Sampler Tool and (b) Capture Tool

3.4.2 Post-processing

In addition to the volumetric performance curves (V vs. L/H), the data collected using the Capture Tool can provide better insight into the behavior of cable-stayed bridges, which include:

1. Determining the effect of bending in the total volume of material, and further assess whether preliminary design of cable-stayed structures based solely on axial forces is acceptable.
2. Identifying a balance between increasing the number of cable supports and its consequent reduction in the volume of material for the deck and tower elements.
3. Defining a range of optimum L/H ratios for different cable-stayed typologies corresponding to a 10% variation of the optimum solution.

4. Understanding the effect of materiality in the overall structural performance of the optimum design solution.
5. Providing a deeper look into the distribution of volume of materials between the tower, deck and cable elements.

3.5 Finite Element Analysis

The analyses performed using Karamba3D in Grasshopper are corroborated by building a finite element (FE) model in a traditional FE software Strand7 (2010). Two FE models: a fan and web typology with symmetric load pattern, are constructed using similar elements, material properties, loads and support conditions. The geometry of the two bridge models are summarized in Table 3.3.

Table 3.3: Geometry of the bridge models simulated in Strand7

	Model 1	Model 2
Type	Fan	Web
Support conditions	Self-anchored	Self-anchored
Load Pattern	Symmetric	Symmetric
Material	Steel	Steel
L (m)	500	500
H (m)	250	50
n (m)	20	20

The purpose of this particular analysis is to confirm the validity of the previously stated design assumptions in Section 3.2.5, where the stay cables in the parametric model are modeled as truss elements, instead of actual cable elements. The two configurations are selected to demonstrate the influence of cable weight on catenary sag and the overall performance of the system, given that the web configuration has a higher quantity of cable based on Phase I or truss analysis.

3.5.1 Finite Element Model

Using a traditional FE software, the elements comprising the cable-stayed system can be defined to match its behaviour accordingly. Using Strand7, the deck and tower elements are modeled as beam elements, while the stays are modeled as cable elements. Their respective cross-sectional shape and dimensions are individually specified. Similar to the parametric model in Karamba3D, the FE model in Strand7 is restricted to

a two-dimensional plane by restraining DZ translation, RX, and RY rotations. For both models, all six degrees of freedom are restrained at the tower-deck connection.

The resulting two FE models developed in Strand7 are depicted in Figure 3-14.

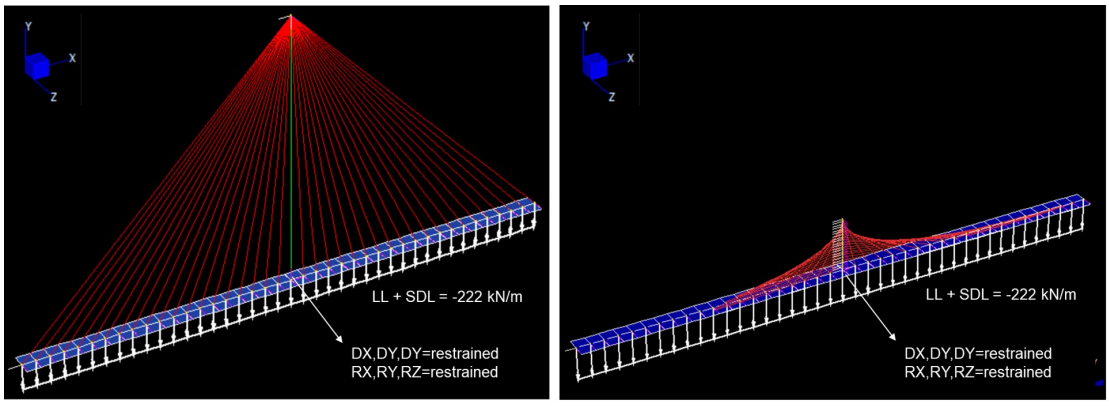

(a) (b)

Figure 3-14: Finite Element Model (FEM) developed in Strand7 for (a) Model 1 and (b) Model 2

It is well understood that the design assumptions imposed on the stay cables play a significant role in governing the final design of the cable-stayed structure. Thus, the aim of this validation study is to clearly establish the design assumptions adopted in the parametric model in Grasshopper and identify the implications of modeling the stay cables as truss elements.

3.5.2 FE Validation

In order to rationalize the design assumption adopted in the parametric model, two FE models with distinct assumptions for the cable elements are generated:

1. Catenary action of the stay cables is entirely taken into account. This would be considered as the lower bound of the design.
2. Sagging of the stay cables is eliminated by defining the cable's free length (FL) as the distance between the two nodes connecting them. The free length should be lesser than the distance between the two connecting nodes to ensure that the cables are always taut and do not sag under gravity. This is considered as the upper bound of the design.

Table 3.4 compares the total volume calculated in Karamba3D and Strand7 for the different assumptions used in modeling the cable elements. The resulting axial force and bending moment diagram for the web configuration (Model 2) with different cable behaviours are provided in Appendix B.

Table 3.4: Final volume of material obtained from Karamba3D and Strand7

		Karamba3D	Strand7	
		Truss element	Accounts for cable sag (1) LB	No cable sag by predefining FL (2) UB
Model 1	Total volume (m^3)	215.55	171.10	208.80
	Variance (%)	-	-21%	-3%
Model 2	Total volume (m^3)	4024.10	1921.11	3869.21
	Variance (%)	-	-52%	-4%

It is clearly evident that the inclusion of cable sag in the cable elements results in a less conservative volume of material. This can be attributed to the cable sag being counteracted by the tensile forces acting on the cable as soon as the deck is loaded. Another critical observation includes the importance of the cable's linear density, as a shorter free length is required to keep a heavier cable in taut. This effect of cable sag in counteracting the tensile forces in the cables is hence, more pronounced in the web typology where the weight of cables per unit length is more considerable.

In reality however, the stay cables in cable-stayed bridges are often pretensioned to prevent the cables from going into slack, which is simulated by defining the free length of the cable in the FE model. Furthermore, the disregard for catenary action of the stay cables in the parametric model provides a more conservative result, which is of particular importance in the early stages of design. This justifies the assumption of modeling the cables as equivalent truss elements in Karamba3D and prestraining it once it undergoes into compression.

Chapter 4

Results

This chapter discusses exhaustively the procedures and justifications adopted in deriving the volume and displacement efficiency curves for different cable-stayed typologies.

The first step involves identifying and examining any observable trends brought about by the design variables investigated in this study. It starts off with a close review on the performance of self-anchored cable-stayed bridges and later extending it to assess the performance of partially-anchored cable-stayed bridges. In addition to this, a comparative study between the optimum design solution produced by an axial-only (Phase I) analysis and an axial and bending (Phase II) analysis is also performed. The main purpose of this is to provide a better idea of representing the efficiency curves that will concisely and clearly capture the effects of various design variables without losing much information on the optimum design solution.

Lastly, the optimization results generated in this study are corroborated against real-world design projects to demonstrate the validity of this simplified parametric approach used in developing the proposed design efficiency curves, thus verifying its applicability in solving conceptual design problems of real-life cable-stayed bridges.

4.1 Morphological indicator validation

Since the parametric model generated by truss analysis of Phase I described in Section 3.3.1 is developed under the same design assumptions as Samyn's (2004) work, volume W and displacement Δ indicators are calculated using Equation 2.4 and 2.5, and then plotted against L/H ratio to obtain the curves shown in Figure 4-1. The curves appear to be agree with the MI curves derived by Samyn (2004) in Figure 2-3.

The minimum point in the efficiency curves represents the optimum design solution of a cable-stayed bridge with a specific typology and boundary condition. The

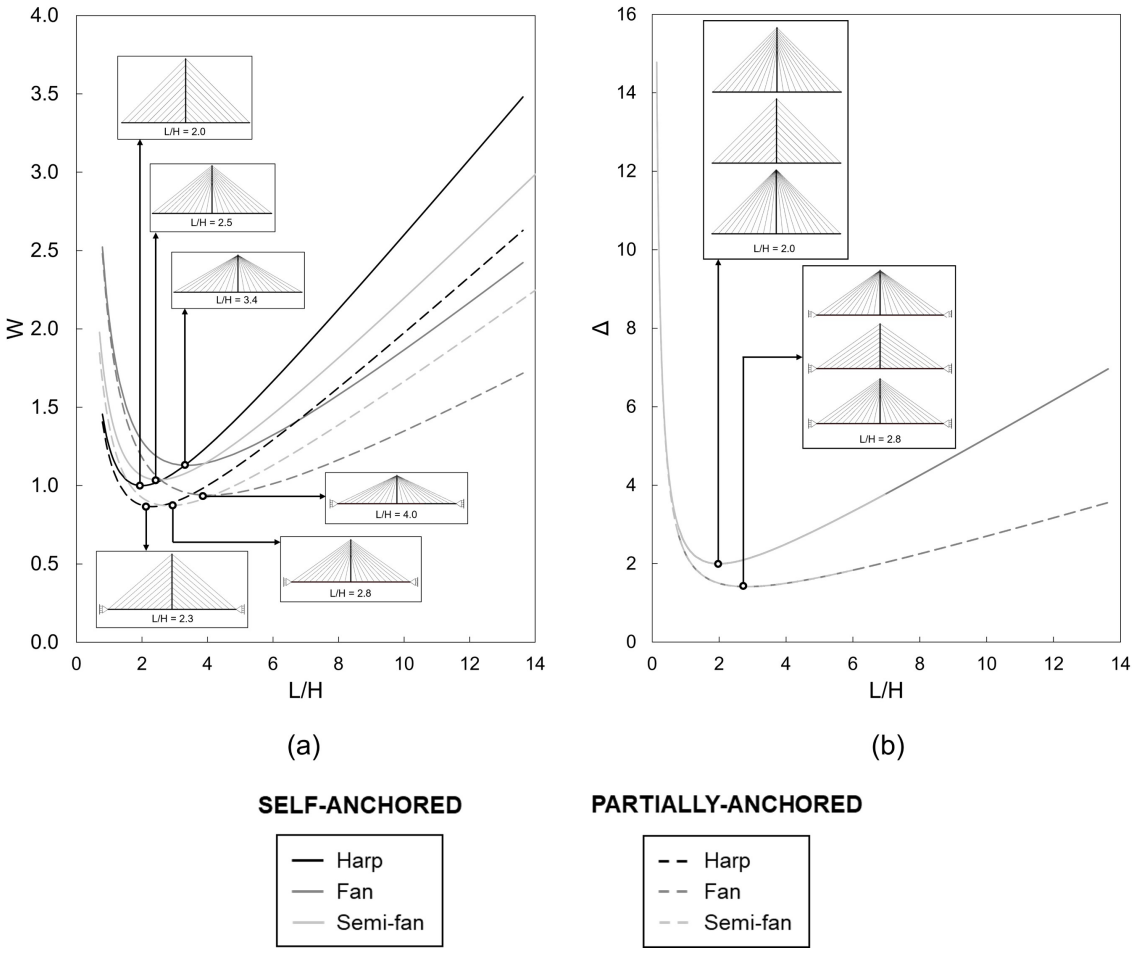

Figure 4-1: (a) Volume indicator W and (b) Displacement indicator Δ plotted against L/H ratio using the results obtained from Phase I: Axial-only model

minimum non-dimensional volume W and displacement Δ for each typology are extracted and compared against Samyn's (2004) results in Table 4.1.

Table 4.1: Volume W and displacement W indicator results against Samyn's (2004) results

	Compression Deck						Compression & Tension Deck					
	Samyn		Par. Model		% Diff.		Samyn		Par. Model		% Diff.	
	W	Δ	W	Δ	W	Δ	W	Δ	W	Δ	W	Δ
Harp	1.00	2.00	1.00	2.00	0%	0%	0.94	1.41	0.87	1.41	8%	0
Fan	1.15	2.00	1.13	2.00	2%	0%	0.96	1.41	0.94	1.41	2%	0%
Semi-fan	-	-	1.04	2.00	-	0%	0.87	1.41	0.87	1.41	1%	0%

Based on the results in Table 4.1, the sampled data from the parametric study are in good agreement with the existing study (Samyn, 2004). For all three typologies, the discrepancy between the two studies are well below 10%, validating the reliability of the axial-only parametric model.

4.2 Influence of bending stiffness

The effect of modeling flexural rigidity EI in the tower and deck elements on the optimum design solution is studied by comparing the results obtained from a truss analysis (Phase I) and beam analysis (Phase II). Members that carry bending moments are generally less efficient compared to those that are axially-loaded, mainly because bending stresses develop non-uniformly over the cross-section. As the stresses are mostly concentrated at the extreme fibers of the cross-section, a large proportion of material is left unutilized, resulting in an inefficient and heavy structure. This is clearly evident for the case when flexural rigidity is introduced into the structural elements of the parametric model.

4.2.1 Symmetric loading condition

Figure 4-2 illustrates the total volume V of the optimum design solutions obtained for a self-anchored, 500 m span cable-stayed bridge with a harp, fan, web, and semi-fan typology under uniform loads over a L/H ratio between 1 to 10. A similar pattern is observed for the short (200 m) and long span (800 m) cable-stayed parametric models.

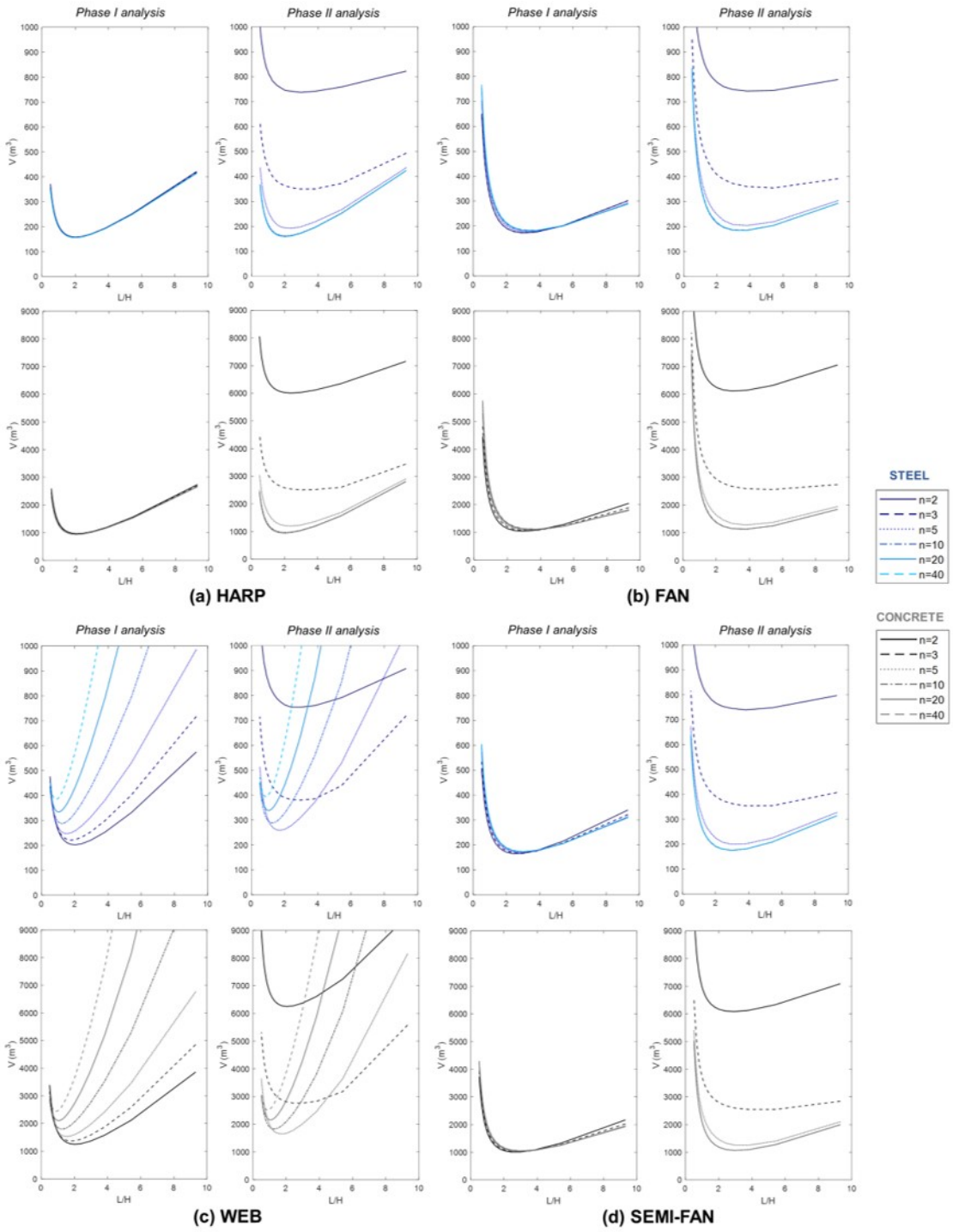

Figure 4-2: Optimal volume of material V determined for a 500 m span self-anchored, cable-stayed bridge with varying number of cable supports n for (a) harp, (b) fan (c) web, and (d) semi-fan typology analyzed as truss members (left) and members with flexural rigidity (right) under uniform load conditions

Relating Maxwell's 'load path' theorem and axial-only analysis

Where the structural elements are modeled without bending rigidities, $EI = 0$ (Phase I analysis), the optimal solution obtained is essentially equivalent to the system's total 'load path.' i.e., $\Sigma|F_i|L_i$ or commonly termed as Maxwell's theorem. This means that the volume V computed using truss analysis in Figure 4-2 can easily be resolved using Equation 3.1 by treating the system as a determinate structure made of truss elements with pinned-connected joints.

Since the overall forces transferred to the deck and tower are equivalent to the resultant of the externally applied loads on the deck, variations in the design curves mainly reflect variations in the axial forces of the cables. Therefore, in cases where a truss analysis is assumed, the difference in efficiency is primarily a result of cable orientation. Figure 4-3 plots the development of the axial forces of the cables at the anchorage points for $n = 10$ and 20 for a harp, fan, web, and semi-fan typology under uniform loads.

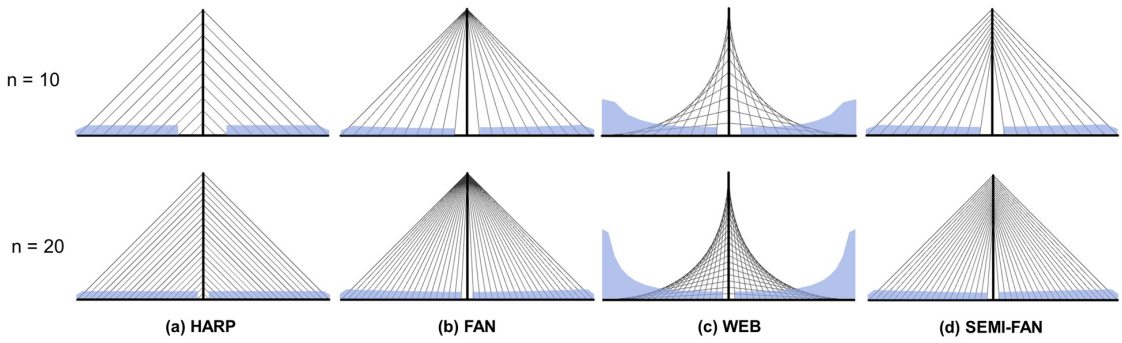

Figure 4-3: Development of axial forces in the cables for a harp, fan, web and semi-fan typology with $n = 10$ and 20 (Note: The axial forces of the cables are plotted along the deck.)

The slight variations in the design curves with changes in the number of stay cables n for a fan and semi-fan typology in Figure 4-2 are a result of the change in the angle of inclination of the cable supports, subsequently altering the axial forces in the cables. On the contrary, where the cables are inclined at a constant angle like a harp configuration, the same total volume of material will be attained for all values of n. For a harp typology, the volume increase by length as the number of cable elements n increases is compensated by the lowered axial forces in each individual cable element. Thus, the optimum design solution equilibrated itself regardless of the number of cable stays.

Understanding the structural performance demonstrated by the web configuration in relation to the number of stay cable n is critical in rationalizing the reduced effi-

ciency of the web typology with increased number of cables n. As the orientation of the stay cables transitions to a near-horizontal gradient with higher number of cables, there is an exponential growth in the axial forces of the cables anchoring the deck further away from the tower, i.e., midspan of deck).

As the orientation of the stay cables transitions to a near-horizontal gradient with increasing number of stay cables, there is an exponential growth in the axial forces of the cables anchoring the deck further away from the tower as indicated by Figure 4-3. By Maxwell's theorem, the increase in axial forces of the cables coupled with the increased length of the cables renders the structure increasingly inefficient with higher number of cables.

Effect of stay cables on flexural rigidity

Two distinct design curves are obtained when the system is analyzed as truss and beam elements. The most evident observation distinguishing the two approaches is the influence the number of cable support n has on the final optimum design. The stay cables anchoring the girders and towers act as intermediate supports, restraining deflections, similar to that of a continuous beam. The development of hogging moments as a result of the cable supports reduces the transfer of bending moments along the longitudinal length of the girder.

The effectiveness of the stay cables in providing vertical restraint to the deck is evident in the case of the harp, fan, and semi-fan configuration, which is demonstrated by the lowering of the efficiency curves with more cables supports. In contrast to the behavior of these conventional configurations is the web typology which becomes heavier and more inefficient with the increase in the number of stay cables.

A closer look at the bending moment diagrams of the decks of the parametric bridge models with $n = 10$ and 20 in Figure 4-4 provides an explanation for the stated observations.

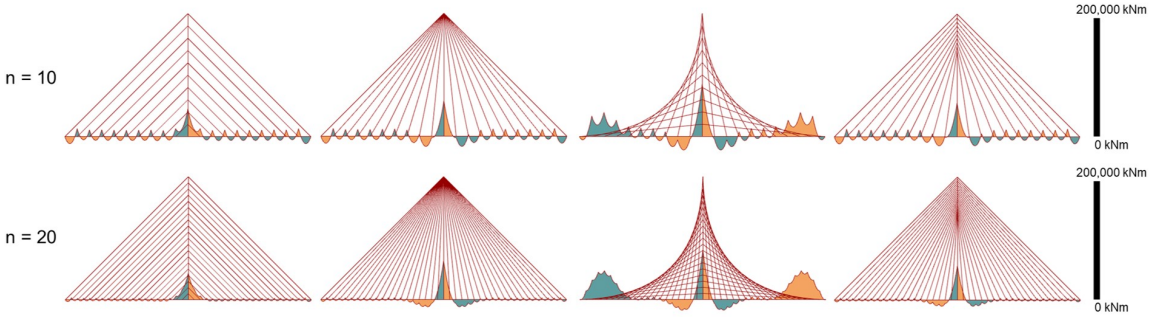

Figure 4-4: Bending moment diagrams of the parametric models of different typologies with $n = 10$ and n = 20

Firstly, the bending moment diagrams for the harp, fan, and semi-fan configurations appear to be analogous to that of a continuous beam, indicating that the vertical restraint provided by the stay cables arranged in this configuration is effective in preventing excessive deflections of the girder. It introduces negative bending moments in the deck and reduces the development of positive sagging moments along the deck.

There appears to be a correlation that exists between the tensile forces in the stay cables displayed in Figure 4-3 with the bending moments in the deck. The tensile forces in the stay cables determine the degree of vertical stiffness it provides to the girder, which leads to the assumption that cables with higher tensile forces provide less vertical restraint to the deck.

When the cables are arranged at a constant angle similar to a harp configuration, the tensile stresses in all the cables remain the same, indicating the same level of vertical stiffness provided to the deck at the cable anchors. With more cable supports, more vertical restraints are located at the deck to prevent bending moments in the deck from escalating significantly. This inference is also supported by the fact that a shorter tower (low L/H ratio) with the cables arranged in a near-horizontal orientation generates a higher volume of material as the cables have higher tensile forces and provide reduced vertical restraint to the deck.

Extending this inference to fan and semi-fan configuration, the slight increase in the axial forces of the cables reduces the development of hogging moments in the deck.

On the contrary, the reduced efficiency of a web typology as the number of cables increases is substantiated by the exponential increase in the tensile forces of the cable stays and the massive bending moments in the deck. As the cables anchoring the deck towards the midspan achieve a near-horizontal gradient, the vertical stiffness (or equivalent vertical reaction force) offered by the cables is significantly reduced. With the cable supports becoming considerably ineffective in providing vertical restraint, the deck behaves more like a simply supported beam with no intermediate supports.

Design curve convergence

The convergence of the design curves obtained from a beam analysis in Phase II and truss analysis in Phase I corroborates the importance of stay cables in alleviating bending moments in the deck, as discussed in the previous section. Figure 4-5 compares the normalized minimum volume V_{min}/L^2 from the optimum design solutions computed for different numbers of stay cables n using Phase I and Phase II analysis. The convergence plots consider different cable-stayed typologies and span lengths.

The minimum volume V_{min} is normalized against L^2 to distinguish the influence brought about by span length L on the convergence of the design curves.

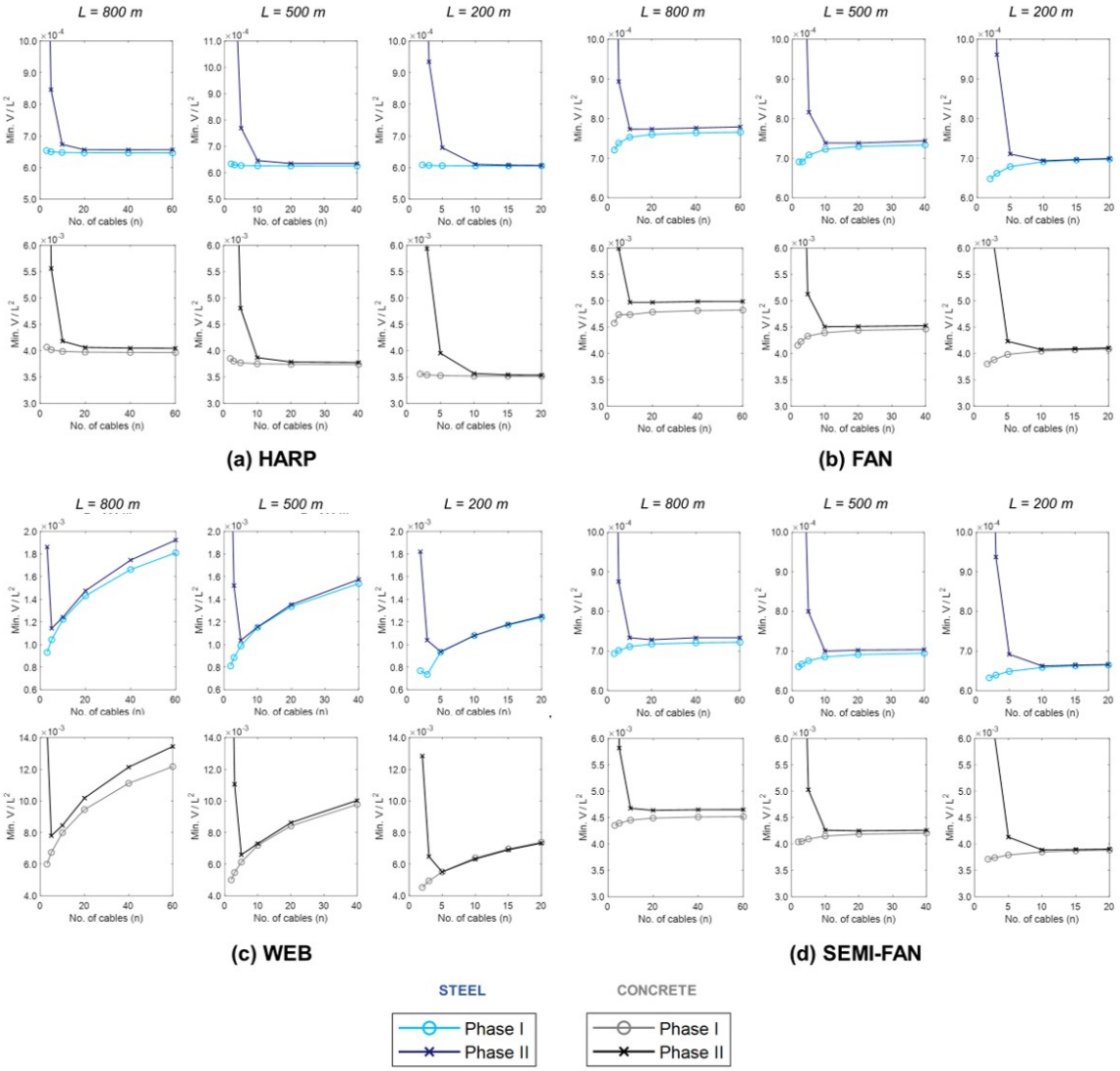

Figure 4-5: Normalized minimum volume V_{min}/L^2 of a self-anchored, cable-stayed bridges with varying number of stay cables n obtained using a truss analysis in Phase I and beam analysis in Phase II (Note: The ordinate axis for the web typology is greater than the other three configurations.)

Based on these graphs, it is quite evident that the effect of bending in the deck becomes negligible as the number of stay cables increases, particularly for the harp, fan, and semi-fan typology. With this particular notion in mind, it would be fair to assume that a simple truss analysis is sufficient in providing a preliminary estimate of the structural efficiency of the system, provided that the number of stay cables is not unreasonably low.

To support the applicability of this simplified design approach, Table 4.2 outlines the variation in the total volume of material of a self-anchored cable-stayed bridge calculated using a truss (Phase I) and beam analysis (Phase II) for different span lengths, materials, and typology, in which the stay cables are spaced at intervals of less than 7 m.

Table 4.2: Percentage variation of the total volume of material predicted using truss (Phase I) and beam analysis (Phase II) with cable spacing of less than 7 m

Typology	Harp			Fan			Web			Semi-fan		
L (m)	800	500	200	800	500	200	800	500	200	800	500	200
Steel (%)	1.5	1.5	0.4	1.7	1.4	0.2	5.9	2.3	0.8	1.6	1.3	0.2
Concrete (%)	2.0	1.0	0.6	3.3	1.4	0.5	9.5	2.5	0.9	2.9	1.3	0.5

The increase in the total volume V predicted with the inclusion of flexural rigidity EI in the analysis are well below 10% for all typologies, reflecting the adequacy of a simple truss analysis as a form of preliminary design check at the early stages of design. However, it is also important to recognize that the web configuration appears to be an anomaly, exhibiting a significantly higher deviation in the total volume than the other conventional typologies. In order to precisely understand how truss and beam analysis varies for a web configuration, Table 4.3 provides a detailed look at the minimum volume V_{min} obtained as a function of the number of stay cables n. Because the general trends between the other three configurations are similar, the table only compares the web typology against a harp typology made of steel.

It is obvious from the beginning, particularly from Figure 4-2 that the web typology is the most inefficient and least adaptable form due to the narrow range of optimum geometric aspect ratio L/H. The table clearly shows that the web typology requires an average of 2.5 times more material relative to the harp typology. While the harp configuration displays convergence of the curves with increasing number of cables, the design curves of a web configuration converge at a specific number of cables, particularly when $n = 15$, 10, and 5 for a long, medium, and short-span cable-stayed bridge. This signifies a point in the design of a web typology where the bending moments in the deck are negligible compared to the axial forces that are governing the design of the system. An increase in the number of cables at this point for a web typology will result in an exponential increase in the tensile forces of the cables (Figure 4-3) as well as higher bending moments in the deck (Figure 4-3).

Therefore, in evaluating the effect of bending rigidities EI in the performance of a cable-stayed structure, there are two critical design scenarios which require flexural rigidity to be included in the conceptual design of cable-stayed bridges, that includes

Table 4.3: Minimum volume V and calculated deviation between a truss analysis and beam analysis for harp and web cable-stayed bridge model made of steel

Typology	Harp						Web					
					$L = 800$ m							
n	3	5	10	20	40	60	3	5	10	20	40	60
Phase I	418	416	414	414	414	414	1192	731	794	944	1118	1231
Phase II	1089	542	431	420	420	420	595	667	782	916	1064	1159
Variance (%)	62	23	4	1	2	2	50	9	2	3	5	6
					$L = 500$ m							
n	2	3	5	10	20	40	2	3	5	10	20	40
Phase I	158	157	157	157	156	119	202	221	247	288	334	385
Phase II	737	350	192	162	159	159	753	380	259	289	338	394
Variance (%)	79	55	18	3	2	2	73	42	5	0	1	2
					$L = 200$ m							
n	2	3	5	10	15	20	2	3	5	10	15	20
Phase I	24	24	24	24	24	24	31	29	37	43	47	50
Phase II	72	37	27	24	24	24	73	41	37	43	47	50
Variance (%)	72	40	11	1	1	1	58	30	0	0	0	1

the design of a conventional harp, fan, and semi fan typology with few numbers of cables and a web configuration with a significant number of cables.

Material distribution

Given the structural indeterminacy of cable-stayed systems, multiple optimum design solutions can be attained by simply proportioning the material differently across the tower, deck, and cables. Consider the two extreme design cases illustrated in Figure 4-6, in which a slender deck is compensated by a stiffer tower and vice versa. Excessive deflections in a slender deck can be prevented by the stiffer tower; similarly, a stiffer deck with improved resistance against deformations would limit axial shortening in the much slender tower, resulting in major savings in the volume of the tower. Both mechanisms satisfy design requirements through different forms of material distribution. Therefore, it is important to be cognizant that the optimum solution provided in this study is just one possible solution to the many optimum design solutions that exist in the design space being explored.

In this study, the stiffnesses of the tower and decks are controlled by the structure's geometrical aspect ratio, since their cross-sectional dimensions are a function of L and H. Figure 4-7 breaks down the the total volume of the structure depicted in Figure 4-2 into their individual components for a medium-span length , self-supported cable-

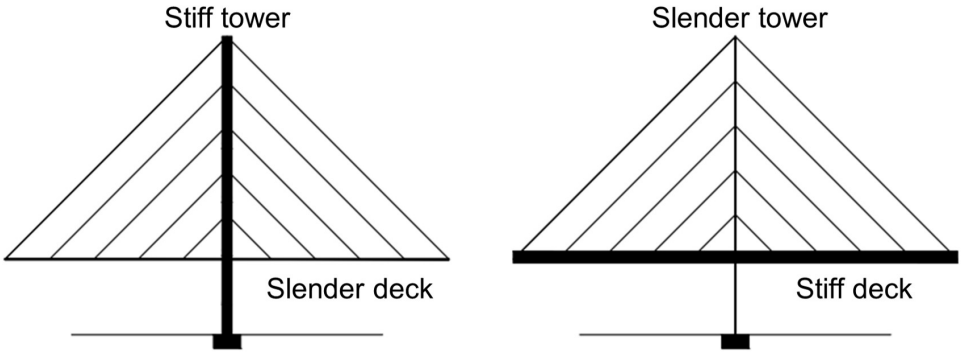

Figure 4-6: Possible optimum design solutions obtained by different material distribution

stayed bridge with $n = 2$, 10, and 40.

The most notable change observed with the additional consideration of bending stiffness EI in the analysis includes the increase in the volume of the deck, which primarily is the case for cable-stayed structures with low number of cables. Where bending is the governing design load instead of the axial loads, the cross-section of the deck would need to have a larger moment of inertia than the minimum cross-sectional area required to resist the axial loads.

The volume of the tower however, remains consistent for both Phase I and Phase II under symmetric loads. Given that the tower does not experience any bending moments due to equal yet opposite forces imposed by the cables anchored to it, the only load that governs its design is the axial compressive force imposed by the dead and live loads acting on the surface of the deck.

As the L/H ratio increases and the tower becomes shorter, a substantial volume of material is allocated to achieve a stiffer deck. Because a shorter tower generally means a near-horizontal orientation of the cables, the lack of vertical stiffness provided by the cables is compensated by increasing the deck's stiffness and allocating more material to it. Hence, a key takeaway obtained from the plots depicted in Figure 4-7 is that the final optimum design solution achieved for a cable-stayed structure with a high L/H ratio is one comprising of a slender tower and stiff deck and vice versa for a low L/H ratio. This trend of increasing deck volume with L/H ratio is exhibited by all typologies, though is most prominent in the web configuration

The volume of stay cables remains relatively consistent for the harp, fan, and semi-fan configurations, despite the change in the number of cables and L/H ratios. The volume of the stays is dependent on two factors: the cable length and the tensile force it has to resist, which is a function of the gradient in which the cables are oriented.

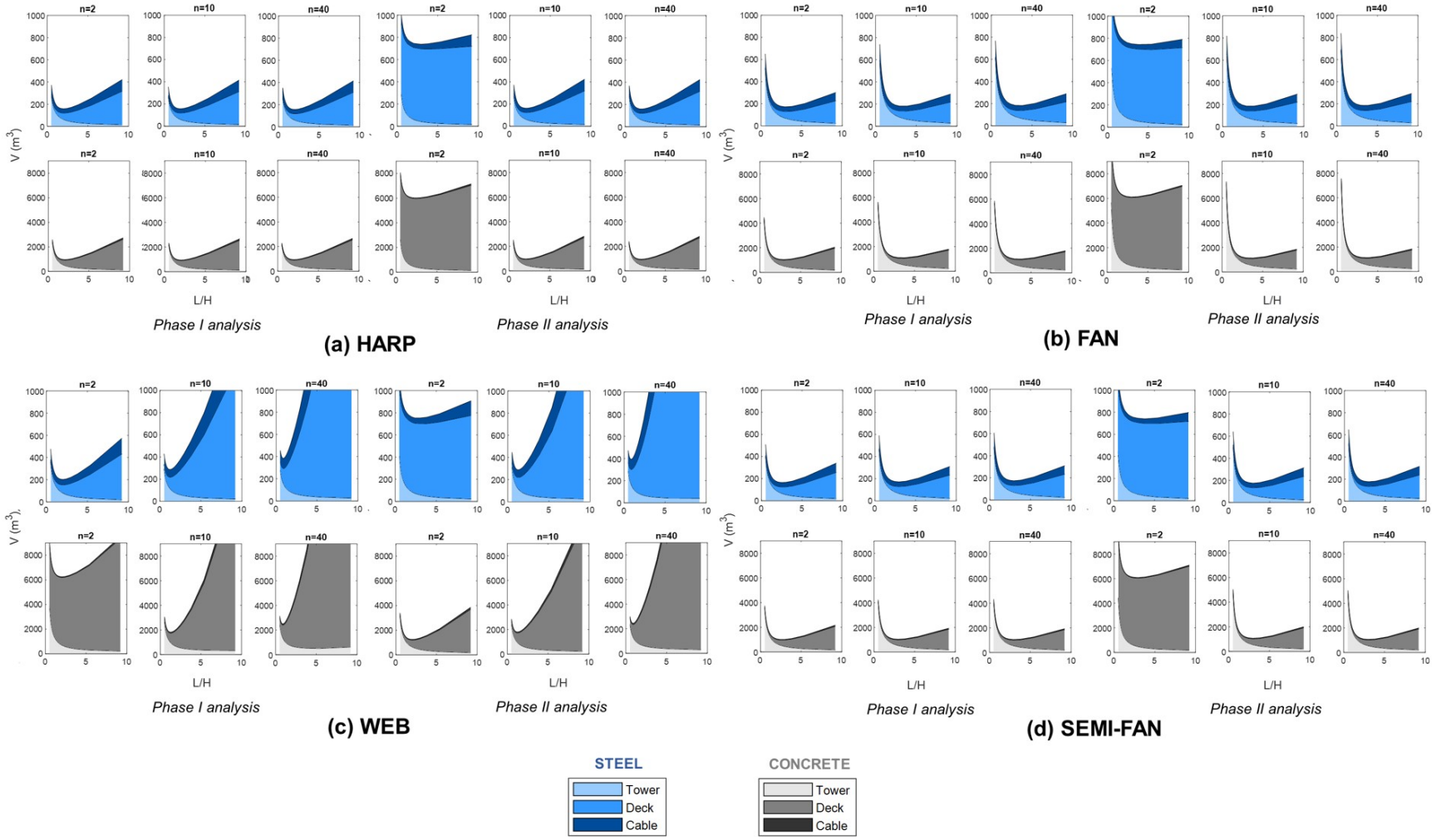

Figure 4-7: Material distribution of the tower, deck and cable elements for a self-anchored, medium-span bridge with $n = 2$, 10, and 40 under uniform loading conditions

As the taller towers (lower L/H) require the cables to span longer distances, the supposedly increase in volume is compensated by the near-vertical orientation of the stay cables, lowering the axial forces in the cables. Likewise, the volume of the stay cables remains the same despite the increase in the number of stay cables, mainly because the tensile forces that the cables have to sustain are reduced.

The conclusions made earlier with regards to the web typology in Section 4.2.1 is corroborated by the plots provided in Figure 4-7. The effectiveness of the cables in providing vertical stiffness to the deck reduces as the number of cables is increased. The volume of the deck and cables increase significantly with higher number of cables as the deck attempts to improve its moment of inertia to resist bending and the cables attempts to improve its cross-sectional area to resist axial loads satisfactorily.

Though the volume of the tower elements appears to vary similarly for all typologies, it is most sensitive to changes in the L/H ratio when the cables are arranged in a fan pattern. At lower L/H ratios where the towers are extremely tall, the loads are concentrated at the cable anchorages located at the top of the tower. Thus, the entire length of the tower is sized to resist the axial compressive force equivalent to the total resultant force of the system. This emphasizes the importance of how load transfer within a system affects the optimal design of the structure.

All in all, the typology of a system plays a crucial role in controlling the distribution of material across the tower, deck, and cable elements. As the flow of forces through the system changes with form, material distribution and the optimum design solution can vary significantly.

3D visualization of the design space

To better understand the scope of the design space with variations in the structure's geometrical aspect ratio L/H and the number of stay cables n, a three-dimensional representation of the overall design space for the four different typologies studied are produced. Given that the shape of the efficiency curves does not change with span length and material type, the normalized volume V/L^2 of a 500 m self-anchored, steel cable-stayed bridge in Figure 4-8 would provide a general overview of the design space for the harp, fan, web and semi-fan typology.

A major distinction that exists between the harp and fan typology is the wide region of flatness demonstrated by the fan typology at higher L/H ratios. This region of flatness however, ends abruptly at a L/H ratio of approximately 1.0 as the gradient of the volume performance becomes considerably steeper. The performance curve for a semi-fan configuration can be generalized to have characteristics that lie in between the harp and fan typology.

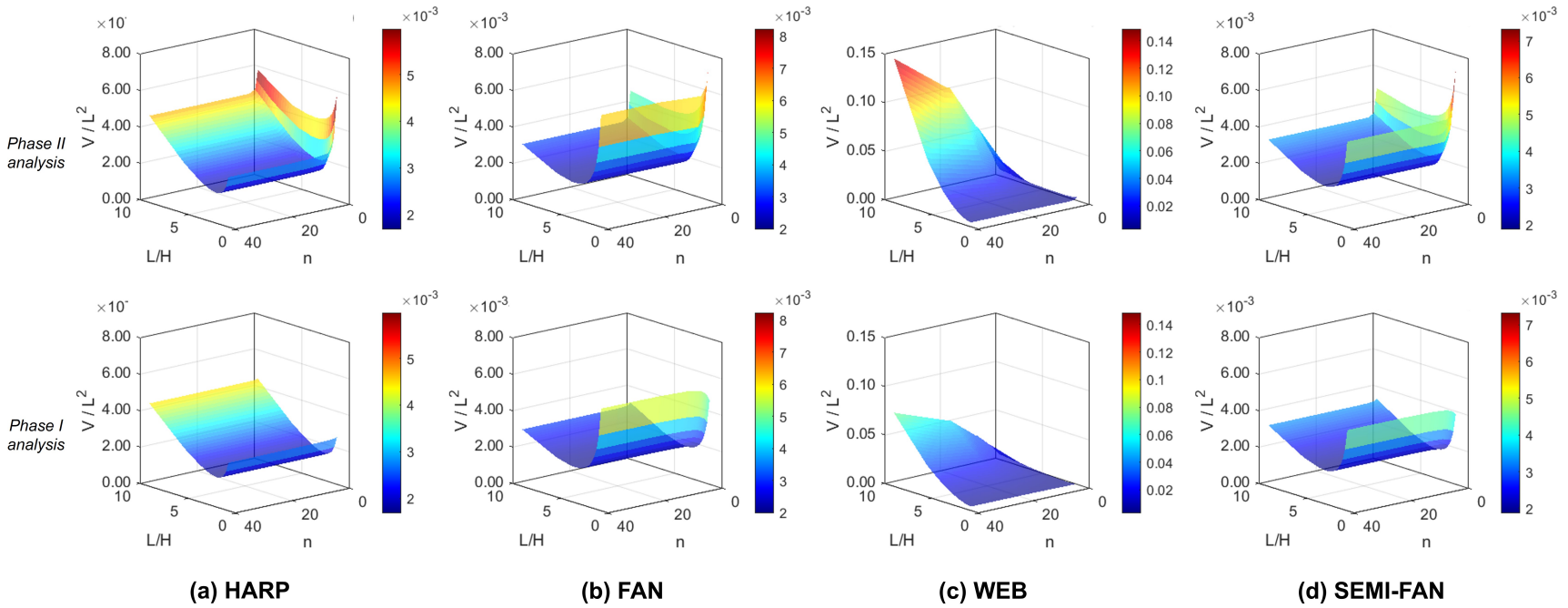

Figure 4-8: 3D design space of the normalized volume V/L^2 performance with respect to L/H ratio and number of stay cables n for a 500 m, self-supported, steel cable-stayed bridge (Note: The ordinate axis for the web typology is greater than the other three configurations.)

The design space presented by the web configuration is highly restrictive, depicted by the small region in the design space in which the optimum design solution yields a reasonably low volume of material. This suggests that the conceptual design of cable-stayed bridges with web configuration must be performed with great attention to its geometric aspect ratio L/H and the number of stay cables n, such that the design procedure does not start with an extremely inefficient system that would be difficult to optimize in the detailed analysis phase.

4.2.2 Asymmetrical loading condition

The results obtained from a similar analysis with asymmetrical loads will be discussed in this section. Since the efficiency curves changes with span length, typology, and material, Figure 4-9 plots the volume performance of the self-anchored cable-stayed parametric models against its geometric aspect ratio L/H.

When compared against the same structural system subjected to symmetric load patterns, there is a significant rise in the total volume of material for all four typologies, mainly brought about by the bending of the towers towards the loaded span. Besides the increase in the material quantity, the efficiency curves appear to be flattened out for all four configurations. The reduction in the gradient of the curves relative to L/H is most notable for the harp, fan, and semi-fan configurations. One benefit of having a system that is governed by asymmetric load conditions would be the larger freedom in manipulating the structure's aspect ratio with minimal consequence to the efficiency of the system.

Given these two major differences between the optimum design solutions obtained for the case of symmetric and asymmetric loads, a simple truss analysis is not recommended as an early-stage design approach for bridges with asymmetric loads governing their design. A simple truss analysis yields a highly unconservative result and an inaccurate optimum geometry L/H of the structure.

Effect of stay cables on design curve convergence

When the effect of stay cables on the convergence of the design curves is analyzed between systems subjected to symmetric and symmetric loads, the design curve for asymmetric loads converges more rapidly with fewer cables. This means that the variation in the converged volume and the volume with minimal stay cables is more prominent in the case of symmetric loads. As an effort to support this hypothesis, Table 4.4 expresses the difference in the total volume for a self-supported, steel cable-stayed bridge with minimal number of cables and the converged volume as a ratio of

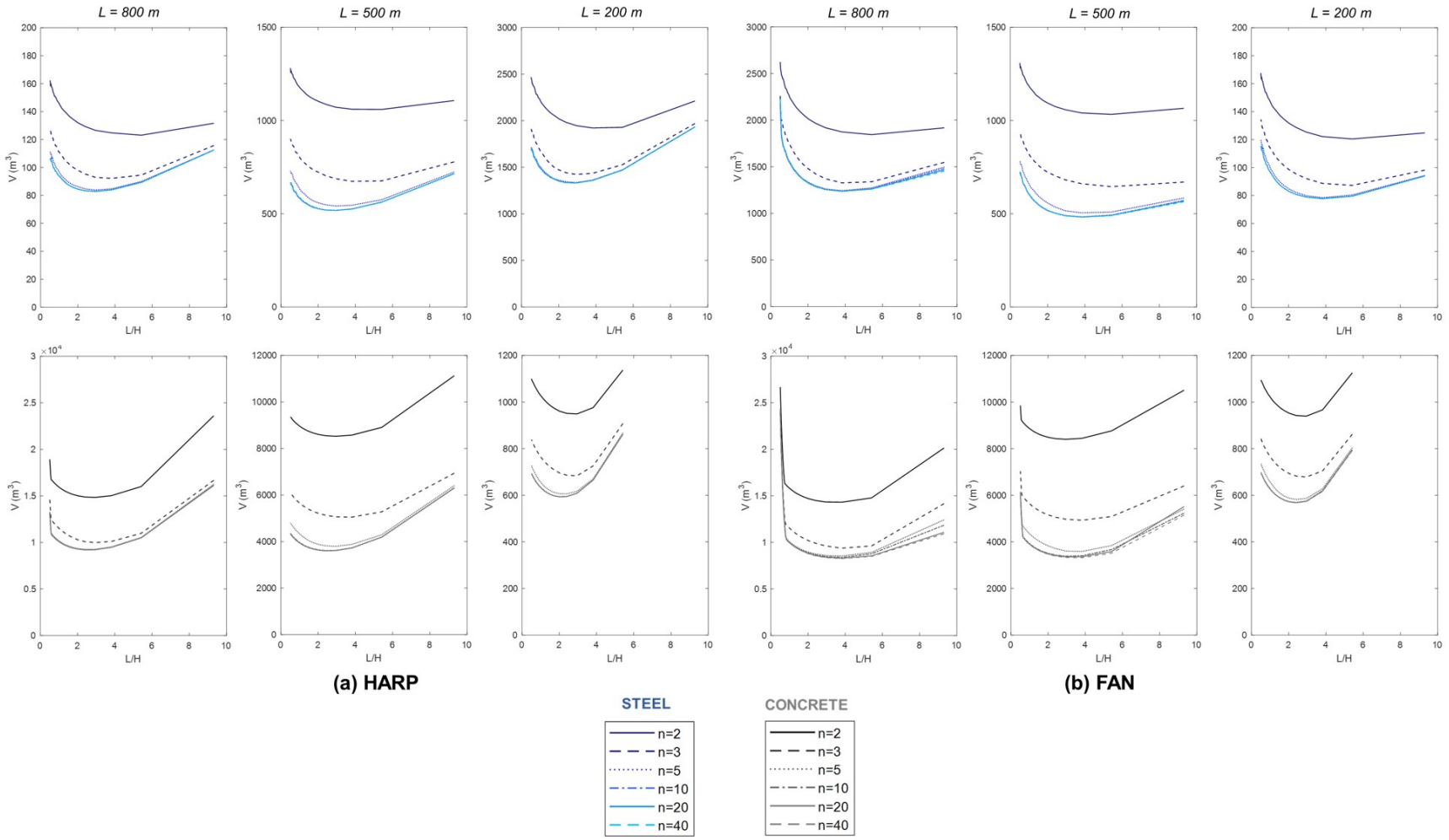

Figure 4-9: Optimal volume V of material determined for self-anchored cable-stayed bridges with varying number of cable supports n for (a) harp, (b) fan (c) web, and (d) semi-fan typology of different span lengths under asymmetric loads

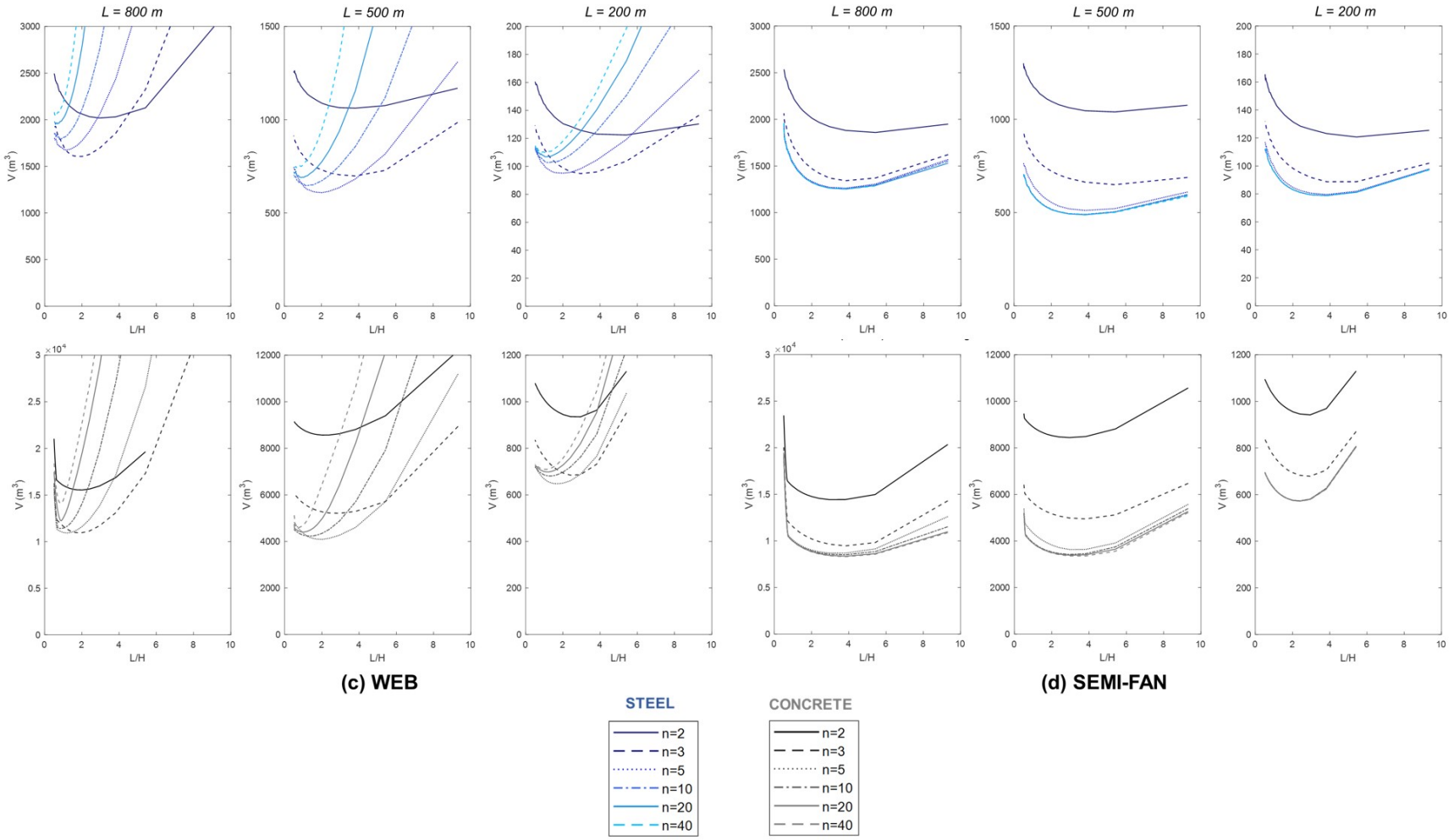

Figure 4-9: Optimal volume V of material determined for self-anchored cable-stayed bridges with varying number of cable supports n for (a) harp, (b) fan (c) web, and (d) semi-fan typology of different span lengths under asymmetric loads

the two. In the table, the total volume of material of a cable-stayed system with n number of cables is denoted as V_n.

Table 4.4: Difference in the total volume of the model with minimal stay cables and the converged volume expressed as a ratio

L (m)	800 m ($\frac{V_2}{V_{60}}$)		500 m ($\frac{V_2}{V_{40}}$)		200 m ($\frac{V_2}{V_{20}}$)	
Typology	Sym.	Asym.	Sym.	Asym.	Sym.	Asym.
Harp	2.59	1.44	4.64	2.05	2.95	1.48
Fan	2.24	1.49	4.00	2.14	2.56	1.55
Web	0.97	0.99	1.91	1.43	1.46	1.12
Semi-fan	2.34	1.48	4.21	2.13	2.69	1.53

The table above supports the notion that the number of cables has greater weight in modifying the volumetric performance of a cable-stayed system under symmetric loading conditions. The ratio of the volume convergence almost doubles by simply analyzing the system under symmetric loads instead of asymmetric loads. Hence, greater consideration needs to be allocated to the number of stay cables n when the system is analyzed under symmetric loading conditions.

Furthermore, the harp, fan and semi-fan configurations are determined to be the most sensitive to the number of stay cables compared to the web configuration under both asymmetric and symmetric loads.

Importance of materiality

Upon investigating the system's performance under asymmetric load patterns, materiality becomes a dominant factor in deriving an optimal design solution. As the allowable stress σ of steel is high, an optimum design solution can be determined satisfactorily for the various design variables being investigated, which explains the smooth and continuous curves obtained in the figure above.

Considering the low allowable stress σ of concrete, there are two instances when a design solution cannot be obtained satisfactorily under the predefined constraints implemented on the deck and tower cross-sections. These include:

- At the most critical design criteria involving a cable-stayed bridge with the least number of stay cables, $n = 3$, and the longest span length $L = 800$ m, the deck depth D_{deck} of 4 m is insufficient in providing stiffness to resist the considerably high bending stresses in the deck.
- Because the cross-sectional dimensions of the towers ($D_{tower} = 0.10H$ and $W_{tower} = 0.02L$ in Section 3.2.1) are described as a function of the bridge's span length

L and height H, in the case of a minimum tower height ($L/H = 10$), the towers of a 200 m bridge cannot resist the applied bending moments under the given cross-sectional area constraint.

The consideration of asymmetrical load pattern emphasizes the importance of materiality in the preliminary design of cable-stayed bridges. Hence, defining an appropriate material that would satisfy the design requirements and specifications early in the design stage would benefit the design process quite significantly.

Material distribution

The volume of the individual elements of the optimum design solutions determined for cable-stayed bridges subjected to asymmetric loads is examined more closely in this section. Because a general trend is observed for the conventional harp, fan, and semi-fan configurations, Figure 4-10 and 4-11 depicts the complete breakdown of the volume of tower, deck and cable elements for a harp, fan, and semi-fan cable-stayed bridges made up of steel and concrete, respectively. Given its unique configuration and atypical behaviour with different number of stay cables and L/H ratios, the volume of the individual elements for the web configuration is broken down separately in Figure 4-12.

The most significant shift in the optimum design solutions obtained for a cable-stayed bridge subjected to symmetric and asymmetric load patterns is the volume increase of the tower elements. The volume of the tower is inversely related to the L/H ratio, which makes sense given that bending moments are a function of span length or in this case, the tower's length between cable supports. Therefore, it becomes intuitive that when asymmetric loads govern the design of the cable-stayed bridge, a shorter tower or a higher L/H ratio would be more favorable.

With the individual volumes disintegrated, it becomes apparent that the number of stay cables n primarily alters the volume of the deck more so than the towers. In order to rationalize this variation in the volume of material across different structural elements better, the bending moment diagram of the cable-stayed bridges under asymmetric load conditions are visualized in Figure 4-13.

The bending moment diagrams supports the findings described earlier from Table 4.4, in which the stay cables are mainly utilized to control the bending moments induced in the deck. The bending moments in the tower remain the same regardless of the increase in the cable supports.

Typology does affect the range of geometric aspect ratio L/H that would provide the most efficient design, though not as significantly as the same system under symmetric loading conditions. For all conventional typologies, there is a substantial

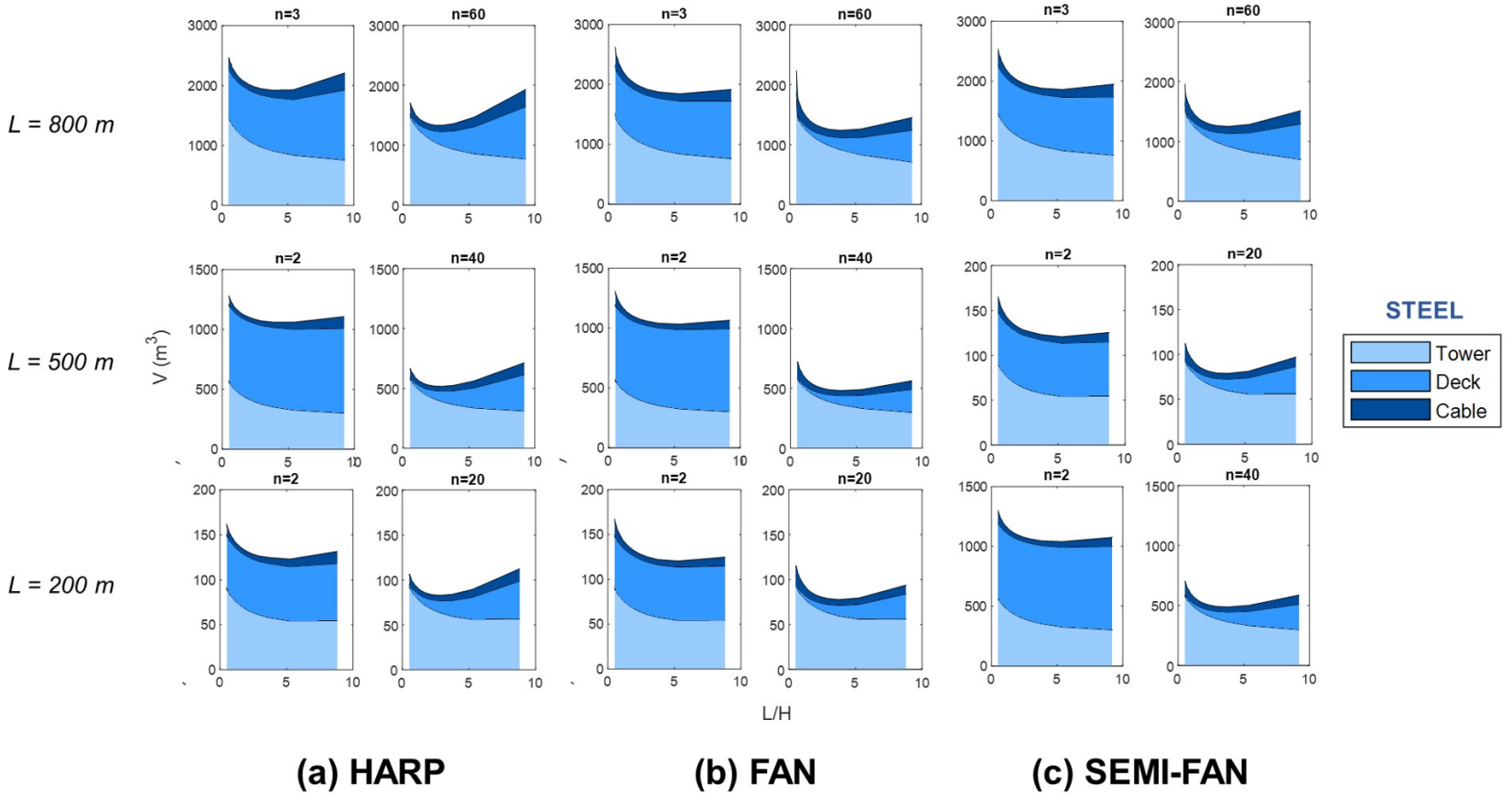

Figure 4-10: Material distribution of the tower, deck and cable elements for a steel bridge of harp, fan and semi-fan configurations with $n = 3$, 60 for L = 800 m, $n = 2$, 40 for $L = 500$ m, and $n = 2$, 20 for $L = 200$ m under asymmetric loading conditions

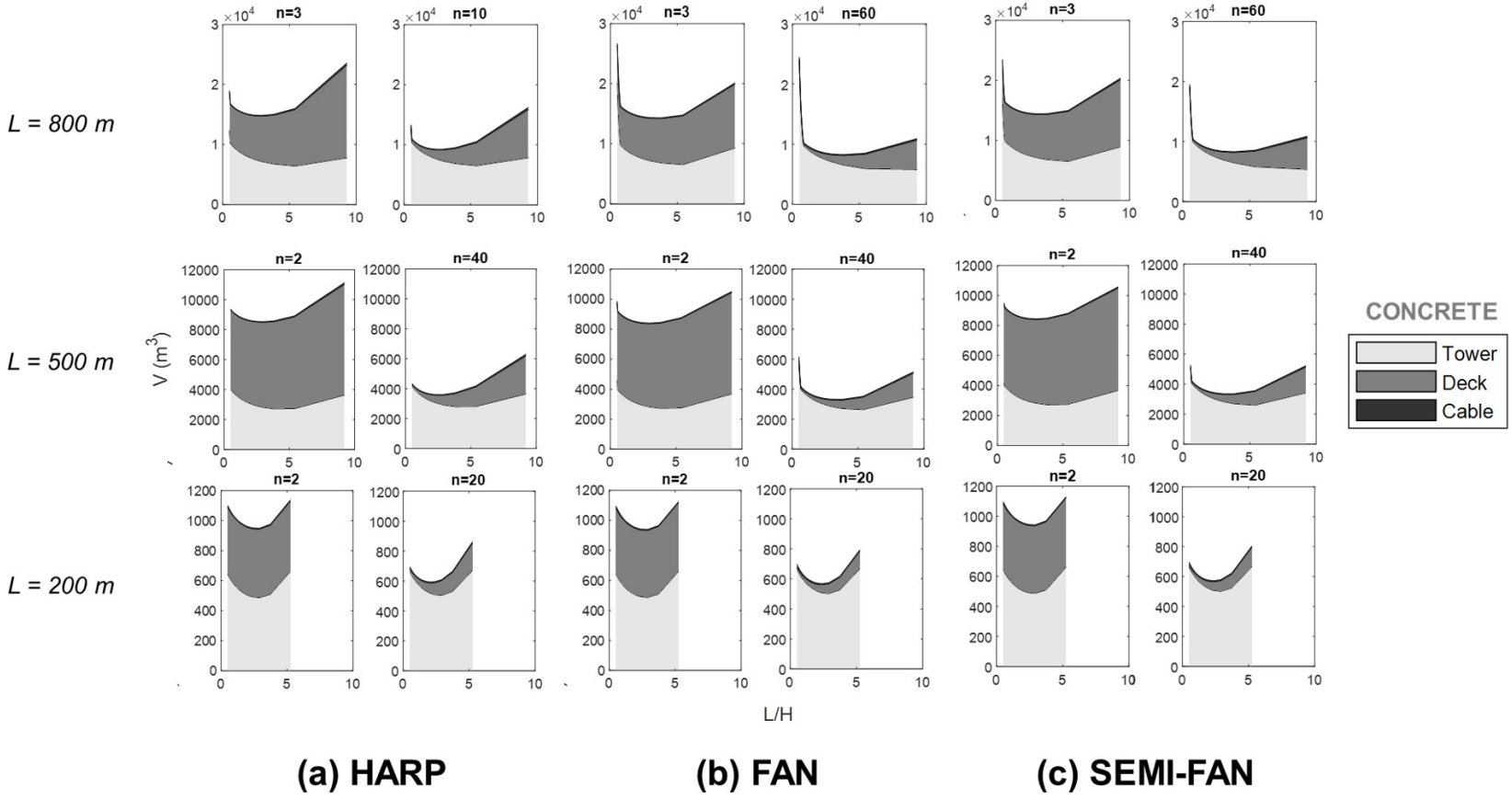

Figure 4-11: Material distribution of the tower, deck and cable elements for a concrete bridge of harp, fan and semi-fan configurations with $n = 3$, 60 for L = 800 m, $n = 2$, 40 for $L = 500$ m, and $n = 2$, 20 for $L = 200$ m under asymmetric loading conditions

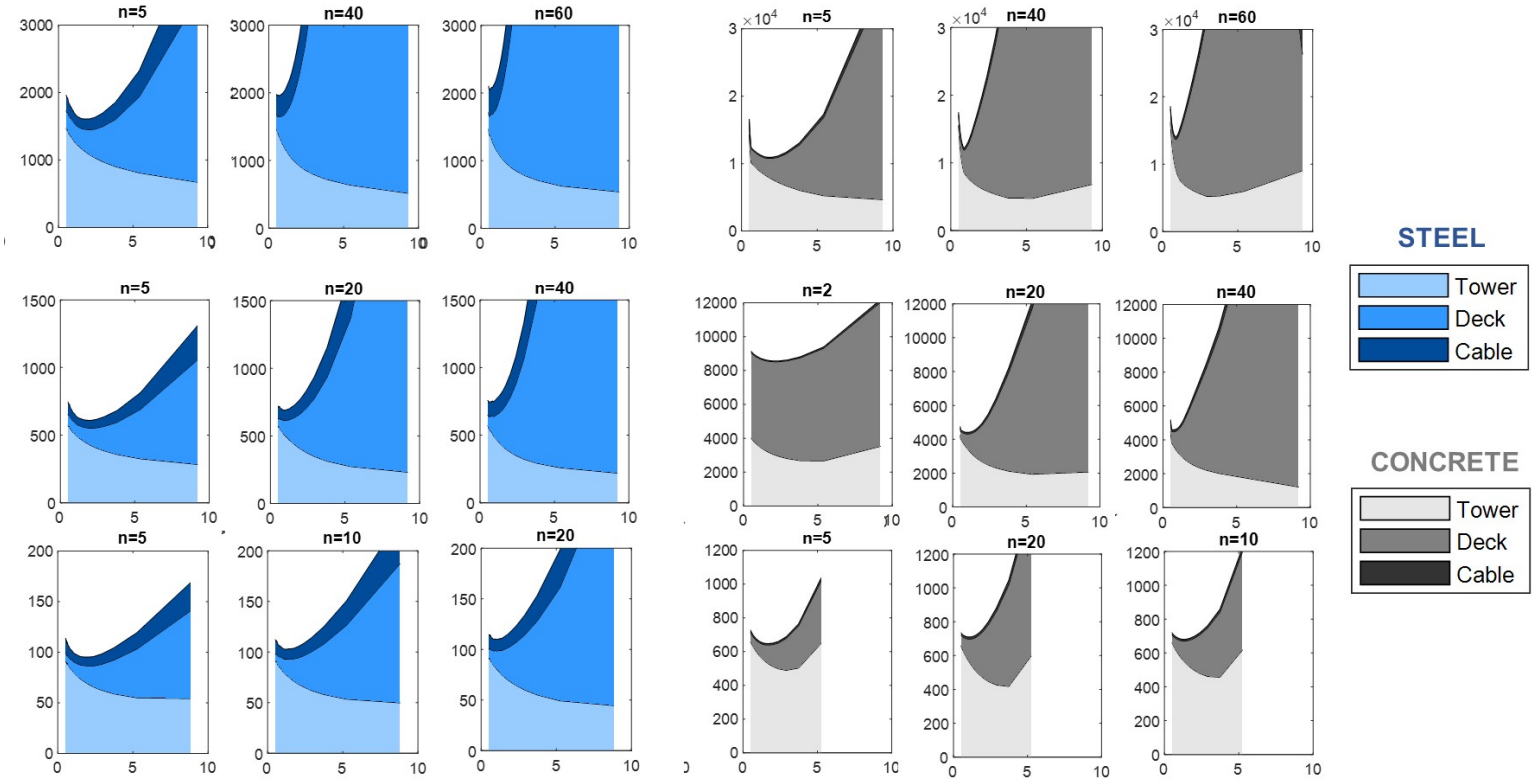

Figure 4-12: Material distribution of the tower, deck and cable elements for a steel and concrete bridge of a web configuration with $n = 3$, 60 for L = 800 m, $n = 2$, 40 for $L = 500$ m, and $n = 2$, 20 for $L = 200$ m under asymmetric loading conditions

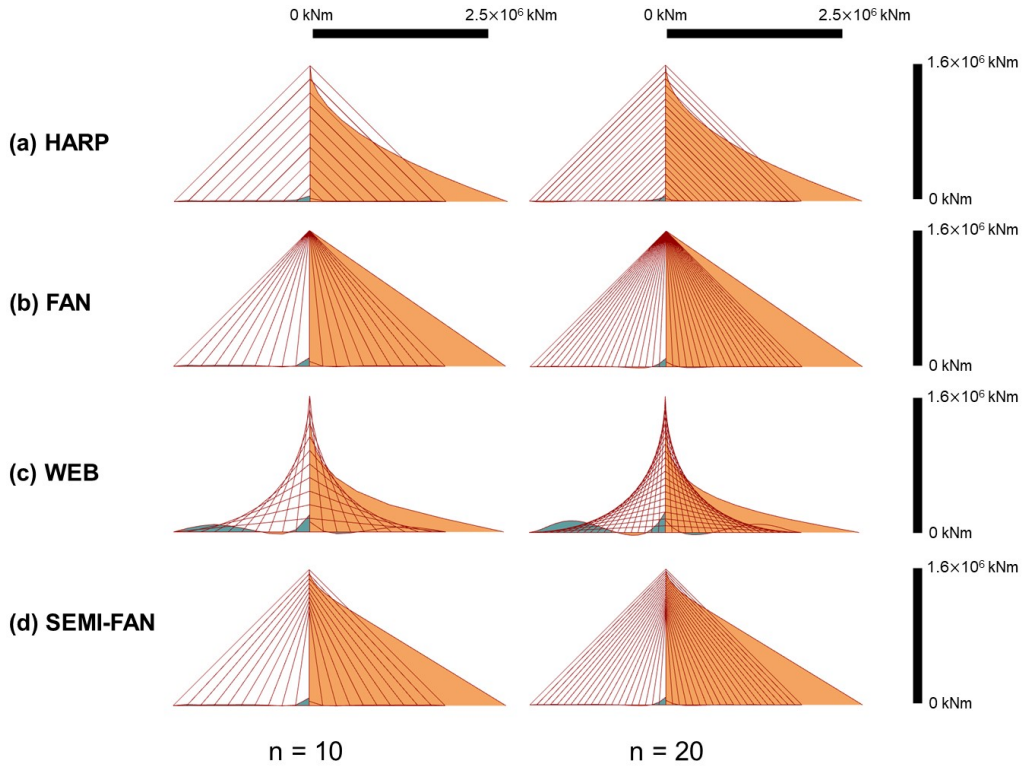

Figure 4-13: Bending moment diagram for a (a) harp, (b) fan, (c) web, and (d) semi-fan cable-stayed bridge models under asymmetric load conditions for n = 10 and 20

overlap in the range of L/H ratios that are deemed efficient given the flatter design curves obtained. Further, the harp configuration no longer remains the most efficient typology and is now replaced by the fan configuration under asymmetric load conditions. This is mainly associated with the slight reduction in the bending moments of the tower when the stay cables are arranged in a fan configuration.

Similar to symmetric loading, the total volume of the deck varies similarly for a web configuration. Not only does the bending moments in the deck (Figure 4-13(c)) increases with the number of cable supports, it also increases at higher L/H ratios.

3D visualisation of the design space

Figure 4-14 illustrates the design space for an asymmetrically loaded cable-stayed bridge in three-dimension with respect to the two design variables, namely the geometric aspect ratio L/H and the number of stay cables n for the harp, fan, web, and semi-fan typology. The plots also encompass the three span length categories of 200 m, 500 m, and 800 m since the shape of the design curve changes, although slightly with span length L.

The design space domain that can be explored freely while remaining within an

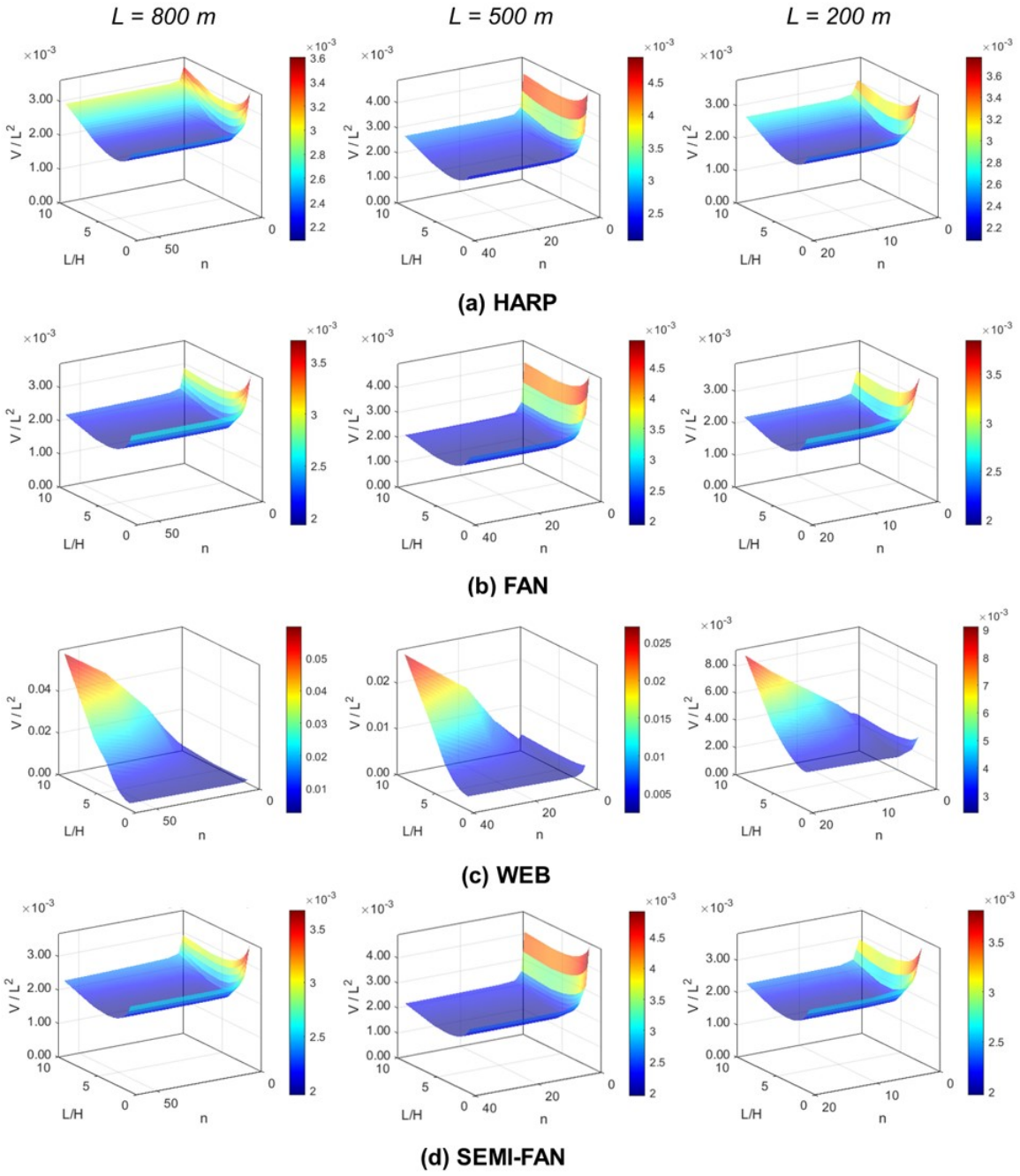

Figure 4-14: 3D design space of the normalized volume V/L^2 performance with respect to L/H ratio and number of stay cables n under asymmetric load pattern (Note: The ordinate axis for the web typology is greater than the other three configurations.)

optimal performance range for the harp, fan, and semi-fan typology appears to overlap, which is indicated by the similarly flattened design space at higher L/H ratios and higher number of cables n.

The shapes of the design curve for a symmetric and asymmetric load condition for the web configuration appear to be quite similar except for the much gentler slope of the design curve obtained for asymmetric loads. This suggests the wider flexibility in navigating around the design space when the web cable-stayed bridge is governed by asymmetric load conditions.

4.3 Influence of span lengths

When the total volume is normalized by L^2, the effect of the bridge's span length L on the total volume of the optimum design can be determined objectively. To assess this relationship fairly, Table 4.5 records the minimum volume of the optimum design solution normalized by L^2 for the three span length categories, each with the same cable spacing of 10 m and subjected to the same uniform loads. The same information is recorded as well in Table 4.6 for asymmetric loading condition.

Table 4.5: Normalized total volume of material V_{min}/L^2 for different span lengths of cable-stayed bridges with 10 m cable spacing under symmetric loads

	Steel ($V_{min}/L^2 \times 10^{-4}$)				Concrete ($V_{min}/L^2 \times 10^{-3}$)			
L (m)	800	500	200	Gradient	800	500	200	Gradient
n	40	25	10	$\times 10^{-7}$	40	25	10	$\times 10^{-6}$
Harp	6.56	6.36	6.10	0.76	4.05	3.78	3.57	0.80
Fan	7.76	7.40	6.93	1.38	4.99	4.52	4.08	1.51
Web	17.5	14.2	10.8	11.1	12.1	9.07	6.32	9.68
Semi-fan	7.33	7.02	6.62	1.19	4.65	4.25	3.89	1.26

With a constant cable spacing of 10 m, the normalized volume V_{min}/L^2 in Table 4.5 and 4.6 are further plotted against their respective span lengths L. The resulting plots are depicted in Figure 4-5. The results for the web typology is provided in a separate graph (bottom) due to its significantly higher volume of material.

Under an imposed symmetric load, a positive linear correlation is discovered between the normalized volume of material and span length (i.e., $V \propto L^3$). This applies for all cable-stayed typology and material. The main difference though exists in the strength of the correlation, which is represented by the gradient of the line plots. The effect of span lengths on the total volume of the material in the following ascending order: harp, semi-fan. fan, and web.

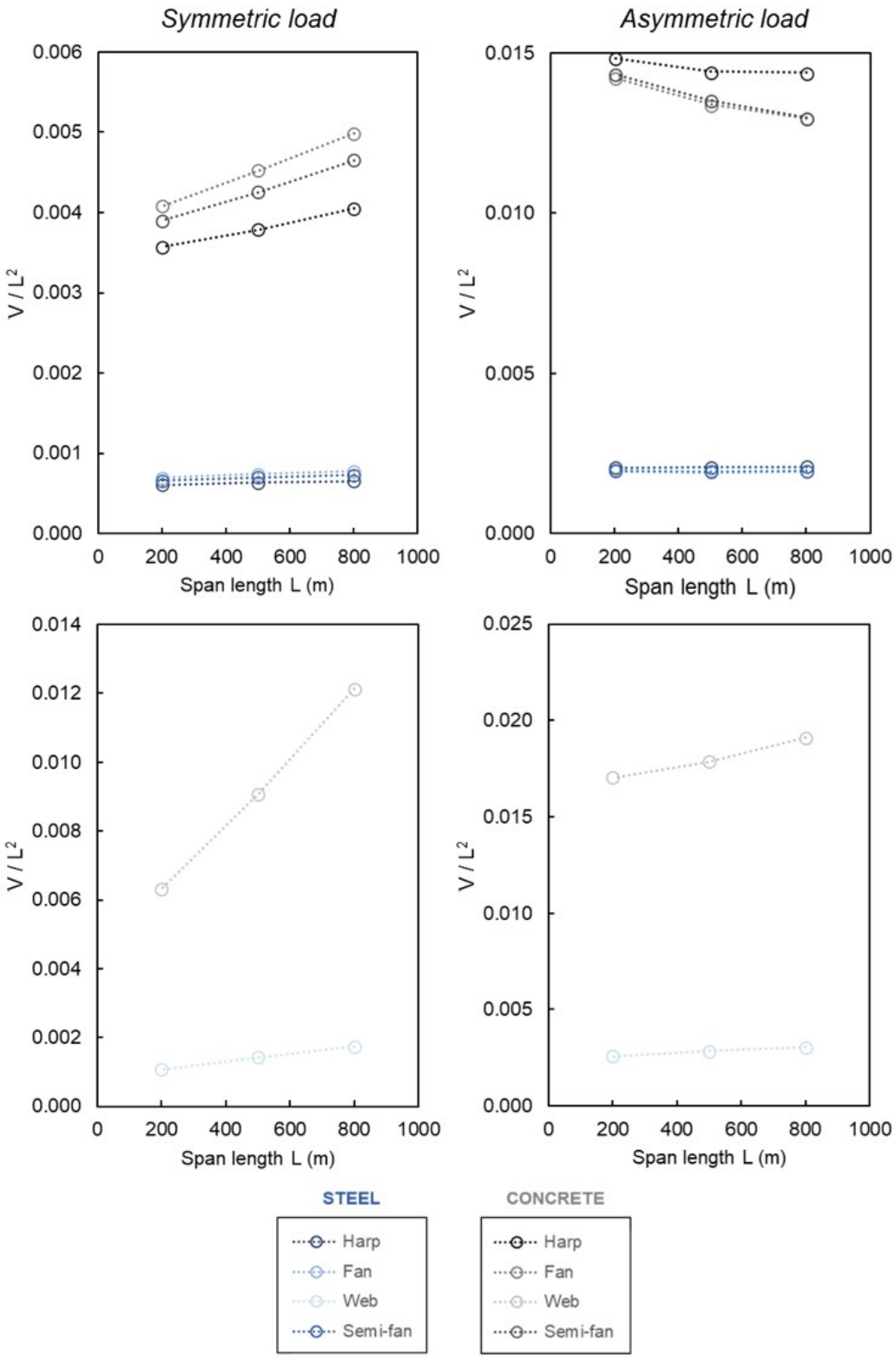

Figure 4-15: Normalized minimum volume V_{min}/L^2 of cable-stayed bridges with stay cables spaced at 10 m plotted against its span length L of 800 m, 500 m, 200 m under symmetric load conditions

Table 4.6: Normalized total volume of material V_{min}/L^2 of different span lengths of cable-stayed bridges with 10 m cable spacing under asymmetric loads

	Steel ($V_{min}/L^2 \times 10^{-3}$)				Concrete ($V_{min}/L^2 \times 10^{-2}$)			
L (m)	800	500	200	Gradient	800	500	200	Gradient
n	40	25	10	$\times 10^{-8}$	40	25	10	$\times 10^{-6}$
Harp	2.08	2.07	2.07	2.10	1.44	1.44	1.48	0.77
Fan	1.93	1.93	1.94	-1.47	1.30	1.34	1.42	-2.09
Web	3.05	2.83	2.57	80.3	1.91	1.79	1.70	3.47
Semi-fan	1.96	1.95	1.97	-2.01	1.30	1.35	1.43	-2.30

An entirely different trend is obtained when the cable-stayed bridge is subjected to asymmetric loads. The volumetric performance of the conventional harp, fan, and semi-fan configurations demonstrate a negative correlation with span length. Given that the volume increase caused by asymmetric loads is mainly attributed to the increase in the tower's moment of inertia to resist bending, the cross-sectional dimensional constraint predefined as a linear function of the span length L and tower height H would justify this negative correlation that arises with increasing span length. Because the optimum design solution for the different span length has a unique tower height H, imposing different constraints on the tower dimensions, the general conclusion made here might not be a fair one.

4.4 Effect of Materiality

It is quite obvious from the beginning of this chapter that the total volume for a steel cable-stayed bridge is considerably lesser than its concrete counterpart, provided that both systems are subjected to the same design variables and loading conditions. This is mainly attributed to the much lower allowable stress σ of concrete, equivalent to barely 15% of the allowable stress of steel.

The effect of materiality is assessed using the results provided in Table 4.5 and 4.6 in Section 4.3. This way, the effect of span length L and number of cables n are eliminated by normalizing the volume with L^2 and keeping a constant cable spacing of 10 m. Thus, the ratio of the total volume of material for a self-anchored, steel and concrete $V_{concrete}/V_{steel}$ cable-stayed bridge for different typologies and span lengths are calculated and are summarized in Table 4.7 below.

Overall, the average ratio of volume for a self-anchored, concrete and steel cable-stayed bridge subjected to symmetric and asymmetric loads are approximately 6.0 and 7.0 respectively. It is important to acknowledge the slight variations in the ratio of the

Table 4.7: Ratio of the total volume of a self-anchored, concrete and steel cable-stayed bridge $V_{concrete}/V_{steel}$ with the same cable spacing of 10 m

	Symmetric loads			Asymmetric loads		
L (m)	800	500	200	800	500	200
Harp	6.17	5.95	5.85	6.91	6.96	7.18
Fan	6.42	6.11	5.88	6.71	6.95	7.32
Web	6.95	6.38	5.86	6.27	6.30	6.63
Semi-fan	6.34	6.06	5.88	6.64	6.92	7.28
Average	6.47	6.13	5.87	6.63	6.78	7.10

volumes of steel and concrete with typology and span length. Under symmetric loads, the ratio of the volumes reduces with span length and increases in the order of harp, semi-fan, fan, and web typology. The reverse is true for the case of asymmetric load conditions. These differences is most likely caused by the structural indeterminancy of the overall cable-stayed system.

Moreover, Figure 4-15 shows that the efficiency of of a concrete cable-stayed bridge reduces more severely with increase in span length when compared against a steel cable-stayed bridge, and is applicable for all cable-stayed typologies. The steeper graphs obtained for concrete also suggests that a steel cable-stayed system might be more favorable for longer span bridges.

4.5 Influence of support conditions

The two types of boundary conditions involving a self-anchored and a partially-anchored cable-stayed bridge described in Section 4.5 will be compared for cable-stayed structures under symmetric and asymmetric load conditions.

4.5.1 Symmetric loading condition

In the plots provided in Figure 4-16, the efficiency curves for the same cable-stayed system under symmetric loads but with different boundary conditions are plotted separately for each typology for easy visualization. It is evident that the horizontal restraint provided by a partially anchored cable-stayed bridge leads to a lowered volume of material specifically when L/H is greater than 1.0. It is also shown that the gradient of the design curve becomes less steep for partially-anchored bridges.

The reduction in the total volume is recorded in Table 4.8 as a ratio of total minimum volume obtained for a self-anchored and partially-anchored cable-stayed bridge.

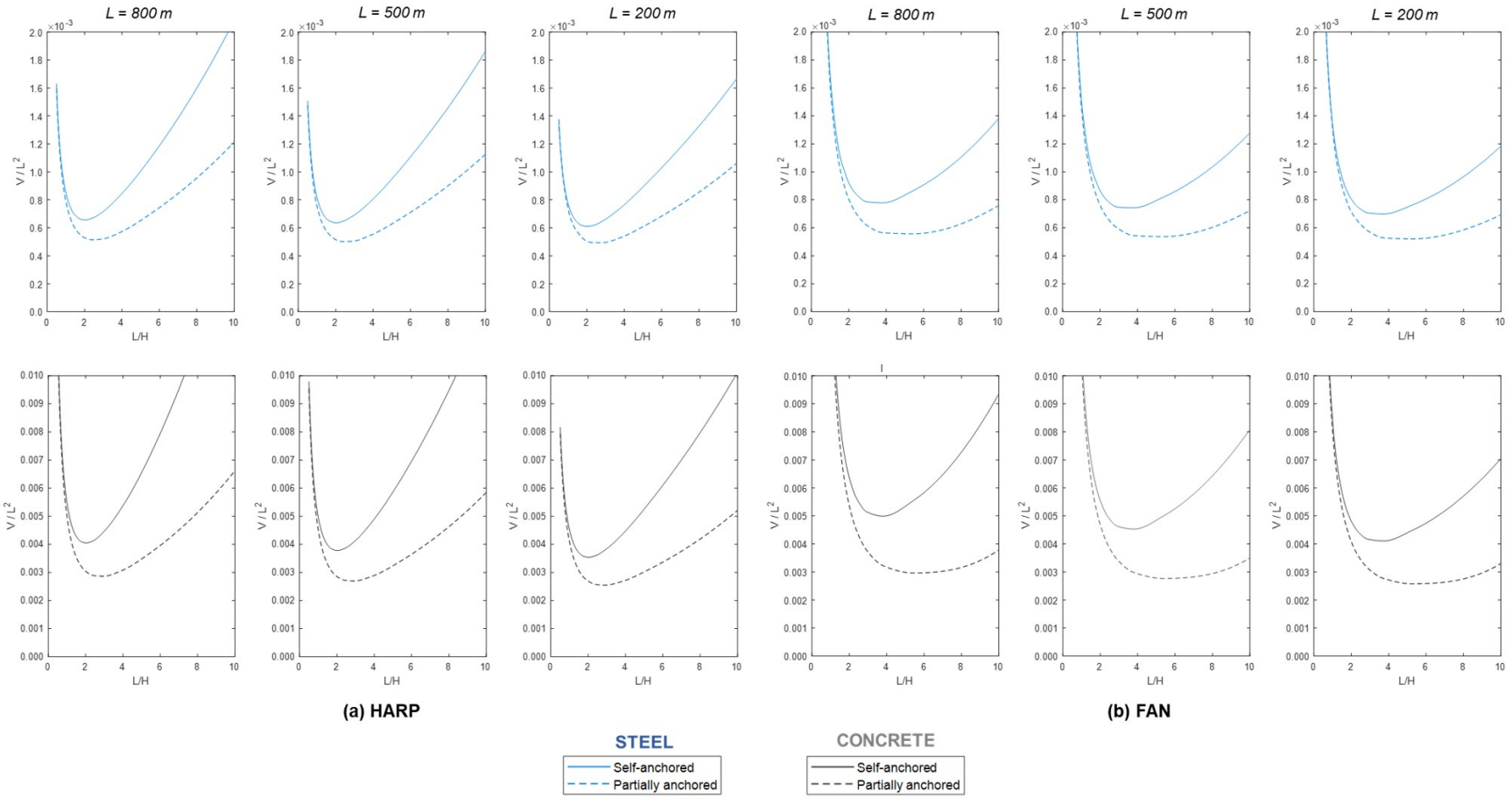

Figure 4-16: Comparison of the optimum volume V of material for a self-anchored and partially anchored cable-stayed bridge under symmetric loads. The design curves for the (a) harp, (b) fan, and (d) semi-fan typology are the converged efficiency curves where n is assumed to be high, while the design curves for the (c) web configuration adopt a value of $n = 10$

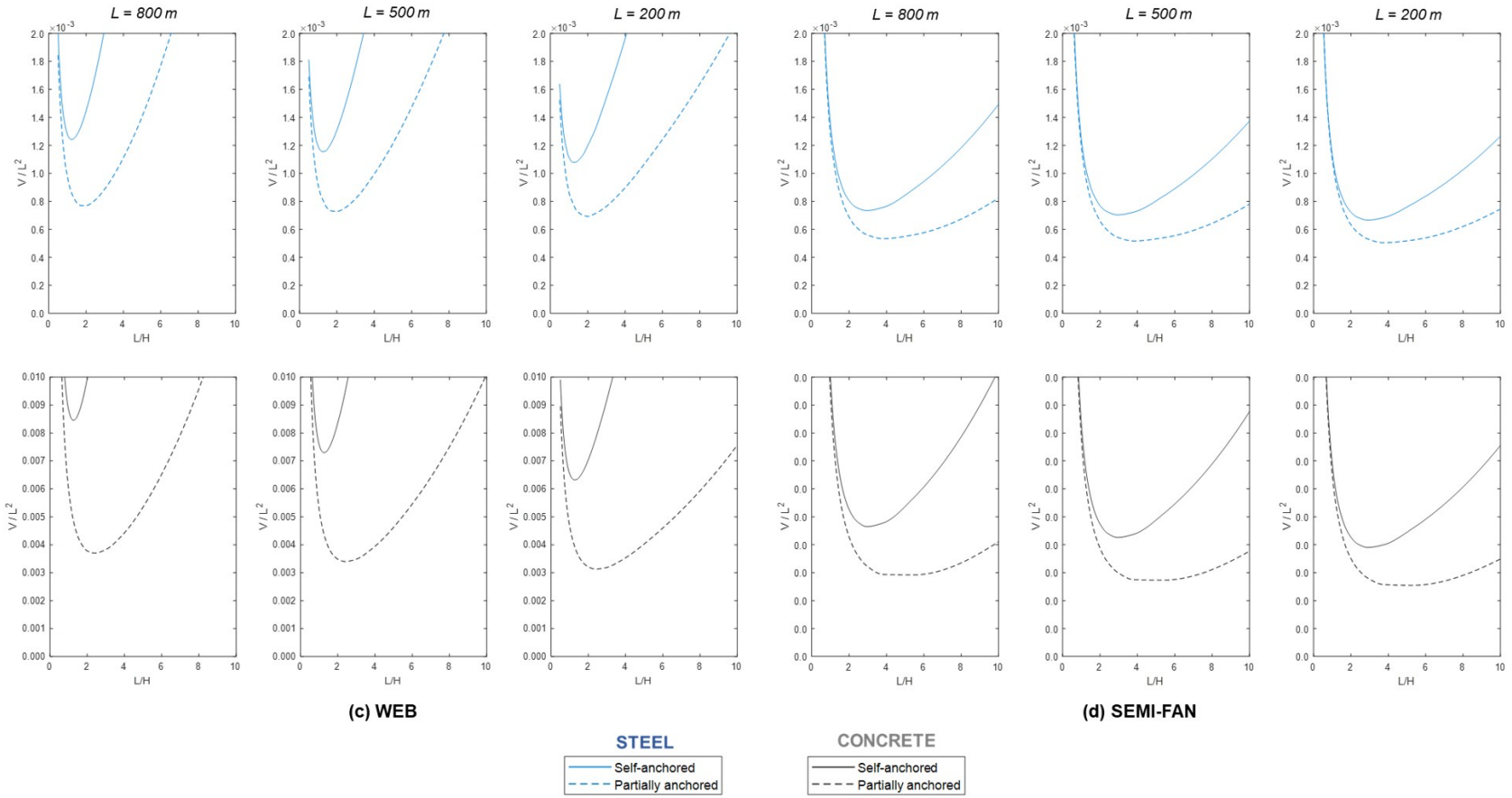

Figure 4-16: Comparison of the optimum volume V of material for a self-anchored and partially anchored cable-stayed bridge under symmetric loads. The design curves for the (a) harp, (b) fan, and (d) semi-fan typology are the converged efficiency curves where n is assumed to be high, while the design curves for the (c) web configuration adopt a value of $n = 10$

It is evident that there is significant reduction in the total volume by simply partially restraining horizontal translations in the deck. This effect is predominantly observed for the web configuration, followed by the fan, semi-fan, and harp configuration. Furthermore, partially-anchored cable-stayed bridges appear to be an effective remedy in improving the efficiency of the structure when a lower strength material is used, which is supported by the higher ratios recorded for concrete cable-stayed bridges compared to its steel counterpart.

4.5.2 Asymmetric loading condition

Under asymmetric loads, Figure 4-17 compares the efficiency curves of a self-anchored and partially-anchored cable-stayed bridges. There is a slight decrease in the total volume of material for the case of a partially anchored cable-stayed bridge. Also listed in Table 4.8 are the ratios of the minimum volume of material for a self-anchored and a partially-anchored cable-stayed bridge made of steel and concrete under asymmetric load pattern.

When compared against the results obtained for symmetric loads, the restraint on the deck ends barely improve the structural efficiency of the cable-stayed bridge, with an average volume reduction of 10% for the harp, fan, and semi-fan typologies and 20% for the web typology. These findings actually supports the results discovered in Section 4.2.2, where most of the volume increase caused by an asymmetrical load pattern is caused by bending of the towers. Since the horizontal restraint at the deck ends do not mitigate the bending moments in the tower, the reduction in the total volume of cable-stayed bridge under asymmetric loads is significantly lesser than of symmetric loads.

Table 4.8: Ratio of the total volume of a self-anchored and a partially anchored cable-stayed bridge made of concrete and steel under symmetric loads

	Symmetric loads						Asymmetric loads					
	Steel			Concrete			Steel			Concrete		
L (m)	800	500	200	800	500	200	800	500	200	800	500	200
Harp	1.28	1.27	1.24	1.41	1.40	1.39	1.11	1.11	1.10	1.12	1.10	1.07
Fan	1.40	1.38	1.34	1.68	1.64	1.59	1.14	1.13	1.11	1.08	1.08	1.06
Web	1.61	1.58	1.56	2.28	2.14	2.02	1.20	1.20	1.20	1.24	1.23	1.19
Semi-fan	1.38	1.36	1.32	1.59	1.56	1.53	1.13	1.13	1.11	1.07	1.08	1.06

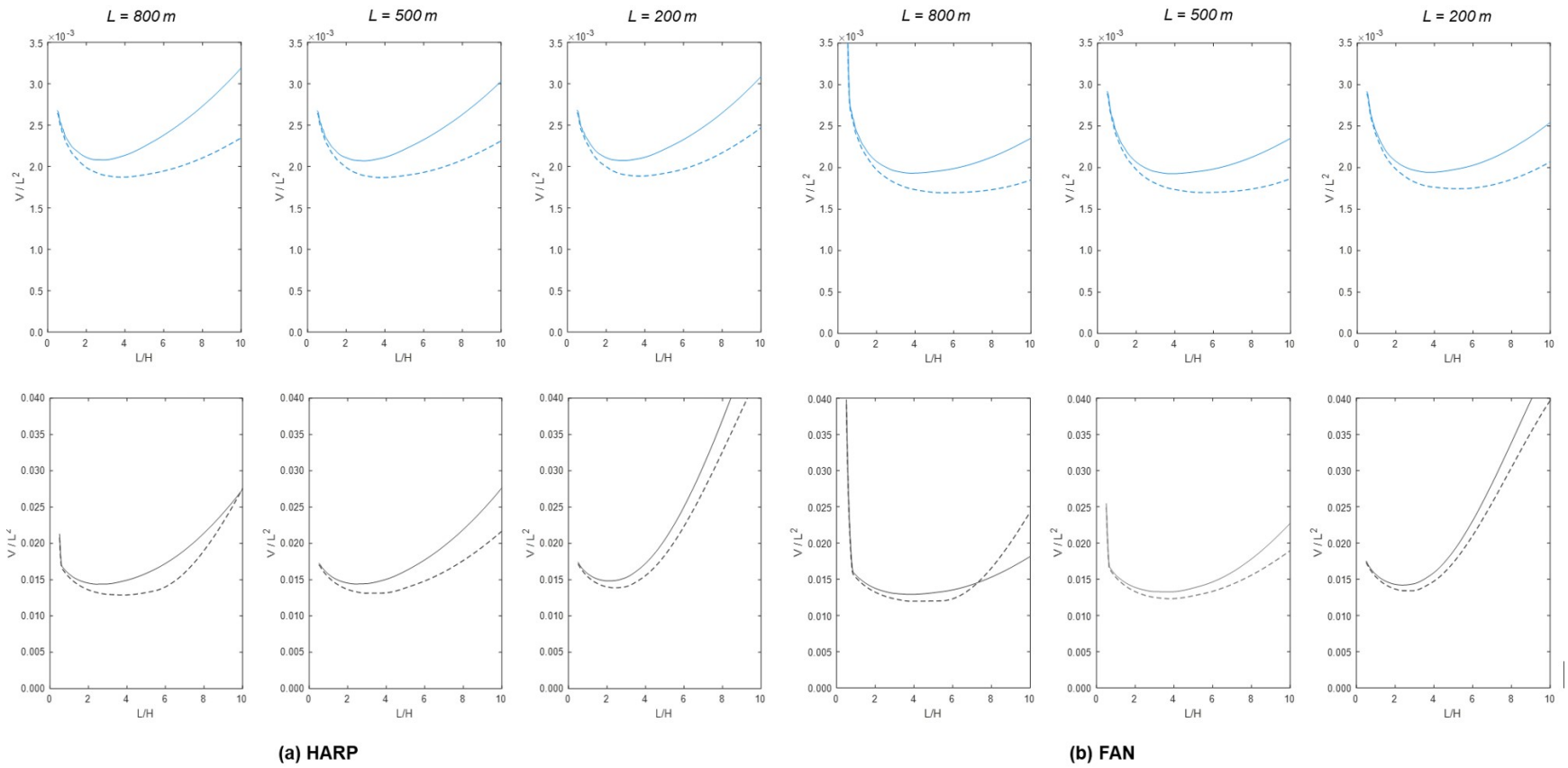

Figure 4-17: Comparison of the optimum volume V of material for a self-anchored and partially anchored cable-stayed bridge under asymmetric loads. The design curves for the (a) harp, (b) fan, and (d) semi-fan typology are the converged efficiency curves where n is assumed to be high, while the design curves for the (c) web configuration adopt a value of $n = 10$

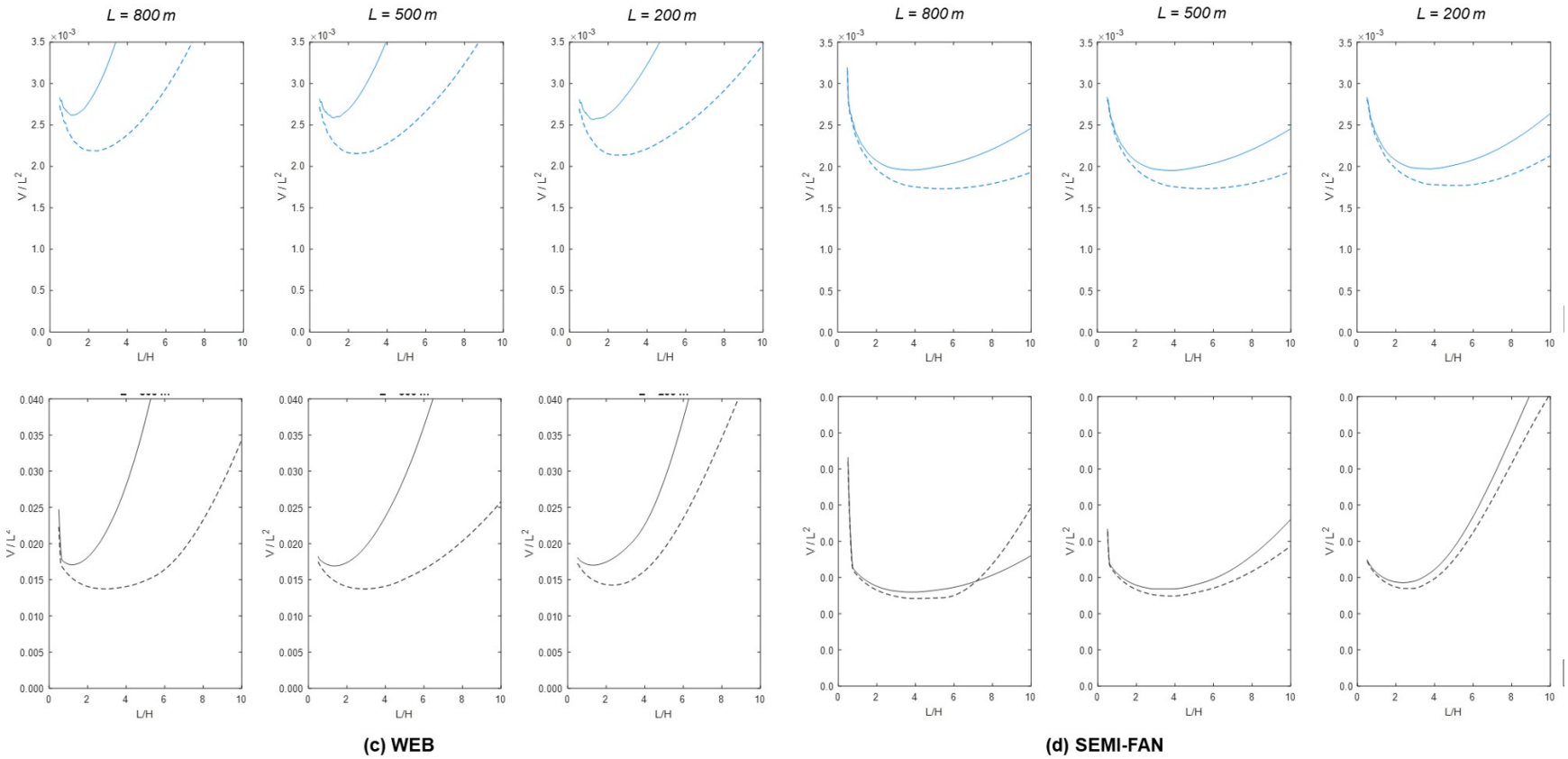

Figure 4-17: Comparison of the optimum volume V of material for a self-anchored and partially anchored cable-stayed bridge under asymmetric loads. The design curves for the (a) harp, (b) fan, and (d) semi-fan typology are the converged efficiency curves where n is assumed to be high, while the design curves for the (c) web configuration adopt a value of $n = 10$

4.6 Case Studies

One approach adopted in this study to verify the results obtained from the parametric study involves comparing the results against nine existing, real-world structures shown in Figure 4-18. This is done by using a mass per unit deck area as a performance metric for the different typologies and material considered.

Figure 4-18: Nine different cable-stayed bridges used for result verification

To simplify the plots and represent essentially the efficiency of different structural forms, the optimum design solution with the least amount of volume is defined as the most efficient design for a given typology and materiality. This design solution is obtained under the assumption that the cable-stayed system has significant number of stay cables where the design curves have converged. It is important to also acknowledge that this optimum design solution which has the least amount of volume corresponds to a specific L/H ratio that would be different for each typology and material considered. The amount of material considered in this study only includes that of the superstructure, and excludes any material associated with the foundations

and piers. Furthermore, since the dead loads of the road deck is assumed as a line load of 130 kN/m, the mass per unit deck area of the structure obtained from the FE analysis in Karamba3D is added an equivalent weight of $\frac{130kN/m}{22m \times 9.81} = 0.6$ tons/m^2.

The details of the nine bridges are summarized in Table 4.9 and the resulting graph is provided in Figure 4-19.

Some general observations inferred from these plots include:

- A positive linear relationship exists between the mass per unit deck area of the cable-stayed bridge and span length. This trend applies for all typologies and material.
- As the span length increases, the increase in the mass per unit deck area increases more drastically for a concrete structure.
- It can be deduced that the variance in total volume between asymmetric and symmetric loading conditions increases with span length. This suggests that for shorter spans, either symmetric or asymmetric load case will govern the design, while asymmetric load patterns will most likely govern the design loads for longer span.
- The effect of span length on the total mass per unit deck area is most severe for a web configuration, followed by the fan, semi-fan and harp condiguration.

Table 4.9: Existing cable-stayed structures considered for result verification

Name	Location	Span length L (m)	Tower height H (m)	Material	Type	Total mass (tons)	Mass per unit deck area (tons/m^2)
Tatara Bridge (Yanaka et al., 1998)	Japan	890	180	Steel	Semi-fan	27,970	1.02
Higashi Kobe (Ganev et al., 1998)	Japan	388	147	Steel	Harp	23,750	1.58
Rio Guama River Bridge (Miranda, 2003)	Brazil	320	98	Concrete	Harp	38,980	1.42
Meiko Central Bridge (Ito, 1998)	Japan	590	141	Steel	Semi-fan	38,700	1.20
Yamuna Bridge (Schlaich et al., 2013)	India	395	151	Steel	Harp	13,800	0.68
Al Emarah City Bridge (Y. Wang et al., 2018)	Iraq	143	49	Concrete	Harp	1,940	0.58
Kanchanapisek Bridge (Jomvinya and Vicat, 2009)	Thailand	500	138	Concrete	Semi-fan	45,510	1.08
Qi Ao Bridge (Jiang and Yang, 1998)	China	320	76	Concrete	Harp	76,800	1.85
Ponte Laterale Sud (Rando et al., 2010)	Italy	180	58	Steel	Web	1,400	0.62

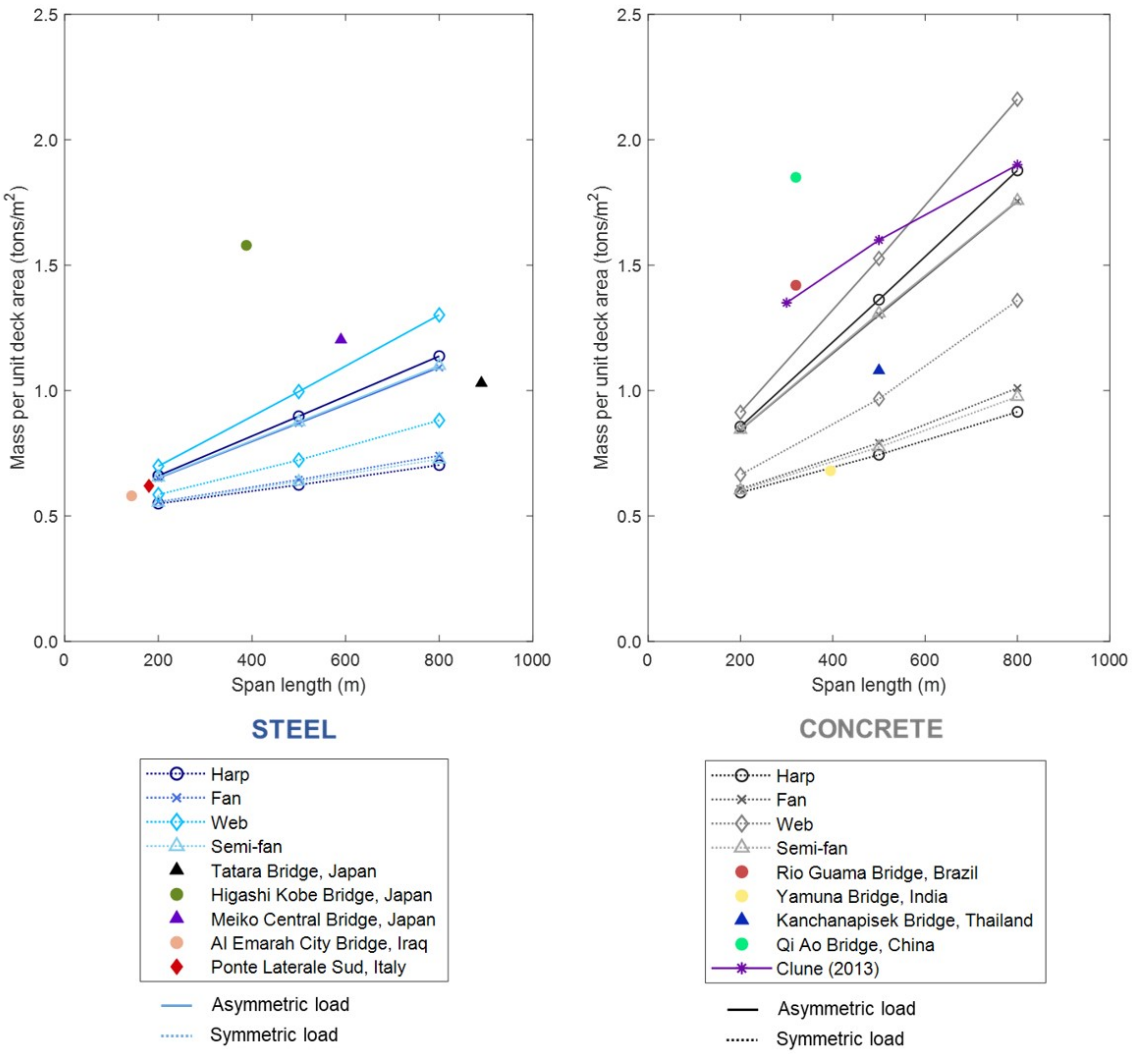

Figure 4-19: Mass per unit deck area plotted against span for steel and concrete cable-stayed bridges, compared against real bridges

In addition to the existing, real-world cable-stayed bridges listed above, the structurally optimized design solutions resolved by Clune (2013) in his PhD thesis is also included in these plots for verification. The results obtained from Clune's study (2013) are in general, more conservative. A possible reason for the variance could be the different material properties of steel and concrete being considered, as well as the LRFD approach that was adopted in his study.

For a majority of the cable-stayed bridges being considered, the mass per unit deck area falls within an acceptable range of the results obtained in this study for a self-supported, cable-stayed bridge. Some anomalies are identified, that includes the steel Higashi Kobe Bridge in Japan and the concrete Qi Ao Bridge in China.

An explanation for the significantly higher volumes of material for the Higashi Kobe Bridge can be accounted to the fact that it is a double-decked cable-stayed bridge, leading to higher design of dead and live loads. Furthermore, its proximity in a highly active seismic zone suggests that its design is mainly governed by dynamic aspects (Ganev et al., 1998) instead of the typical static design loads. The similar dynamic design aspects of wind also governs the design of the Qi Ao Bridge, which would explain the variance in the designs.

Two particular case studies highlight the importance of materiality as well as the element stiffnesses on the structural efficiency of the system, namely the Tatara Bridge and Ponte Latarale Sud.

While the Tatara Bridge is the second longest cable-stayed bridge in the world with a main span of 890 m, its performance in Figure 4-19 lies below the optimum design solution results for a semi-fan configuration. It is able to achieve such high level of efficiency with an extremely slender deck of 2.7 m depth due to the use of steel orthotropic deck.

The Ponte Laterale Sud in Reggio Emilia of Italy are two (twin) of the three bridges designed by Santiago Calatrava which has a web configuration similar to the Margaret Hunt Hill Bridge in Dallas, Texas. Similar to the Tatara Bridge, the use of steel orthotropic decks would explain for the relatively efficient performance despite the high bending moments generated in the deck, which is previously determined in Section 4.2.1.

4.7 Flatness of design curve

As the efficiency curves are derived, there lies an optimum design solution in which the system is capable of working most efficiently in resisting the same applied loads with the least volume of materials. This notion led to the question of how freely the designer can explore the design space or more specifically, how wide is the range of geometry L/H that still performs relatively efficiently given the different gradients of efficiency curves exhibited by different forms.

Therefore, this section of the thesis aims at proposing a range of geometry aspect ratio L/H that corresponds to design solutions that lie within a 10% range of the optimum design solution. The purpose of this is to aid the conceptual design stage of cable-stayed bridges such that a relatively suboptimum initial design is achieved to streamline the design process and achieve a perfectly optimized structure in the end under the existing design requisites.

It must be noted that for the harp, fan, and semi-fan typologies, the converged

design curves are adopted to derive these efficiency curves. This means that the design curves assumes that the cable-stayed bridges do not have unreasonably low number of stay cables n. For the case of the web typology, the number of stay cables n is taken as 10.

4.7.1 Symmetrical loading condition

The efficiency curves for cable-stayed bridges subjected to symmetric loads are provided in Figures 4-20 and 4-21 for steel and concrete bridge respectively. In addition to the design curves, the minimum volume and the corresponding L/H ratio are recorded in Table 4.10, 4.11 and 4.12 for span lengths L of 800 m, 500 m, and 200 m, respectively.

4.7.2 Asymmetrical loading condition

The efficiency curves for cable-stayed bridges subjected to asymmetric loads are provided in Figures 4-22 and 4-23 for steel and concrete bridge respectively. The minimum volume and the corresponding L/H ratio are summarized in Table 4.13, 4.14 and 4.15 for span lengths L of 800 m, 500 m, and 200 m, respectively.

L = 800 m

Table 4.10: Normalized volume V of the optimum design solution with their corresponding geometry L/H, and the range of optimum L/H ratios for bridges of span length $L = 800$ m subjected to symmetric load pattern

	Self-anchored						Partially-anchored					
	Steel ($\times 10^{-4}$)			Concrete ($\times 10^{-3}$)			Steel ($\times 10^{-4}$)			Concrete ($\times 10^{-3}$)		
	V/L^2	L/H	10% L/H Range	V/L^2	L/H	10% L/H Range	V/L^2	L/H	10% L/H Range	V/L^2	L/H	10% L/H Range
Harp	6.56	2.05	1.35 - 3.00	4.05	2.05	1.40 - 2.95	5.15	2.40	1.70 - 3.85	2.86	2.95	1.85 - 4.20
Fan	7.79	3.80	2.30 - 5.30	4.99	3.80	2.55 - 5.30	5.57	5.40	3.05 - 7.65	2.96	5.45	3.70 - 8.45
Web	12.4	1.25	0.85 - 1.80	8.45	1.25	0.90 - 1.75	7.69	1.75	1.30 - 2.75	3.70	2.40	1.65 - 3.45
Semi-fan	7.34	2.95	2.00 - 4.55	4.65	2.95	2.15 - 4.60	5.33	3.85	2.65 - 6.25	2.92	5.40	3.05 - 7.50

L = 500 m

Table 4.11: Normalized volume V of the optimum design solution with their corresponding geometry L/H, and the range of optimum L/H ratios for bridges of span length $L = 500$ m subjected to symmetric load pattern

	Self-anchored						Partially-anchored					
	Steel ($\times 10^{-4}$)			Concrete ($\times 10^{-3}$)			Steel ($\times 10^{-4}$)			Concrete ($\times 10^{-3}$)		
	V/L^2	L/H	10% L/H Range	V/L^2	L/H	10% L/H Range	V/L^2	L/H	10% L/H Range	V/L^2	L/H	10% L/H Range
Harp	6.35	2.00	1.35 - 3.05	3.78	2.00	1.35 - 3.00	5.00	2.40	1.65 - 3.90	2.69	2.95	1.85 - 4.25
Fan	7.43	3.80	2.25 - 5.35	4.53	3.80	2.40 - 5.30	5.37	5.35	3.05 - 7.70	2.76	5.40	3.60 - 8.50
Web	11.5	1.25	0.85 - 1.85	7.30	1.25	0.90 - 1.85	7.28	2.00	1.30 - 2.85	3.40	2.40	1.65 - 3.60
Semi-fan	7.04	2.95	2.00 - 4.65	4.26	2.95	2.10 - 4.60	5.17	3.80	2.65 - 6.40	2.73	5.35	3.00 - 7.55

L = 200 m

Table 4.12: Normalized volume V of the optimum design solution with their corresponding geometry L/H, and the range of optimum L/H ratios for bridges of span length $L = 200$ m subjected to symmetric load pattern

	Self-anchored						Partially-anchored					
	Steel ($\times 10^{-4}$)			Concrete ($\times 10^{-3}$)			Steel ($\times 10^{-4}$)			Concrete ($\times 10^{-3}$)		
	V/L^2	L/H	10% L/H Range	V/L^2	L/H	10% L/H Range	V/L^2	L/H	10% L/H Range	V/L^2	L/H	10% L/H Range
Harp	6.07	2.00	1.30 - 3.05	3.54	2.00	1.35 - 3.05	5.00	2.40	1.65 - 3.95	2.55	2.90	1.80 - 4.30
Fan	6.99	3.75	2.25 - 5.35	4.11	3.75	2.30 - 5.35	5.37	5.35	2.95 - 7.70	2.58	5.25	3.50 - 8.45
Web	10.8	1.25	0.85 - 1.95	6.32	1.25	0.85 - 1.90	7.28	2.00	1.30 - 2.95	3.13	2.40	1.65 - 3.75
Semi-fan	6.66	2.90	1.95 - 4.60	3.90	2.90	2.00 - 4.65	5.17	3.80	2.60 - 6.50	2.55	5.25	2.95 - 7.50

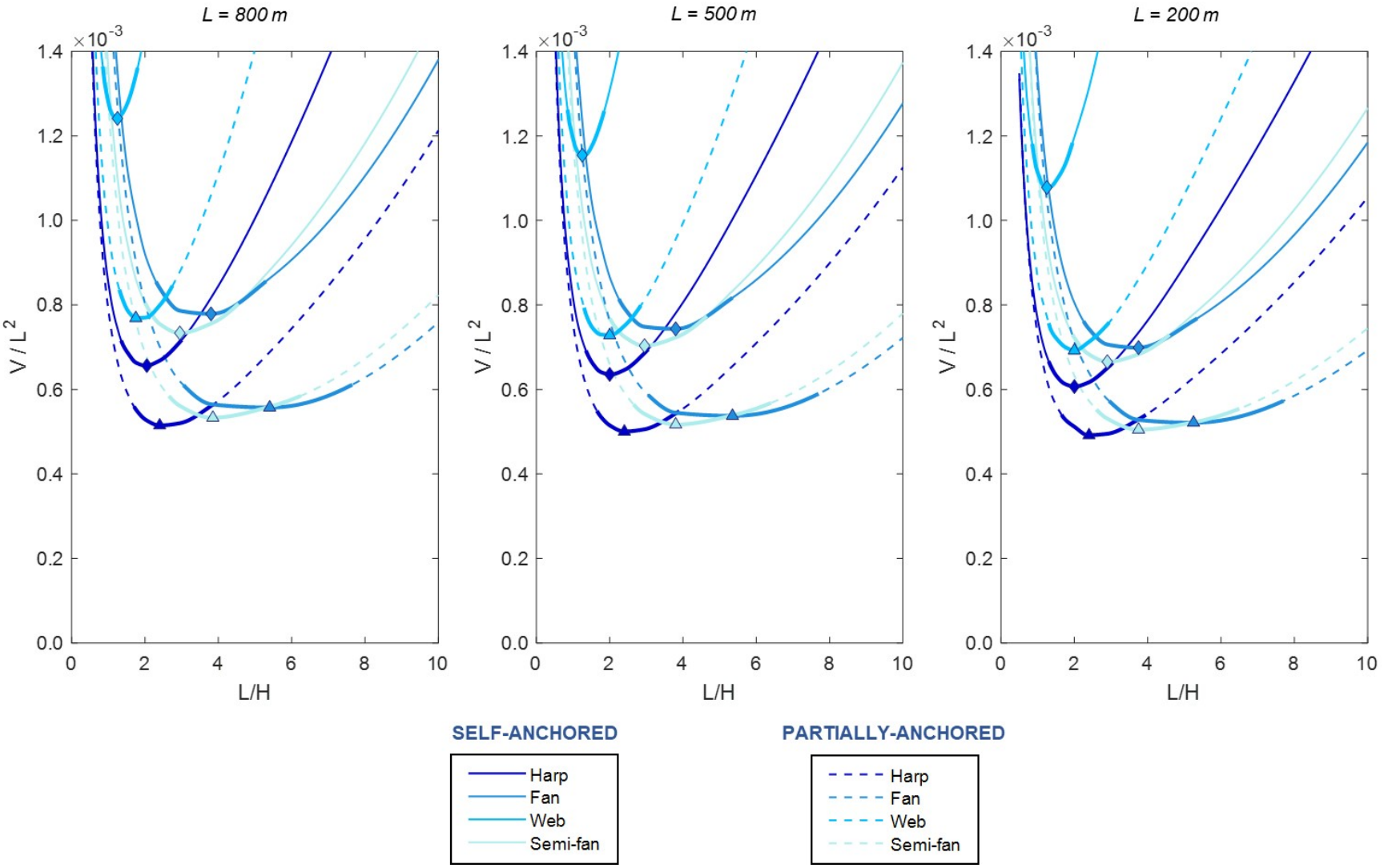

Figure 4-20: Range of optimum L/H ratios that lie within 10% of the optimum design solution for a steel, self-anchored and partially-anchored cable-stayed bridges of different span lengths and typology under symmetric load conditions

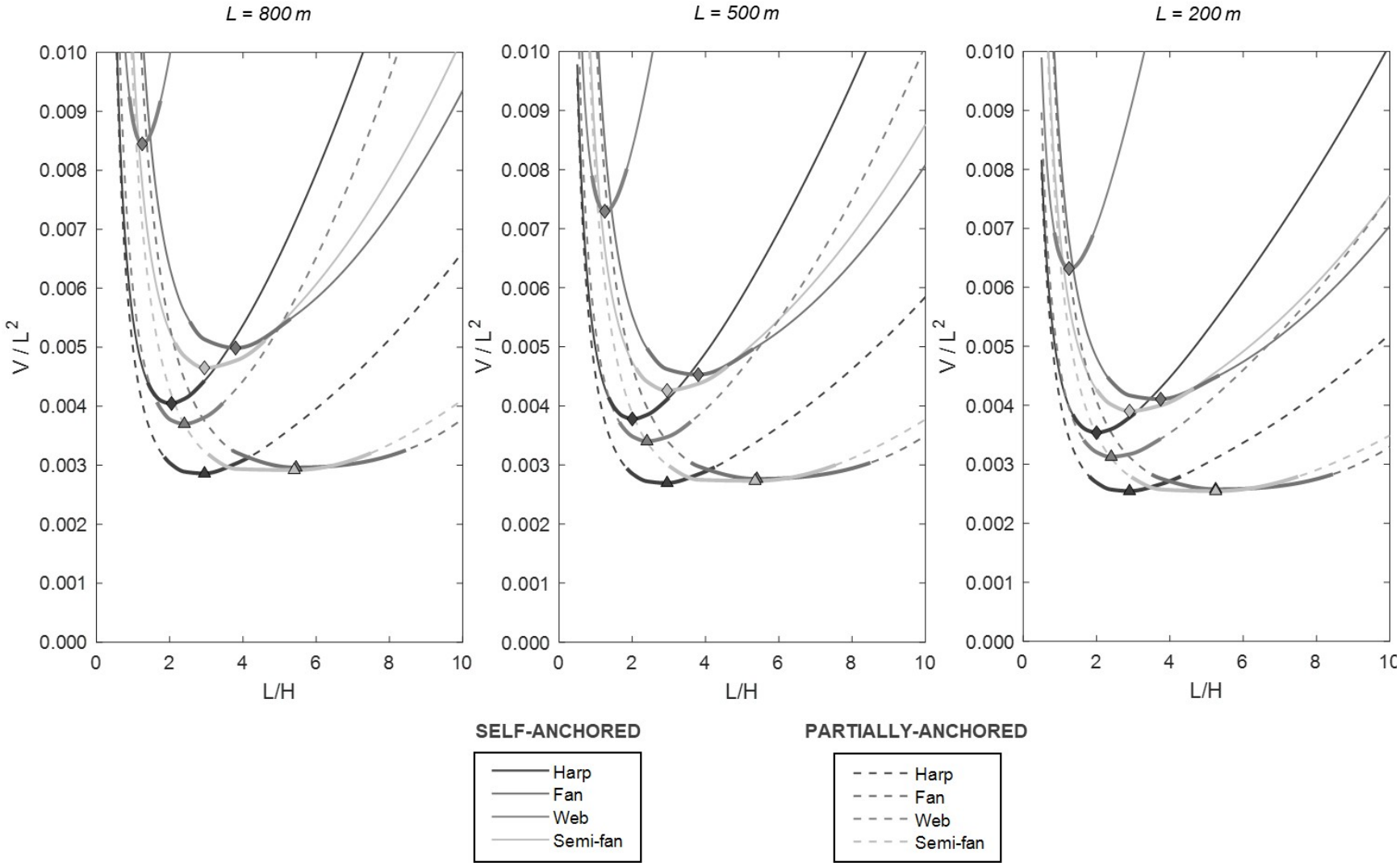

Figure 4-21: Range of optimum L/H ratios that lie within 10% of the optimum design solution for a concrete, self-anchored and partially-anchored cable-stayed bridges of different span lengths and typology under symmetric load conditions

L = 800 m

Table 4.13: Normalized volume V of the optimum design solution with their corresponding geometry L/H, and the range of optimum L/H ratios for bridges of span length $L = 800$ m subjected to asymmetric load pattern

	Self-anchored						Partially-anchored					
	Steel ($\times 10^{-3}$)			Concrete ($\times 10^{-2}$)			Steel ($\times 10^{-3}$)			Concrete ($\times 10^{-2}$)		
	V/L^2	L/H	10% L/H Range	V/L^2	L/H	10% L/H Range	V/L^2	L/H	10% L/H Range	V/L^2	L/H	10% L/H Range
Harp	2.08	2.95	1.15 - 5.30	1.44	2.40	1.00 - 4.95	1.87	3.80	1.70 - 7.50	1.44	2.40	1.60 - 6.10
Fan	1.93	3.80	1.80 - 7.95	1.29	3.80	1.70 - 6.90	1.70	5.45	2.60 - 10.0	1.29	3.80	2.05 - 6.60
Web	2.62	1.15	0.50 - 2.25	1.71	1.25	0.65 - 2.20	2.19	2.40	1.00 - 4.10	1.71	1.25	1.25 - 5.15
Semi-fan	1.96	3.80	1.65 - 7.40	1.30	3.80	1.65 - 6.90	1.73	5.40	2.35 - 9.70	1.30	3.80	2.00 - 6.55

L = 500 m

Table 4.14: Normalized volume V of the optimum design solution with their corresponding geometry L/H, and the range of optimum L/H ratios for bridges of span length $L = 500$ m subjected to aymmetric load pattern

	Self-anchored						Partially-anchored					
	Steel ($\times 10^{-3}$)			Concrete ($\times 10^{-2}$)			Steel ($\times 10^{-3}$)			Concrete ($\times 10^{-2}$)		
	V/L^2	L/H	10% L/H Range	V/L^2	L/H	10% L/H Range	V/L^2	L/H	10% L/H Range	V/L^2	L/H	10% L/H Range
Harp	2.07	2.95	1.15 - 5.60	1.44	2.40	1.00 - 4.70	1.87	3.80	1.70 - 7.70	1.44	2.40	1.45 - 5.60
Fan	1.93	3.80	1.80 - 7.90	1.33	3.80	1.50 - 5.95	1.70	5.40	2.55 - 10.00	1.33	3.80	1.85 - 6.20
Web	2.59	1.25	0.50 - 2.50	1.69	1.35	0.50 - 2.60	2.16	2.40	1.05 - 4.55	1.69	1.35	1.25 - 5.00
Semi-fan	1.95	3.80	1.65 - 7.40	1.34	3.80	1.40 - 5.95	1.73	5.40	2.35 - 9.60	1.34	3.80	1.75 - 6.10

L = 200 m

Table 4.15: Normalized volume V of the optimum design solution with their corresponding geometry L/H, and the range of optimum L/H ratios for bridges of span length $L = 200$ m subjected to asymmetric load pattern

	Self-anchored						Partially-anchored					
	Steel ($\times 10^{-3}$)			Concrete ($\times 10^{-2}$)			Steel ($\times 10^{-3}$)			Concrete ($\times 10^{-2}$)		
	V/L^2	L/H	10% L/H Range	V/L^2	L/H	10% L/H Range	V/L^2	L/H	10% L/H Range	V/L^2	L/H	10% L/H Range
Harp	2.07	2.90	1.20 - 5.60	1.48	2.00	0.80 - 3.55	1.89	3.75	1.60 - 7.15	1.48	2.00	1.20 - 3.95
Fan	1.94	3.75	1.75 - 7.20	1.42	2.35	1.05 - 3.80	1.75	5.25	2.35 - 8.65	1.42	2.35	1.00 - 3.70
Web	2.57	1.25	0.50 - 2.80	1.70	1.35	0.50 - 2.75	2.14	2.40	1.10 - 5.05	1.70	1.35	1.25 - 4.00
Semi-fan	1.97	3.75	1.55 - 6.90	1.43	2.35	1.00 - 3.80	1.77	5.25	2.15 - 8.40	1.43	2.35	1.10 - 3.80

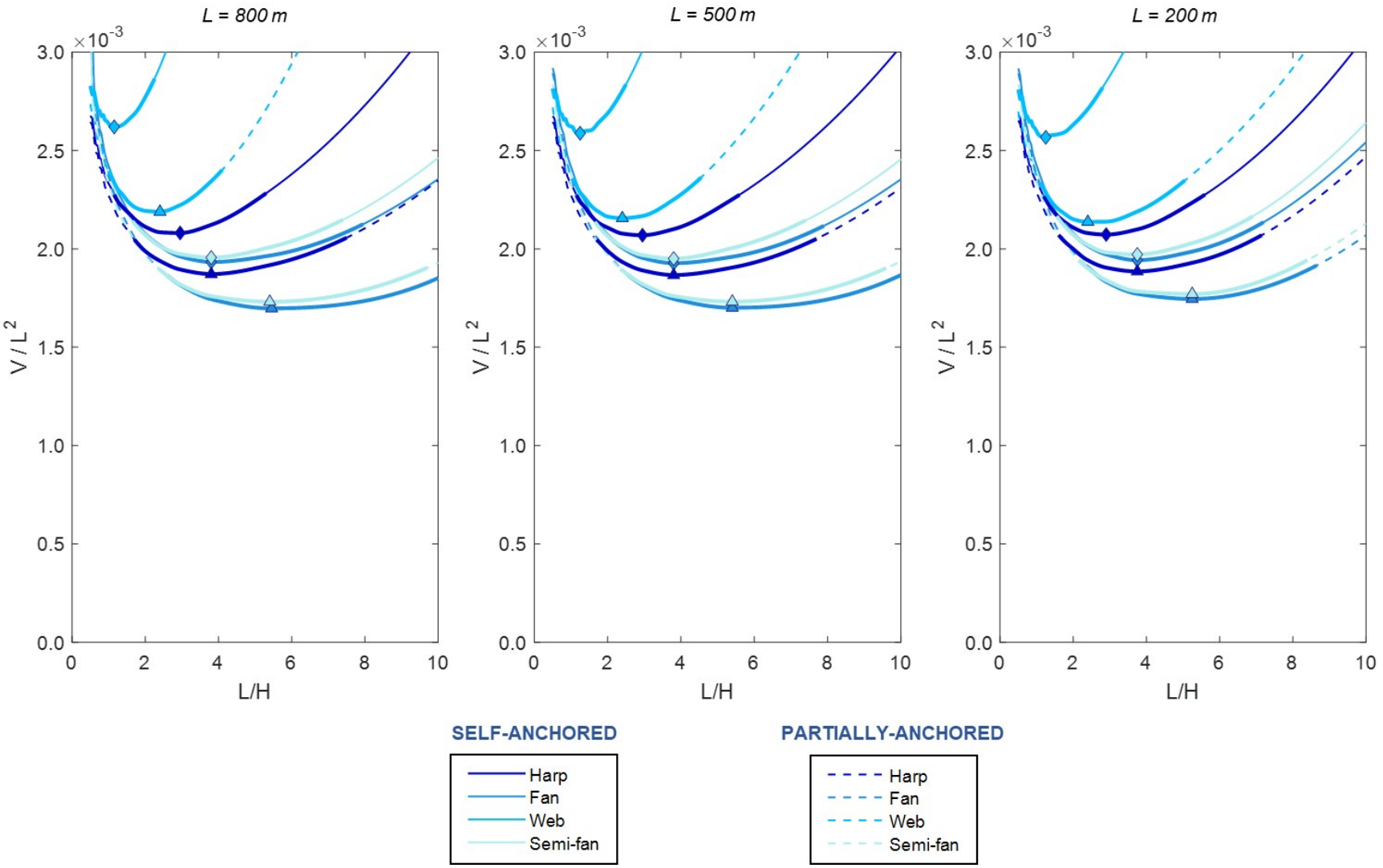

Figure 4-22: Range of optimum L/H ratios that lie within 10% of the optimum design solution for a steel, self-anchored and partially-anchored cable-stayed bridges of different span lengths and typology under asymmetric load conditions

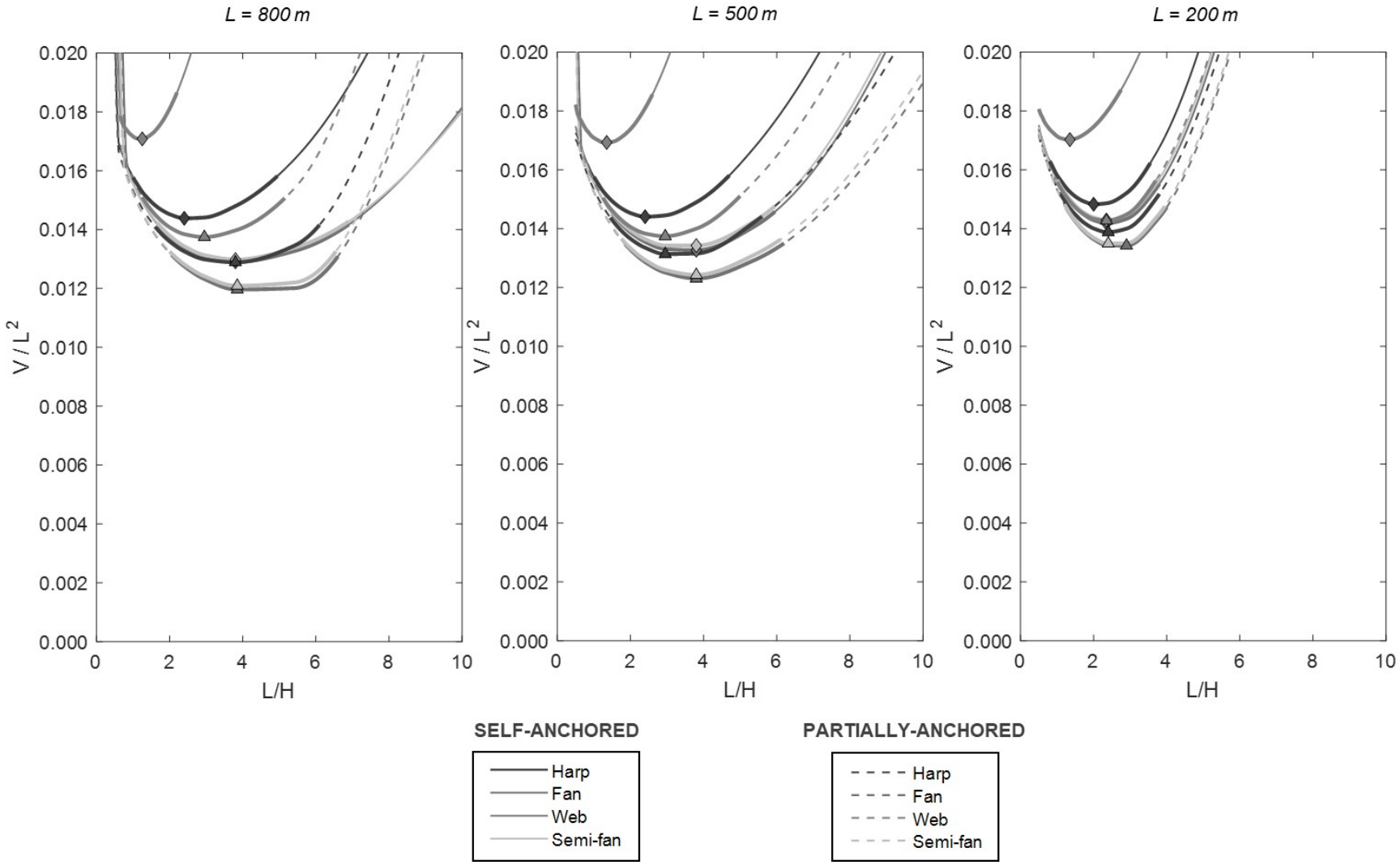

Figure 4-23: Range of optimum L/H ratios that lie within 10% of the optimum design solution for a concrete, self-anchored and partially-anchored cable-stayed bridges of different span lengths and typology under asymmetric load conditions

Chapter 5

Conclusion

This thesis explores the idea of structural optimization at the conceptual level through the use of user-friendly volume efficiency curves. The emphasis on user-friendly conceptual design tools is critical to allow for free exploration of the design space, while still considering important design variables in the preliminary design phase of cable-stayed bridges. Despite the importance of the conceptual design phase, the lack of conceptual design tools that serves the aforementioned purposes continues to persist, which leads to designers being stuck in an iterative design loop and attaining a highly inefficient system. With these design problems in mind, the aim of this thesis is to:

- Analyze various cable-stayed typologies while considering additional design variables that represent realistic structural design problems.
- Incorporate the effect of bending stiffnesses and materiality into the main structural elements.
- Consider both symmetric and asymmetric load patterns.
- Derive a series of efficiency curves with respect to the system's geometry L/H and propose a range of geometry L/H that lies within an acceptable 10% range of the optimum design solution for different cable-stayed typologies.

Based on this study, several key findings are discovered and will be presented in the next section. Furthermore, future research that needs to be undertaken given the limitations of the study will also be discussed. The proposed future work mainly attempts at increasing the scope of the study for the design curves to be more applicable for use in the conceptual design stage of cable-stayed bridge design.

5.1 Key findings

Number of stay cables n

- With the added consideration of flexural rigidity EI in the tower and deck elements, the number of cables n becomes a critical design variable. Under a simple truss analysis, the total volume of the system is independent of the number of cables n; this however, does not apply for the web configuration.
- The vertical stiffness provided by the stay cables which prevents excessive deflections in the deck depends on the orientation of the stay cables. Generally, where the orientation of the stays are close to vertical, sufficient vertical stiffness is provided to the deck, limiting the development of bending moments in the deck.
- For the harp, fan, and semi-fan configuration, the vertical stiffness provided by the stay cables is sufficient in limiting bending moments in the deck. Hence, an increase in the number of stay cables leads to the reduction of total volume of the system. This causes the design curve to eventually converge with the design solution obtained from a truss analysis.
- The near horizontal orientation of the stays in the web configuration prevents adequate restraint to be developed in the deck. Hence, the increase in the number of cables is ineffective in controlling bending moments in the deck. Thus, the design curves do not converge with the solution obtained from a truss analysis.
- A truss analysis is deemed effective in the preliminary design of a harp, fan, and semi-fan cable-stayed bridges provided that the system has a considerable number of stay cables. The conceptual design of a web typology would need the consideration of flexural rigidity depending on the number of cables and boundary conditions.
- Since the stay cables primarily influence bending moments in the deck, it barely affects the total volume of a cable-stayed bridge under asymmetric loads. This is because under asymmetric load, increase in the total volume is mainly attributed to the increased moment resistance required by the tower elements.

Span length L

- A linear correlation is observed between the normalized volume V/L^2 and span length L. Hence, the absolute volume V can be described as a function of L^3.
- The strength of the correlation is dependent on the material properties of the structural elements, typology, loading conditions, and boundary conditions.

- Under symmetric loads, the effect of span length is most pronounced in the following order of typology: harp, semi-fan, fan, and web.
- The influence of span length L on the efficiency of the system becomes more severe for a material with lower allowable stress σ.
- The volume increase caused by asymmetric loads becomes more severe with the increase in span length.

Materiality

- Concrete, which has a lower allowable stress than steel requires a higher volume of material than steel by approximately a factor of 6.

Typology

- The efficiency of a cable-stayed structure is generally governed by how the cables are oriented and anchored between the tower and deck. The form of a system defines the flow of forces within the system.
- Out of all the different forms investigated, the web configuration is determined to be least efficient due to the extremely gentle sloping cables connecting the midspan of the deck to the towers, especially with the increase in the number of cables, resulting in higher tensile forces in the cables.
- Under symmetric loads, the most efficient form is determined to be in the following order: harp, semi-fan, fan, web. When the same system is subjected to asymmetric loads, the efficiency of the system is slightly reverse: fan, semi-fan, harp, web.
- The flatness of the design curve represent just how flexible the designer is in manipulating the geometry L/H of the cable-stayed structure. The fan configuration is the most forgiving out of all typologies, since the design curve has a much gentler gradient than the others. The steepest design curve is the web configuration.

Boundary conditions

- In general, a partially-anchored cable-stayed bridge performs better than a self-anchored cable-stayed bridge. The most significant improvement is observed for the web configuration. Under symmetric loads, a reduction of approximately 35% and 50% is seen for a steel and concrete bridge, respectively for a harp, fan, semi-fan typology.

- By simply restraining horizontal translation in the main span of the decks, the efficiency of the web configuration is significantly mitigated under the influence of uniform loads, making it comparable with the other conventional typologies. The reduction is amounted to at least 60% for steel and 100% for concrete.
- The design curves of a partially anchored cable-stayed bridge are not only lowered but also flatter in shape. The reduced slope of the design curve indicates that the designer can navigate through the design space more freely with regards to the structure's geometry L/H without much sacrifice on the performance of the system.
- Partial anchoring of the deck is effective to a lesser extent under asymmetric load patterns in comparison to uniform loading conditions. This is because the restrains on the deck does not mitigate the bending induced in the towers caused by asymmetric loads.

5.2 Future works

The work in this thesis only addresses the performance of a cable-stayed bridge in terms of its structural efficiency or in other words, the minimum volume of material required to resist the imposed design loads. It is important to realize that there are other design criteria that needs to be considered in the design of cable-stayed bridges such as serviceability, stability, dynamic aspects caused by wind and seismic, and railroads loading conditions. This suggests that further research need to be done to develop design curves with these performance objectives. A displacement performance, buckling load, and first mode natural frequency for different cable-stayed typologies and geometry are some of the objective parameters that can be used to assess serviceability, buckling and dynamic performances.

Advancements in materiality and typology emphasizes the need for these performance curves to accommodate increasing design variables. As the span lengths of cable-stayed bridges continue to improve, there is a widespread prevalence for lighter steel orthotropic decks and composite deck sections with higher stiffnesses. The inclusion of these type of deck cross-section can provide better insight to the performance of cable-stayed bridges at the preliminary design stage.

Furthermore, this study assumes that the towers and decks are made of the same element, either steel or concrete. It would be worthwhile to explore the possibility of a hybrid design, where the deck is composed of steel and towers of concrete, given the high compressive strength of concrete.

Future work on these design curves, which aims at relating the geometry L/H to

various performances should be encompassing of the different design variables and requirements of modern cable-stayed bridges, while still being simple to implement.

Appendix A

Structural optimization

This appendix demonstrates the general design procedure in structural optimizing the members of the cable-stayed systems described in Section 3.3. The calculations looks at the design of a cable-stayed bridge with the geometry listed in Table A.1.

Table A.1: Details of the cable-stayed bridge being considered

Typology	Harp
Support conditions	Self-anchored
Load Pattern	Symmetric
Material	Steel (σ = 250 MPa)
L (m)	500
H (m)	250
n	5

The structural elements comprising the cable-stayed bridge are labeled in detail in Figure A-1.

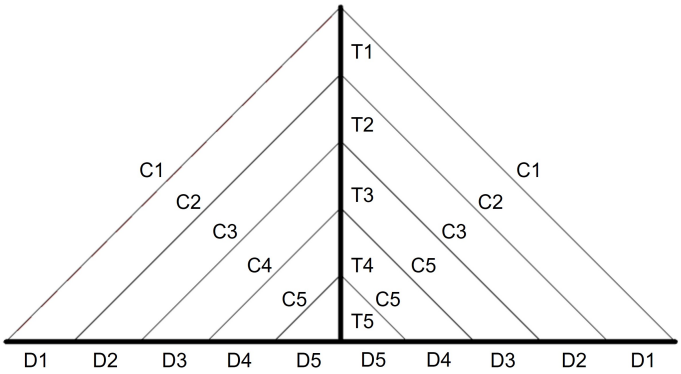

Figure A-1: Structural elements of the cable-stayed system labeled

A.1 Phase I Analysis

Based on a truss analysis performed in Karamba3D, the axial forces N acting on each elements is summarized in Table A.2. Negative axial forces indicate compression and positive axial forces indicate tension.

Table A.2: Axial load N of individual members of a harp cable-stayed model with L = 200 m, H = 100 m, and n = 5 calculated using Karamba3D (Note: The labels D, T, and C indicates deck, tower and cable elements)

Element	N (kN)	Area (m^2)	Length (m)
D1	-5738	0.023	50
D2	-17244	0.069	50
D3	-28865	0.115	50
D4	-40604	0.162	50
D5	-52459	0.210	50
T1	-11939	0.048	50
T2	-35936	0.144	50
T3	-60398	0.242	50
T4	-85326	0.341	50
T5	-110719	0.443	50
C1	8217	0.011	354
C2	16435	0.022	283
C3	16559	0.022	212
C4	16682	0.022	141
C5	16806	0.022	71

Considering the deck, tower and cable elements D1, T1 and C1, the minimum area A of a member required to resist the applied axial load N is determined using Equation 3.4. For the tower and deck elements made up of steel with an allowable stress σ of 250 MPa, the minimum cross-sectional area required to resist the axial force is:

$$A_{D1} = \frac{5738kN}{250MPa} = 0.023m^2 \tag{A.1}$$

$$A_{T1} = \frac{11939kN}{250MPa} = 0.048m^2 \tag{A.2}$$

The allowable stress for the stay cables is defined as 0.45 of the ultimate tensile strength of a 1675 MPa prestressing strand. Thus, for an allowable stress σ of 754 MPa, the minimum area required for the stay cable C1 is:

$$A_{C1} = \frac{8217kN}{754MPa} = 0.011m^2 \tag{A.3}$$

The total volume of the system is given by:

$$\begin{aligned} V &= \Sigma A_i L_i \\ &= (0.023 \times 50) + (0.069 \times 50) + ... + (0.022 \times 71) \\ &= 157.60m^3 \end{aligned} \tag{A.4}$$

The resulting system is now in a fully-stressed state and is used as an input for beam analysis to be performed on.

A.2 Phase II Analysis

Sizing of the tower and deck elements as beam elements is done by first defining the overall dimension of tower and deck cross-section, which is a function of the bridge's span L and tower height H. These dimensions are provided in Table A.3.

Table A.3: Cross-section dimensions of the tower and deck elements

Deck		Tower	
W_{deck}(m)	D_{deck} (m)	W_{tower} (m)	D_{tower} (m)
22	3	10	25

The axial force N and bending moments M for the cable-stayed bridge analyzed using Karamba is summarized in Table A.4.

Table A.4: Axial load N and bending moment M of individual members of a harp cable-stayed model with $L = 200$ m, $H = 100$ m, and $n = 5$ calculated using Karamba3D (Note: The labels D, T, and C indicates deck, tower and cable elements)

Element	N (kN)	M (kNm)	Thickness / Cable area. (mm/m^2)	Length (m)
D1	-4357	69301	4.1	50
D2	-17884	69301	4.1	50
D3	-28622	52158	3.1	50
D4	-40755	52158	3.4	50
D5	-52508	50573	4.3	50
T1	-9196	0	0.6	50
T2	-37289	0	2.2	50
T3	-60073	0	3.5	50
T4	-85922	0	5.0	50
T5	-111290	0	6.4	50
C1	6265	-	0.008	354
C2	19298	-	0.026	283
C3	15313	-	0.020	212
C4	17244	-	0.023	141
C5	16665	-	0.022	71

The sizing optimization for the same deck, tower and cable elements D1, T1, and C1 are demonstrated here.

Because the deck is subjected to both bending moments and axial forces, the two requisites listed in Equation 3.6 and 3.7 have to be satisfied. For deck D1, the applied bending moments govern the thickness of the section to 4.1 mm.

$$
\begin{aligned}
A_{D1} &= (22 \times 3) - (22 - 3 \cdot 0.0004 \times 2 - 2 \cdot 0.0004) \\
&= 0.02m^2 \\
\sigma_{T1} &= \frac{4357kN}{0.02m^2} \\
&= 218MPa < \sigma = 250MPa
\end{aligned}
\tag{A.5}
$$

$$
\begin{aligned}
I_{D1} &= \frac{(22 \times 3^3)}{12} - \frac{[(22 - 3 \cdot 0.0041] \times [2 - 2 \cdot 0.0041]^3)}{12} \\
&= 0.423m^4 \\
\sigma_{T1} &= \frac{69301kNm \times 1.5}{0.423m^4} \\
&= 246MPa < \sigma = 250MPa
\end{aligned}
\tag{A.6}
$$

Therefore, the minimum thickness for the deck cross-section is taken as 0.007 m.

$$
\begin{aligned}
t_{D1} &= max(t_{axial}, t_{bending}) \\
&= max(0.0004, 0.0041) = 0.0041m
\end{aligned}
\tag{A.7}
$$

For the case of the tower, a minimum thickness of 0.001 m provides sufficient axial capacity to resist the applied 9196 kN compresisve load.

$$
\begin{aligned}
A_{T1} &= (10 \times 25) - (10 - 2 \cdot 0.0006 \times 25 - 2 \cdot 0.0006) \\
&= 0.04m^2 \\
\sigma_{T1} &= \frac{9196kN}{0.04m^2} \\
&= 219MPa < \sigma = 250MPa
\end{aligned}
\tag{A.8}
$$

The cross-sectional area for the stay cable C1 is calculated similarly to Equation A.3

Therefore, the total volume of the new system is given by:

$$
\begin{aligned}
V &= \Sigma A_i L_i \\
&= (0.205 \times 50) + (0.205 \times 50) + ... + (0.022 \times 71) \\
&= 195.48m^3
\end{aligned}
\tag{A.9}
$$

.

Appendix B

FEA Results from Strand7

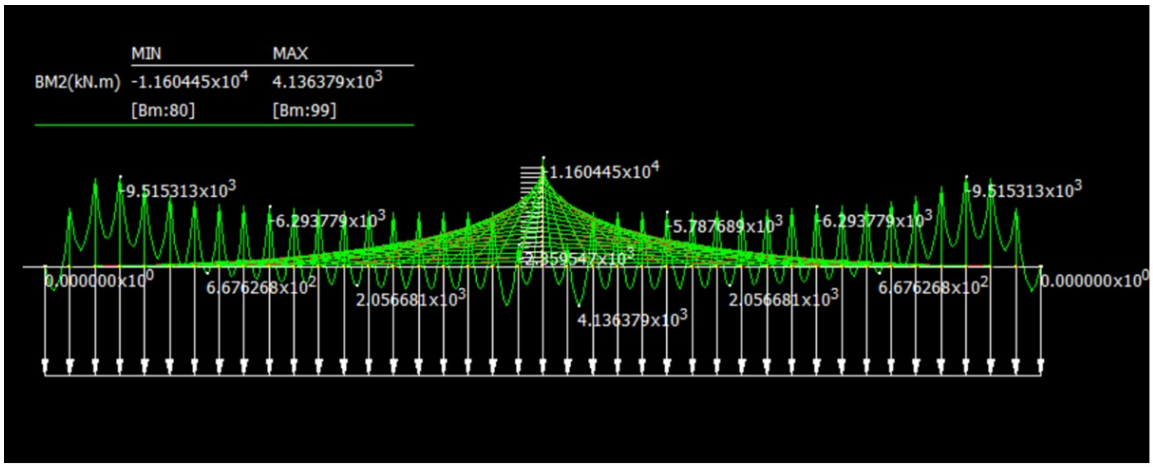

(a)

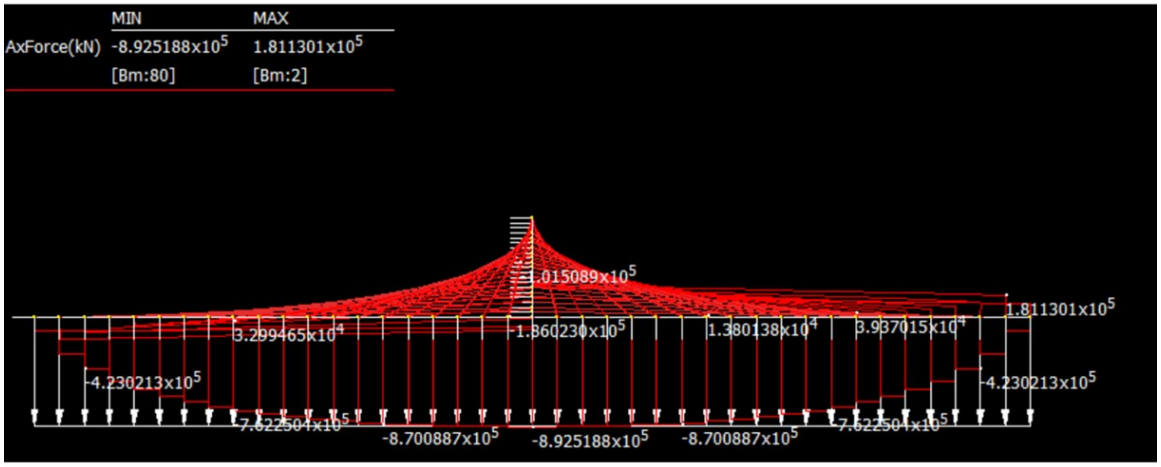

(b)

Figure B-1: (a) Bending moment diagram and (b) Shear force diagram of Model 2 obtained from Strand7 where effect of sag is counteracted

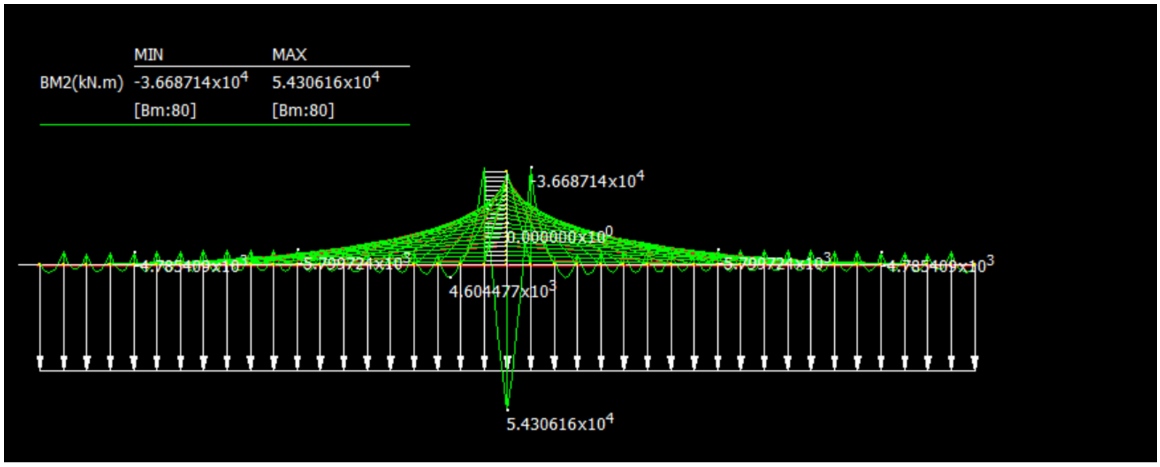

(a)

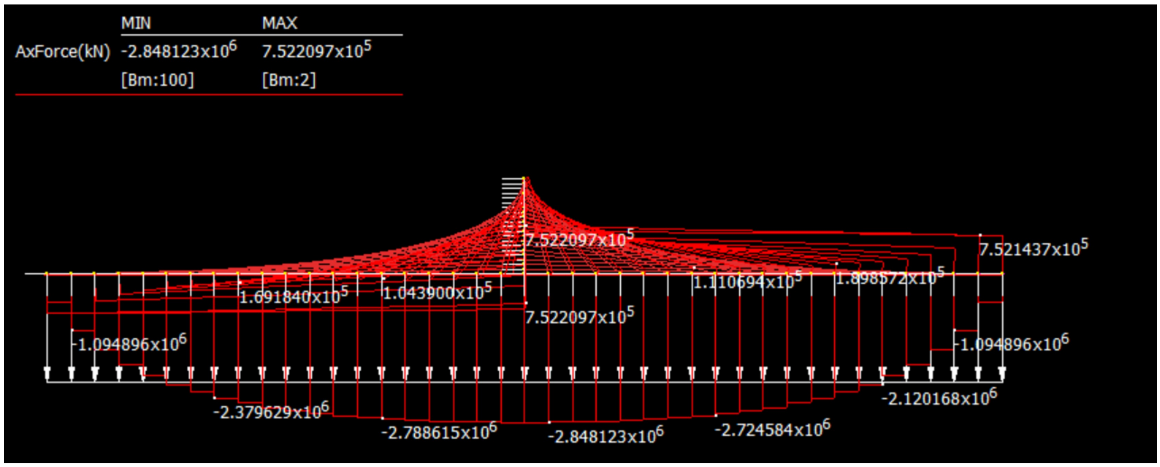

(b)

Figure B-2: (a) Bending moment diagram and (b) Shear force diagram of Model 2 obtained from Strand7 where cable sag is counteracted by defining a free length

Bibliography

AASHTO. (2015). Aashto load and resistance factor design (lrfd) for highway bridge superstructures. American Association of State Highway; Transportation Officials: FHWA-NHI-15-047.

ACI. (2014). Building code requirements for structural concrete. *Aci 318-14*. ACI.

Agrawal, T. (1997). Cable-stayed bridges - parametric study. *Journal of Bridge Engineering*, *2*(2), 61–67.

Akhoondzade-Noghabi, V., & Bargi, K. (2016). Study on different cable configurations of cable-stayed bridges using developed seismic risk assessment. *Structural Engineering International*, *26*(4), 312–323.

ASTM. (2019a). Standard specification for carbon structural steel. *A36/a36m-19*. ASTM.

ASTM. (2019b). Standard specification for low-relaxation, seven-wire steel strand for prestressed concrete. *A416/a416m-18*. ASTM.

Baker, W. F., Beghini, L. L., Mazurek, A., Carrion, J., & Beghini, A. (2015). Structural innovation: Combining classic theories with new technologies. *Engineering Journal*, *52*, 203–217.

Bessas, G. (2005). *Design optimization of cable-stayed bridges* (Doctoral dissertation). Massachusetts Institute of Technology. Cambridge, USA.

Clune, R. (2013). *Algorithm selection in structural optimization* (PhD Dissertation). Massachusetts Institute of Technology. Department of Civil, Environmental Engineering.

De Wilde, W. P., Vandenbergh, T., & Debacker, W. (2015). Structural optimisation and sustainable design. *International Journal of Computational Methods and Experimental Measurements*, *3*(3), 187–204.

Fairclough, H., Gilbert, M., & Tyas, A. (2022). Layout optimization of structures with distributed self-weight, lumped masses and frictional supports. *Structural and Multidisciplinary Optimization*, *2*(2), 1–17.

Ganev, T., Yamazaki, F., Ishizaki, H., & Kitazawa, M. (1998). Response analysis of the higashi-kobe bridge and surroounding soil in the 1995 hyogoken-nanbu earthquake. *Earthquake Engineering & Structural Dynamics*, *27*(6), 557–576.

Hassan, M., Nassef, A., & Damatty, A. (2013). Optimal design of semi-fan cable-stayed bridges. *Canadian Journal of Civil Engineering*, *40*(3), 285–297.

Ito, M. (1998). The cable-stayed meiko grand bridges, nagoya. *Structural Engineering International*, *8*(3), 168–171.

Jiang, F., & Yang, W. W. (1998). Design of the qi ao bridge, china. *Structural Engineering International*, *8*(2), 81–82.

Jomvinya, K., & Vicat, E. (2009). Kanchanapisek bridge over the chao phraya river, thailand. *Structural Engineering International*, *19*(1), 58–62.

Kawashima, K., Unjoh, S., & Tunomoto, M. (1993). Estimation of damping ratio of cable-stayed bridges for seismic design. *Journal of Structural Engineering*, *119*(4), 1015–1031.

Maxwell, J. C. (1864). On reciprocal figures and diagrams of forces. *Philosophical Magazine*, *26*(7), 250–261.

McNeel, R. (2020). Rhinoceros 3d, version 7.0. *Robert McNeel & Associates*.

Miranda, M. D. (2003). Cable-stayed bridge over the guama river, brazil. *Structural Engineering International*, *13*(3), 171–173.

Brown, N. (2017). *Design space exploration user manual version 1.1*. MIT Digital Structures. Massachusetts, MIT.

Ochsendorf, J., & Billington, D. (1998). Record spans in japan. *Civil Engineering - ASCE*, *68*(2), 60–63.

PTI. (2015). Recommendations for stay cable design, testing, and installation. Post-Tensioning Institute.

Rando, M., Lomax, S., & Goberna, E. (2010). The three santiago calatrava bridges in reggio emilia, italy. *Structural Engineering International*, *20*(1), 18–20.

Reich, Y., & Fenves, S. J. (1995). System that learns to design cable-stayed bridges. *Journal of Structural Engineering*, *121*(7), 1090–1100.

Romo, J., Bögle, A., & Meyboom, A. (2015). Geometry and parametric modeling in the conceptual design of bridges. *Iabse conf. - structural engineering: Providing solutions to global challenges*.

Samyn, P. (1999). *Etude comparée du volume et du déplacement de structures isostatiques bidimensionnelles sous charges verticales entre deux appuis. vers un outil d'évaluation et de prédimensionnement des structures (4 tomes)* (Doctoral dissertation). Université de Liège. Liège, Belgium.

Samyn, P. (2004). *Étude de la morphologie des structures à l'aide des indicateurs de volume et de déplacement*. Académie royale de Belgique.

Schlaich, M., Subbarao, H., & Kurian, J. (2013). A signature cable-stayed bridge in india — the yamuna bridge at wazirabad in new delhi. *Structural Engineering International*, *23*(1), 14–17.

Strand7. (2010). Introduction to the strand7 finite element analysis system. *Sydney: Strand7 Pty Ltd.*, *3*.

Stroh, S. (2015). Proportioning and design considerations for extradosed prestressed bridges. *Sustainable bridge structures: Proceedings of the 8th new york city bridge conference* (pp. 150–170).

Svensson, H. (2011). State of the art of cable-stayed bridges. *8th austroads bridge conference*. Austroads.

Virloguex, M. (2001). Bridges with multiple cable-stayed spans. *Journal of International Association for Bridge and Structural Engineering (IABSE)*, *11*(1), 61–82.

Wang, P., Tseng, T., & Yang, C. (1993). Initial shape of cable-stayed bridges. *Computers & Structures*, *46*(6), 1095–1106.

Wang, Y., Wei, M., Gao, Z., & Hadid, H. (2018). Al emarah city bridge, iraq. *Structural Engineering International*, *28*(3), 370–375.

Yanaka, Y., Takazawa, T., & Hirahara, N. (1998). Erection of the tatara bridge's superstructure. *Iabse symposium: Long-span and high-rise structures* (pp. 75–80).

Zalewski, W., & Kus, S. (1996). Shaping structures of least weight. *Proceedings of the international association for shells and spatials structures* (pp. 376–383).